| | |
|---|---|
| 学位論文題目<br>Title | Vulnerability Assessment and Disaster Management in Tsunamis by Integrated Approach of GIS and Remote Sensing(GISとリモートセンシングの統合アプローチによる津波に対する脆弱性評価と災害マネージメント) |
| 氏名<br>Author | MOHAMMAD REZA POURSABER |
| 専攻分野<br>Degree | 博士（学術） |
| 学位授与の日付<br>Date of Degree | 2016-03-25 |
| 公開日<br>Date of Publication | 2018-03-25 |
| 資源タイプ<br>Resource Type | Thesis or Dissertation / 学位論文 |
| 報告番号<br>Report Number | 甲第6646号 |
| 権利<br>Rights | |
| JaLCDOI | |
| URL | http://www.lib.kobe-u.ac.jp/handle_kernel/D1006646 |

Doctoral Dissertation

# Vulnerability Assessment and Disaster Management in Tsunamis by Integrated Approach of GIS and Remote Sensing

# GIS とリモートセンシングの統合アプローチによる 津波に対する脆弱性評価と災害マネージメント

**Mohammad Reza Poursaber**

Graduate School of System Informatics

Kobe University

*February, 2016*

# Acknowledgement

I am very grateful to Kobe University, Japan. I would like firstly express my sincere gratitude and thanks towards my supervisor Professor Yasuo Ariki for his guidance, kindness and patience. I will forever be thankful for encouraging me on my research and his very valuable advices on both my research and career. He provided the vision necessary for me to proceed through this program and this research would not have been possible without his help and support.

My sincere thank also goes to Professor Atsushi Iizuka and Associate Professor Shoji Kato for their useful comments and lectures. I will forever be thankful to Associate Professor Tetsuya Takiguchi for all his kindness and encouragement and other kind students in the Ariki Laboratory of Kobe University for their friendship and helps. I would kindly appreciate to Dr. Ryoichi Takashima, Mr. yasuhiro kakihara, Mr. Ryo Aihara, Dr. Toru Nakashika Dr. Ian Chen for their kind cooperation during my research and special thanks to Mr. Keisuke Sasajima for his efforts and kind cooperation in data processing.

I would like also to appreciate and my sincere thanks to the committee members, Professor Yasuo Ariki, Professor Takenao Ohkawa, Professor Yukio Tada, Professor Akihiko Hokugo and Associate Professor Tetsuya Takiguchi for their helpful comments on my dissertation and oral defense.

My sincere thanks to Professor Shiro Takada, Hyogo International Association organization, Professor Nemat Hassani, Mr. Mansouri and Mr. Mostafa Akbar for their consultant and support to start in Kobe University and their guidance. Special thanks for Dr. M. Safi, Mr. S. Beheshti, Dr. A. Mahdipour, Mr. A. Vasei, Mr. M. Arwan and Mr. R. Pourfathi, my dear friends for their helps and supports. This is a must for me to appear my heart thanks feeling to Prof. M. M. Tehranchi, president of USB and Prof. A. Afzalian, president of Abbaspour Campus for their support to my Ph. D course in Japan.

Last, but by no means the least, I thank my family. Words cannot express how grateful I am to my parents for their kindness and for supporting me every time during my study. And most of all for my patient and supportive wife and my son for all their efforts and patience during last four years.

Finally, the best of best thanks goes to almighty God for blessing my life on this research for saving the lives against natural disasters.

*Mohammad Reza Poursaber*
*February, 2016*

# Abstract

Japan has suffered great damage in terms of both human life and infrastructures due to "Tsunami" attacks over the years. Among them the "Tohoku earthquake and Tsunami" event in March 2011 magnitude 9.0 Honshu, Japan earthquake (38.297 N, 142.372 E, depth 30 km) generated a tsunami that was observed all over the Pacific region and caused widespread destruction. The earthquake and tsunami resulted in 15,890 deaths and many injuries and missing in 12 prefectures with $220 billion damage in Japan. Such big accident is normally resulted in a disaster. A disaster occurs when a significant number of vulnerable people experience a hazard and suffer severe damage and disruption of their livelihood system in such a way that recovery is unlikely without external aid. Management of a disaster requires an effective process to reduce and mitigate the effects. A general strategy for disaster risk reduction must firstly establish the risk management context and criteria, and characterize the potential threats to a community and its environment (hazard); secondly, it should analyze the social and physical vulnerability and determine the potential risks from several hazardous scenarios in order to, finally, implement measures to reduce them. The final goal is reduction of disaster risk in the presence and control of future disaster risk.

In order to manage tsunami disasters and minimize damage in the region, a tsunami disaster vulnerability map is necessary to visualize a graphical presentation of necessary information. The critical information on the tsunami disaster vulnerability map includes vulnerable areas to assess the expected amount of damage in case of possible tsunami attack. Moreover, the tsunami disaster management map can be created from this vulnerability map which indicates the effectiveness and weakness of structural buildings. By examining the weakness revealed on the map, disaster administrators can improve countermeasures and enhance their capability of tsunami disaster prevention and reduction through the establishment of comprehensive disaster prevention and reduction systems. A vulnerability map gives the precise location of sites where people, the natural environment or property are at risk due to a potential catastrophic event that could result in death, injury, pollution or other destruction. Such maps are made in conjunction with information about different types of risks. Vulnerability maps are most often created with the assistance of geographic information systems (GIS), satellite images and land survey designed for use in the studied area. However, vulnerability maps can also be created manually using background maps such as satellite imagery, property boundaries, road

maps, or topographic maps. Vulnerability maps can be of use in all phases of disaster management: prevention, mitigation, preparedness, operations, relief, recovery and lessons-learned. In the prevention stage, planners can use vulnerability maps to avoid high risk zones when developing areas for housing, commercial or industrial use. The vulnerability map can also include evacuation routes to test their effectiveness for saving lives. To create such tsunami vulnerability map, including the distribution of damage area and vulnerable areas, integration of remote sensing technology with spatial analysis applications including Geographical Information System (GIS) is widely employed by the researchers. In the field of disaster management, in particular, remote sensing can help to analyze areas that are prone to natural and man-made hazards and potential damages. Risk and vulnerability assessments are an important part of disaster management and can be supported by remote sensing for pre-disaster analyses. Regarding tsunami risk and vulnerability assessment and modeling, remote sensing techniques have been used in damage assessment and rapid mapping to support the emergency response phase immediately after a disaster has occurred. Remote sensing also gives a contribution to vulnerability and risk assessment in the pre-disaster phase by deriving relevant information such as land use, settlement areas and buildings, elevation, etc. and monitoring of reconstruction and rebuilding in the post-disaster phase.

In this research, we proposed the combined analysis of digital elevation data, very high resolution satellite images, tsunami historical data, together with an Analytical Hierarchy Process (AHP) method with proper factors and suitable scores to produce the vulnerability and damage maps. It is a first attempt for assessing tsunami vulnerability by using the factors of shoreline distance, river distance, elevation, vegetation, and slope through applying the AHP method combined with raster overlay tools through GIS processing in Ishinomaki area. The AHP has been extensively applied to decision-making problems, and extensive research has been carried out to apply AHP to risk assessment. For spatial multi-criteria analysis by means of GIS, the input data as a set of maps and attribute tables that include the spatial information of the study area, are grouped, standardized and weighted. The output is one or more composite index maps, which indicates the realization of the vulnerable hazardous areas. The chapters of this dissertation are organized as follows:

Chapter 1 discusses the introduction and basic motivation of this research, including the research problem and the research objectives. For instance tsunami definition and the origin of a tsunami and vulnerable areas around the world are described.

Chapter 2 represents literature review of this research. This chapter contains the remote sensing concept explanation, Geographical Information System in disaster observation and vulnerability concept. The definition of vulnerability described in this chapter is related to several factors, mostly in some of previous frameworks are mentioned as physical, economic, social and environmental factors. The Application of GIS for preparation of vulnerability maps are described and the methods of utilizing GIS for remote sensing purposes are reviewed.

Chapter 3 discusses a more complicated analysis GIS data that used in this research in the Ishinomaki city in the Miyagi Prefecture as a case study. The technical procedures and issues and necessary steps, including factor definition, processing of raw data, and application of remote sensing and GIS in vulnerability assessment are also explained in this chapter concentrating on the case study defined.

Chapter 4 discusses a simple process and analysis of geospatial image (using GeoEye-1 satellite image) for land use purpose via Environment for Visualizing Images (ENVI) software. Damage classification and change detection in a study area (Inshinomaki city) is investigated by using ENVI software based on the pixel-based image analysis (PBIA) and Object-based image analysis (OBIA). PBIA and OBIA methods are compared by analyzing the damage classification results. It has been shown that object-based approach to classify imagery is giving much accurate result. In the next step, OBIA approach is selected to classify the damage and change detection in two study areas of Ishinomaki city. It analyses the change detection results and discusses about the accuracy, errors and also the correlation between the results in the study areas.

Chapter 5 discusses the steps toward creation of the tsunami vulnerability map by using DEM data. Tsunami vulnerability mapping over the coastal area of Ishinomaki city of Miyagi Prefecture is produced by using GSI DEM. The elevation, slope, coastal proximity, distance from the river and water canal and vegetation were used as the input factors, and weighed raster overlay together with AHP concept was applied to generate the tsunami vulnerability map. Hydrological analysis shows the potential affected area of tsunami wave may spread far into the hinterland by the role of the river of water canal. Most of the high vulnerability area was spread near coastal area. The output result represented similarity to the historical data of a tsunami event in the research area, where 13.44 km2 inundated areas were reported.

Chapter 6 discusses the building damage characteristics based on damage levels (in six classes) and inundation depth where buildings are classified according to their

structural types (Reinforced Concrete (RC), steel, wooden and others). Several statistical figures are plotted based on the MLIT survey data for the whole Ishinomaki city area and specifically for the plane coast area that gives insight to understand the damage dependency to structural material used in buildings. Moreover, in order to consider the impact of coastal topography, a suitable method based on GIS is adopted for extracting the required information from satellite images for the purpose of tsunami-affected area observation in the coastal area. Consequently, potentially affected area by the tsunami is extracted among spatial data and raster calculator output.

Chapter 7 the disaster management and mitigation scopes and framework was described in this chapter. The aim is to reduce the consequences of tsunami event which include saving of lives and capitals. As a prerequisite for this purpose the extent of the damages was obtained from vulnerability studies. Then the quantities to enable us for an appropriate preparedness program can be estimated based on the framework presented. The more exact the data of the vulnerabilities, the more effective the management of its effects. It was shown that which data from vulnerability analysis can more help in disaster management and how we can extract these data for quantifying the needs for disaster management and also planning and preparedness issues.

Chapter 8 presents the conclusion of this dissertation. It has been shown that remote sensing can be capable to achieve information about the input factors for tsunami vulnerability mapping and impact assessment. In the study area, several indicators of vulnerability can be achieved using a very high resolution satellite. It is very useful to derive data about the DEM in high spatial resolution so the output of the research will have more accuracy.

It is shown that a suitable set of factors, including elevation, slope, coastal proximity, hydrological feature, vegetation can be used to obtain an appropriate output, which is close enough to the actual event such as tsunami vulnerability, tsunami disaster management, and tsunami impact assessment. Using very high resolution satellite images and GIS approach, recovery and reconstruction progress can be monitored and studied in future works. This study proposes an effective approach to assess the vulnerability of an area to tsunamis and it is useful for researchers in field of disaster management to create the tsunami vulnerability and damage maps.

# Contents

# List of Figures

# List of Tables

# Abbreviation

| | |
|---|---|
| **AHP** | **A**nalytical **H**ierarchy **P**rocess |
| **ASTER** | **A**dvanced **S**paceborne **T**hermal **E**mission and **R**eflection |
| **A.U.** | **A**stronomical **U**nit |
| **CI** | **C**onsistency **I**ndex |
| **CR** | **C**onsistency **R**atio |
| **CRATER** | **C**oastal **R**isk **A**nalysis for **T**sunamis and **E**nvironmental **R**emediation |
| **CRED** | **C**entre for **R**esearch on the **E**pidemiology of **D**isasters |
| **DEM** | **D**igital **E**levation **M**ap |
| **DN** | **D**igital **N**umber |
| **DT** | **D**ecision **T**rees |
| **ENVI** | **E**nvironment for **V**isualizing **I**mages |
| **FCC** | **F**alse **C**olor **C**omposite |
| **GIS** | **G**eographical **I**nformation **S**ystem |
| **GPS** | **G**lobal **P**ositioning **S**ystems |
| **GSI** | **G**eospatial **I**nformation |
| **HVR** | **H**azard, **V**ulnerability and **R**isk |
| **JMA** | **J**apan **M**eteorological **A**gency |
| **JST** | **J**apan **S**tandard **T**ime |
| **MCDA** | **M**ulti-**C**riteria **D**ecision-making **A**nalysis |
| **MCDM** | **M**ulti **C**riteria **D**ecision **M**aking |

| | |
|---|---|
| **MLIT** | **M**inistry of **L**and, **I**nfrastructure and **T**ransportation of Japan |
| **NDVI** | **N**ormalized **D**ifference **V**egetation **I**ndex |
| **NGDC/WDS** | **N**ational **G**eophysical **D**ata **C**enter/**W**orld **D**ata **S**ervice |
| **NIR** | **N**ear **I**nfrared |
| **NOAA** | **N**ational **O**ceanic and **A**tmospheric **A**dministration |
| **OBIA** | **O**bject-**B**ased **I**mage **A**nalysis |
| **OBIC** | **O**bject-**B**ased **I**mage **C**lassification |
| **OFDA** | **O**ffice of **F**oreign **D**isaster **A**ssistance |
| **PBIA** | **P**ixel-**B**ased **I**mage **A**nalysis |
| **PBIC** | **P**ixel-**B**ased **I**mage **C**lassification |
| **PCM** | **P**air-Wise **C**omparison **M**atrices |
| **PTVA** | **P**apathoma **T**sunami **V**ulnerability **A**ssessment |
| **RC** | **R**einforced **C**oncrete |
| **RH** | **R**isk-**H**azard |
| **ROI** | **R**egions **O**f **I**nterest |
| **SDI** | **S**patial **D**ata **I**nfrastructure |
| **SVM** | **S**upport **V**ector **M**achine |
| **UNICEF** | **U**nited **N**ations **I**nternational **C**hildren's **E**mergency **F**und |
| **UNU-EHS** | **U**nited **N**ations **U**niversity - Institute for **E**nvironment and **H**uman **S**ecurity |
| **U.S.** | **U**nited **S**tates |

| | |
|---|---|
| **VHR** | **V**ery **H**igh spatial **R**esolution |
| **WLC** | **W**eighted **L**inear **C**ombination |

# Chapter 1

## Introduction

### *1.1 Natural Disaster around the World*

Currently about 80 countries around the world are considered susceptible to natural disasters. Large-scale natural disasters, once they occur, take a heavy toll on the lives of people. They can also instantaneously destroy years of development efforts by countries. Disaster risk management should be accounted as a major challenge in the world's future development especially in areas where the poor and vulnerable are at a much higher risk from natural disasters. Consequently, the international organizations such as UNICEF and World Bank Group in general and Japan's government in particular, continue to support the importance of implementing disasters risk management into development programs worldwide. A summary of natural disasters dating from the year 2000 shows in **Table 1.1** [1].

It is evident that the Great East Japan Earthquake brought unprecedented destruction in Japan so that local residents, businesses, local governments, and the national government are now combining their strength in a determined attempt toward rebuilding. The bitter experiences and tough lessons faced in this disaster must be passed on as a testament and also must lead to greatest insight for building from local communities upwards totally disaster resilient nation.

**Table 1.1** Main disasters in the 21th century (Data Source: EM-DAT: The OFDA/CRED International Disaster Database, Centre for Research on the Epidemiology of Disasters (CRED) NOAA)

| No. | Month/Year | Disaster Type | Country | Killed | Total Affected | Estimated Damage (US$ Million) |
|---|---|---|---|---|---|---|
| 1 | January 2010 | Earthquake | Haiti | 222,570 | 3,700,000 | 8,000 |
| 2 | December 2004 | Earthquake | Indonesia | 165,708 | 532,898 | 4,452 |
| 3 | May 2008 | Storm | Myanmar | 138,366 | 2,420,000 | 4,000 |
| 4 | May 2008 | Earthquake | China | 87,476 | 45,976,596 | 85,000 |
| 5 | October 2005 | Earthquake | Pakistan | 73,338 | 5,128,309 | 5,200 |
| 6 | June-August 2010 | Heat wave | Russia | 55,736 | | 400 |
| 7 | December 2004 | Earthquake | Sri Lanka | 35,399 | 1,019,306 | 1,317 |
| 8 | December 2003 | Earthquake | Iran | 26,796 | 267,628 | 500 |
| 9 | July-August 2003 | Heat wave | Italy | 20,089 | | 4,400 |
| 10 | January 2001 | Earthquake | India | 20,005 | 6,321,812 | 2,623 |
| 11 | March 2011 | Earthquake | Japan | 19,846 | 368,820 | 210,000 |
| 12 | August 2003 | Heat wave | France | 19,490 | | 4,400 |
| 13 | December 2004 | Earthquake | India | 16,389 | 654,512 | 1,023 |

| No. | Month/Year | Disaster Type | Country | Killed | Total Affected | Estimated Damage (US$ Million) |
|---|---|---|---|---|---|---|
| 14 | August 2003 | Heat wave | Spain | 15,090 | | 880 |
| 15 | August 2003 | Heat wave | Germany | 9,355 | | 1,650 |
| 16 | December 2004 | Earthquake | Thailand | 8,345 | 67,007 | 1,000 |
| 17 | November 2013 | Storm | Philippines | 7,986 | 16,106,807 | 10,000 |
| 18 | June 2013 | Flood | India | 6,054 | 504,473 | 1,100 |
| 19 | May 2006 | Earthquake | Indonesia | 5,778 | 3,177,923 | 3,100 |
| 20 | April 2010 | Earthquake | China | 2,968 | 112,000 | 500 |
| 21 | September 2004 | Storm | Haiti | 2,754 | 315,594 | 50 |
| 22 | August 2003 | Heat wave | Portugal | 2,696 | | |
| 23 | May-June 2004 | Flood | Haiti | 2,665 | 31,283 | |
| 24 | May 2003 | Earthquake | Algeria | 2,266 | 210,261 | 5,000 |
| 25 | December 2012 | Storm | Philippines | 1,901 | 6,246,664 | 1,693 |
| 26 | August-September 2005 | Storm | United States | 1,833 | 500,000 | 125,000 |

| No. | Month/Year | Disaster Type | Country | Killed | Total Affected | Estimated Damage (US$ Million) |
|---|---|---|---|---|---|---|
| 27 | May-August 2010 | Flood | China | 1,691 | 134,000,000 | 18,000 |
| 28 | October 2005 | Storm | Guatemala | 1,513 | 475,314 | 988 |
| 29 | July 2006 | Heat wave | France | 1,388 | | |
| 30 | August 2003 | Heat wave | Belgium | 1,175 | | |
| 31 | July 2003 | Heat wave | Switzerland | 1,039 | | 280 |
| 32 | July 2006 | Heat wave | Netherlands | 1,000 | | |
| 33 | November 2001 | Flood | Algeria | 921 | 45,423 | 300 |
| 34 | January 2011 | Flood | Brazil | 900 | 45,000 | 1,000 |
| 35 | January 2001 | Earthquake | El Salvador | 844 | 1,334,529 | 1,500 |
| 36 | January-February 2006 | Extreme winter Conditions | Ukraine | 801 | 59,600 | |
| 37 | July 2003 | Heat wave | Croatia | 788 | | |
| 38 | July 2013 | Heat Wave | United Kingdom | 760 | | |

| No. | Month/Year | Disaster Type | Country | Killed | Total Affected | Estimated Damage (US$ Million) |
|---|---|---|---|---|---|---|
| 39 | May-June 2004 | Flood | Dominican Republic | 688 | 10,002 | |
| 40 | February 2004 | Earthquake | Morocco | 628 | 13,465 | 400 |
| 41 | October 2011 | Earthquake | Turkey | 604 | 32,938 | 1,500 |
| 42 | August 2007 | Earthquake | Peru | 593 | 658,331 | 600 |
| 43 | February 2010 | Earthquake | Chile | 562 | 2,671,556 | 30,000 |
| 44 | April-June 2013 | Heat Wave | India | 557 | | |
| 45 | February 2002 | Drought | Malawi | 500 | 2,829,435 | |
| 46 | July 2007 | Heat wave | Hungary | 500 | | |
| 47 | August 2006 | Flood | Ethiopia | 498 | 10,096 | 3 |
| 48 | April 2010-March 2011 | Flood | Colombia | 418 | 2,791,999 | 1,000 |
| 49 | September 2013 | Earthquake | Pakistan | 399 | 185,749 | 100 |
| 50 | August-September 2006 | Flood | Ethiopia | 364 | 8,000 | |

The Tohoku Earthquake, of 2011, created a mega earthquake and tsunami that went far further than any pre-disaster anticipations. It caused enormous damage, and the greatest loss of human life in a single disaster in Japan since the Second World War. Enormous measures have been taken to face natural disasters and tsunamis up to today. The central disaster management council founded the committee for technical investigation on countermeasures for earthquakes and tsunamis based on the lessons learned from the 2011 off the pacific coast of Tohoku earthquake. This has revealed the essential role of risk assessment information gathering, processing how this information should lead to a better understanding of how higher more efficient countermeasures should lead to greater protection of physical, human and financial resources in times of natural disasters.

Several factors such as the magnitude of the earthquake, the height and strength of the tsunami, the extent of the flooded zone, the incidence of subsidence across wide regions, and the extensive human and material harm should be considered by local and international risk management organizations. While disaster management actions had been developed according to many disaster management plans based on pre-disaster assumptions and their implementation, these actions probably exacerbated the damage in some areas [2].

In this study the general description and theory of tsunami dynamics will be discussed.

## *1.2 Overview of Tsunami*

### *1.2.1 General Description*

Tsunami is defined as a series of giant waves which are created by an impulsive disruption in a body of water. Tsunami can cause tremendous damage to coastal areas. A tsunami wave could be less than 1 meter high in the open ocean and traveling at up to 800 km/h in which the wave energy will be boosted from the surface to the ocean floor. They build up to higher and higher heights as the depth of the ocean decreases. So the speed of tsunami waves is mainly associated with ocean depth rather than the distance from the source of the wave. The wave energy of a tsunami is compressed into a much shorter distance when it approaches the coast, generating a potentially large destructive force when it reaches the shore.

When the sea floor abruptly deforms and vertically displaces the overlying water tsunamis are created. A tectonic earthquake is one kind of earthquake that is correlated to the crustal deformation of the earth. When these earthquakes happen on the sea bed, the water layer above the deformed area is displaced from its equilibrium location. Waves are formed as a displaced water mass, occurs due to the impact of gravity. A tsunami can be generated when large areas of the sea floor subside. Tsunami waves slow significantly when approaching the coast, but its height can be 10 times or more and have catastrophic consequences to the areas where it lands on the coast. Low-lying regions of the coast and the areas near bay mouths or tidal flats are highly vulnerable to tsunamis [3].

Large tsunamis are well-known to rise to over 30 meters. Although a tsunami with 3–6 meters height can be very damaging and cause many deaths and damage. Tsunamis are serious menace to life and property for all coastal residents. Since 2014, 245

confirmed tsunamis have triggered more than 600,000 deaths, with about 90% of the casualties from local tsunamis that hit within one hour. Approximately 90% of tsunamis are created by earthquakes or earthquake-generated landslides. During the 1990s, over 4,300 people were killed by 16 tsunamis, including 1100 lives lost in 1992 in Flores, Indonesia, and 2200 lives in the 1998 Aitape, Papua New Guinea tsunamis. The estimated financial damage was nearly one billion U.S. dollars. While most tsunamis (>70%) occur in the Pacific, they can threaten coastlines in the Indian Ocean, Mediterranean Sea, Caribbean region, and the Atlantic Ocean. Since 2000, there have been 14 tsunamis. The most devastating tsunami ever occurred in December 2004, when a M 9.1 earthquake off of northwestern Sumatra, Indonesia produced a destructive tsunami that struck coasts all around the Indian Ocean, killing 227,000 people, relocating more than one million people, and causing billions of dollars of property damage. Other important tsunami happened in March 2011 where a 9.0 Magnitude earthquake generated a tsunami that claimed 17,000 lives in Tohoku, Japan [4].

**Figure 1.1** shows tsunami diagrams in which tsunamis can be divided into four categories.

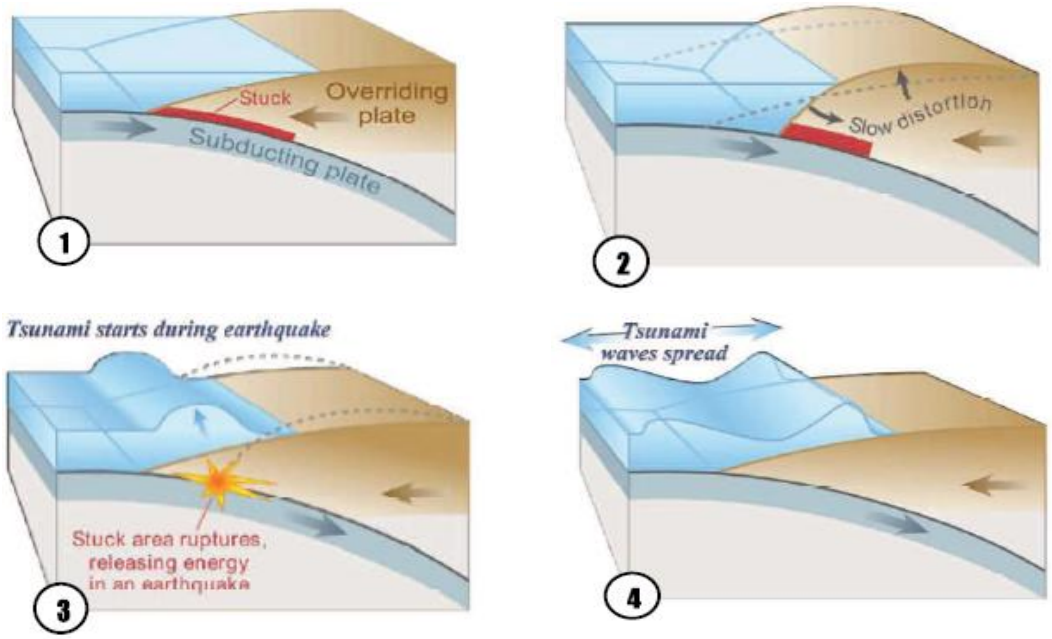


**Figure 1.1** Four different possible causes of tsunamis [5].

**1) Subduction zone**

One of the many plates that make up earth's outer shell descends under an adjacent plate. This kind of boundary is called a subduction zone. When plates move abruptly in an area where they have been struck or stopped from moving. By their own opposing forces over an extended period of time an earthquake will occur.

**2) Between earthquakes**

Stopped or stuck by a sub ducting tectonic plate, the overriding plate gets compressed. Its leading edge is dragged down, while the area behind bulges upward. This movement over an extended period of time, may be even decades or centuries, slowly builds up stress.

**3) During earthquakes**

An earthquake along a subduction zone happens when the leading edge of the overriding plate breaks free and springs upwards, raising the sea floor and the water above it. This uplift starts a tsunami. Meanwhile, the bulge behind the leading edge collapses violently, flexing the plate downward and lowering the area immediately behind the leading edge of the riding plate.

**4) After earthquakes**

Part of the tsunami races toward nearby land, growing taller as it comes in to shallower water. The other part goes in the opposite direction.

**Figure 1.2** shows the distribution of tsunami in the world wide based on the historical occurrence of tsunamis. Tsunamis arise from the sudden displacement of water masses due to earthquakes on the seabed, volcanic eruptions above and under water, landslides or meteorite impacts. About 86 % of all Tsunamis result from so-called seaquakes.

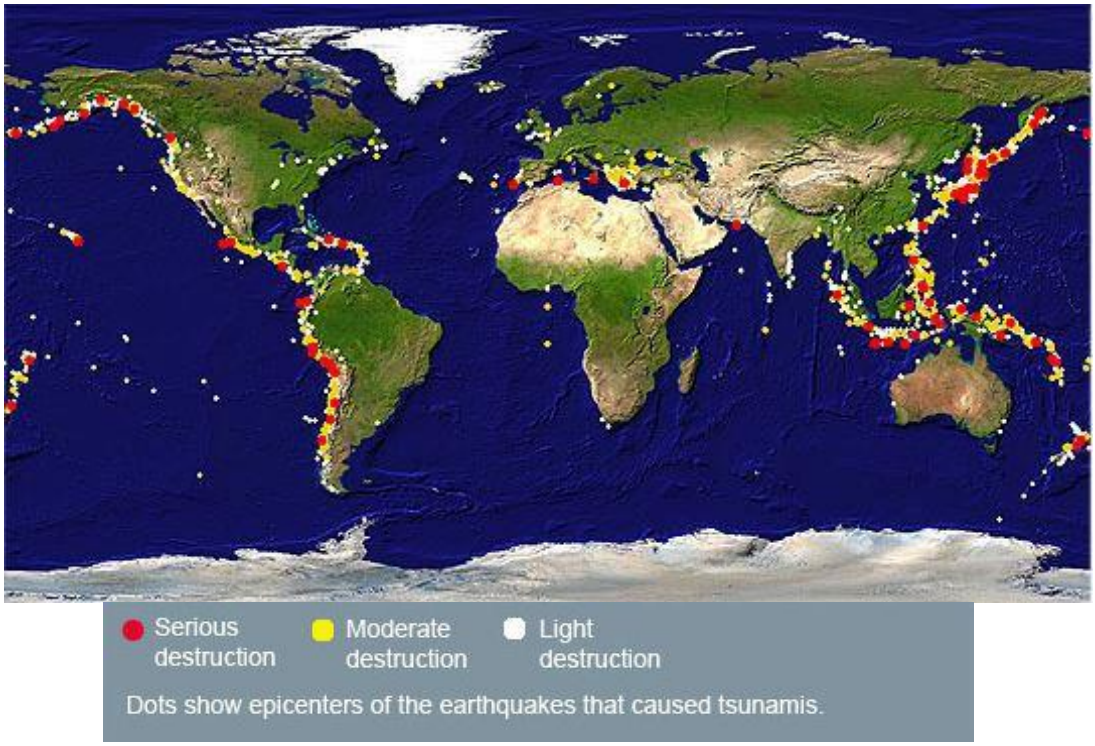


**Figure 1.2** Tsunami distribution in the world based on the historical occurrence [6].

### *1.2.2 Japan Tsunami*

Japan has one of the highest levels of urban risk of natural disaster in the world because all the three values determining the risk-hazard, vulnerability, and exposed value-are very high. Thus, Japanese society has struggled against natural disasters throughout history [1].

Tsunami is a Japanese word represented by two characters "津" "tsu" meaning "harbor" and "波" "nami" meaning "wave". Now generally accepted by the international scientific community to describe a series of travelling waves in water produced by the displacement of the sea floor associated with submarine earthquakes, volcanic eruptions, or landslides and coastal rockfalls can also generate tsunamis, as can a large meteorite impacting the ocean. These waves may reach enormous dimensions and travel across entire ocean basins with little loss of energy. They proceed as ordinary gravity waves with a typical period between 10 and 60 minutes [7] [8].

Located in one of the most active seismic and volcanic zones in the world, Japan is frequently affected by earthquakes and volcanic disasters. As a result, Japan Meteorological Agency (JMA) operationally monitors seismic and volcanic activities all

over the country and issues relevant warnings and information to mitigate damage caused by disasters such as earthquakes, tsunamis, volcanic eruptions and other natural disasters.

From April 2006 until April 2013, the JMA reported at least 51 events of earthquake around Japan with a magnitude above 4.5, also shown in **Table 1.2** is a list of other historic tsunamis on the Tohoku coast. Distribution of major earthquakes that occurred in Japan is shown in **Figure 1.3**, while **Figure 1.4** describes the different magnitude of recent earthquake and shows the comparison between Japan tsunami and tsunami events in some other countries.

**Table 1.2** Historic tsunami on the Tohoku coast [9]

| Year | Earthquake | Magnitude | Max. run up height (m) |
|---|---|---|---|
| 869 | Jogan-Sanriku | 8.3-8.6 | Paleo-tsunami found 4 km inland on Sendai plain |
| 1611 | Keiho-Sanriku | 8.1 | 20 |
| 1896 | Meiji-Sanriku | 8.2-8.5 | 38 |
| 1933 | Showa-Sanriku | 8.1 | 28.7 |
| 2011 | Great East Japan | 9 | 38-40 |

On Friday, at 14:46 Japan Standard Time (JST) 11$^{th}$ March 2011 an earthquake with a 9.0 magnitude occurred in the Pacific Ocean off (the Japan main Island of Honshu) the northeastern coast of Honshu, facing the Tohoku area caused catastrophic damage. The JMA named this earthquake “The Tohoku Earthquake” [10].


**Figure 1.3** Epicenter distribution of the major earthquakes that occurred in Japan (after 1995) [11].

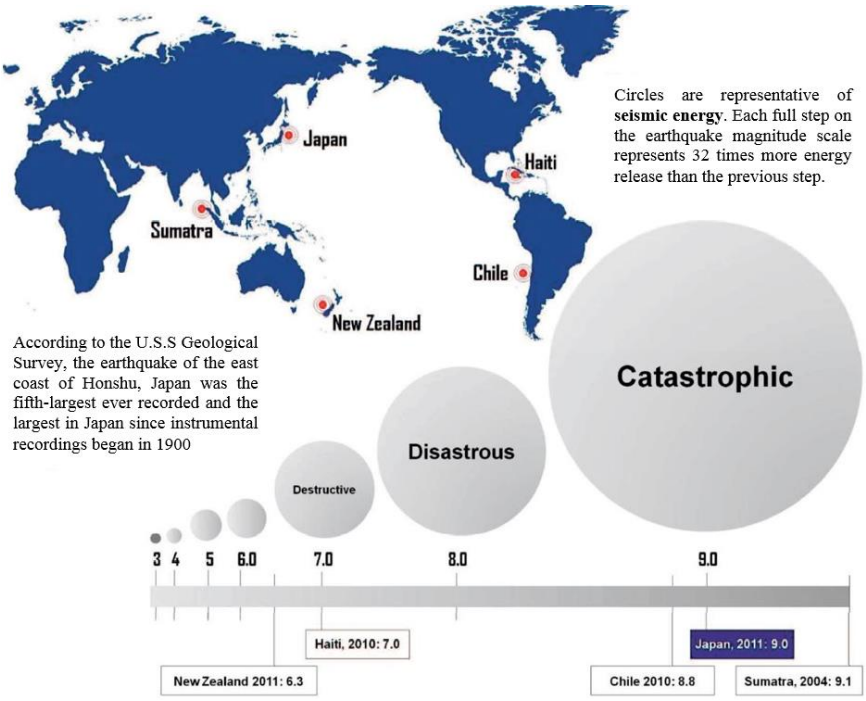


**Figure 1.4** The different Magnitudes of recent earthquakes [12].

The scale and severity of the loss of life, economic losses, and debris generation were extraordinary creating unexpected challenges for emergency management, sheltering, housing, and recovery planning. Current loss estimates indicate 22,626 persons killed or missing nationwide (of which 15,534 are confirmed deaths), 107,000 buildings totally collapsed, and another 111,000 partially collapsed [13].

After the earthquake occurred, the 2011 Tohoku Earthquake Tsunami Joint Survey Group reported the potential tsunami inundation and run up on the Tohoku coast. This report describes that the tsunami inundation run up, concentrated on the coastal areas of Miyagi and Iwate Prefectures. (See **Figure 1.5 (a)** and **(b)**)

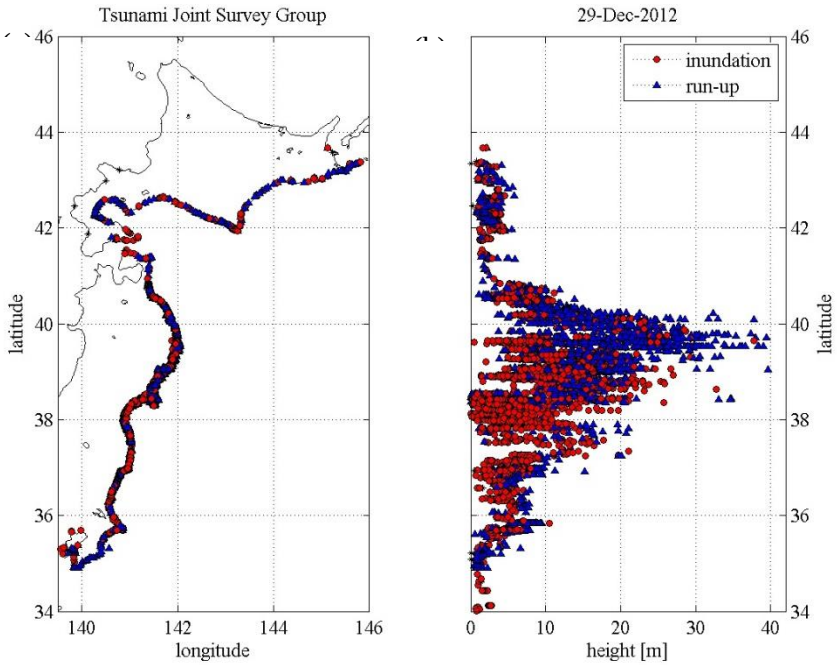


**Figure 1.5** (a) Tsunami inundation and Run-up from the 2011 Tohoku Earthquake Tsunami Joint Survey Group based on Latitude and longitude information; (b) Tsunami inundation and run-up from the 2011Tohoku Earthquake Tsunami Joint Survey Group on 29 December 2012 based on height (m) [14].

According to the report represented by U.S Geological Survey, the shake map in **Figure 1.6** is a geographic representation of the ground shaking produced by the 2011 Tohoku earthquake, and **Table 1.3** its intensity relative to the damage caused.

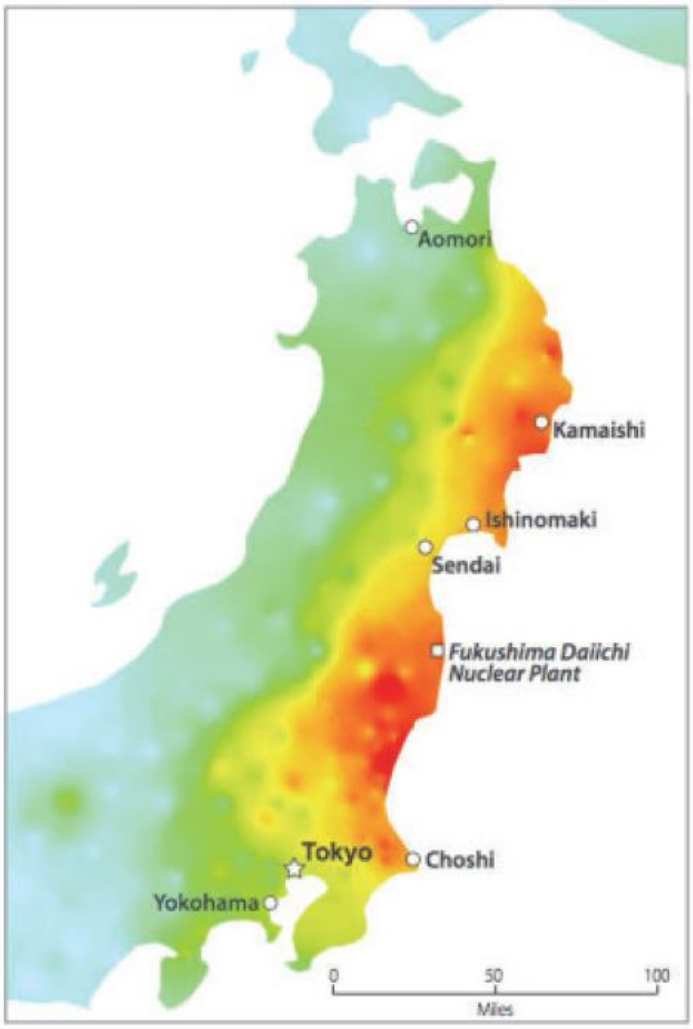


**Figure 1.6** Shake map of the 2011 Tohoku earthquake [15].

**Table 1.3** The intensity classes of ground shaking [16]

| PERCEIVED SHAKING | POTENTIAL DAMAGE | Instrumental Intensity | What Happen at each Intensity? |
|---|---|---|---|
| Not felt | none | I | People do not feel any earth movement. |
| Weak | none | II-III | II-Felt by persons at rest, on upper floors of tall buildings<br>III- Felt by people indoors. Hanging objects swing back and forth. Vibration from the earthquake may seem like the passing of light trucks. May not be recognized as an earthquake. |
| Light | none | IV | Hanging objects swing.<br>Vibration may seem like the passing of heavy trucks or a jolt, like a heavy ball striking the walls. Parked vehicles may rock noticeably. Windows, dishes, doors may rattle and glasses clink. In the upper range of IV, walls of wood frame buildings may creak. |
| Moderate | Very light | V | Felt outdoors .sleepers wakened Liquids disturbed, some spilled. Small unstable objects displaced or upset. Doors swing pictures move. Pendulum clocks stop. |
| Strong | light | VI | Felt by all; some are frightened and take cover. People have difficulty walking due to motion. Objects fall from shelves and dishes, glassware and ceramics may be broken. Pictures fall off walls. Furniture moves or is overturned. Weak plaster and masonry cracked. Damage slight in poorly constructed buildings. Trees, bushes shaken visibly or are heard rustling. |
| Very Strong | Moderate | VII | People have difficulty standing. Drivers on the road feel their cars shaking. Furniture broken. Damage to poorly built masonry buildings. Weak chimneys may break at the roofline. Damage is slight to moderate in well-built structures; considerable in poorly constructed buildings and facilities. |
| Severe | Moderate/ Heavy | VIII | Drivers have trouble steering. Tall structures such as towers, monuments and chimneys may twist and fall. Wood frame houses that are not bolted to their foundations may shift and sustain serious damage. Damage is slight to moderate in well-constructed buildings, considerable in poorly constructed buildings. Branches are broken and fall from trees. Changes occur in flow or temperature of springs and wells. Cracks appear in wet ground and on steep slopes. |
| Violent | Heavy | IX | Masonry structures and poorly constructed buildings suffer serious damage or collapse. Frame structures, if not bolted, shift off foundations. Serious damage to reservoirs. Underground pipes broken.<br>Conspicuous cracks in the ground. In alluvial areas, sand and mud ejected and sand craters are formed. |
| Extreme | Very Heavy | X+ | Most masonry and frame structures destroyed along with their foundations. Some well-built wooden structures and bridges are destroyed. Serious damage to dams, dikes, and embankments. Large landslides occur. Water thrown on the banks of canals, rivers and lakes. Sand and mud shift horizontally on beaches and flat land. Rails bent. |

### *1.2.3 Tsunami sources*

In some ways, tsunamis look like the ripples radiating outward from the spot where a stone has been thrown into the water, but tsunamis can occur in an enormous scale with much higher intensity. Tsunamis are created by any large, impulsive displacement of the sea bed. The movement of the sea floor leading to tsunami can be produced by earthquakes, landslides and volcanic eruptions.

#### *1.2.3.1 Earthquake tsunamis*

Most tsunamis, including almost all of those traveling across entire oceans with destructive force, are caused by submarine faults associated with earthquakes. Tsunamis are produced when a block of the ocean floor is thrust upward, or suddenly drops, or when an inclined area of the seafloor is thrust upward or suddenly thrust sideways. In any event, a huge mass of water is displaced, producing a tidal wave. Such fault movements are referred to as "tsunami genic earthquakes". Most tsunami genic earthquakes take place at the great ocean trenches, where the tectonic plates that make up the earth's surface collide and are forced under or over each other. When the plates move gradually or in small thrusts, only small earthquakes are produced; however, periodically in certain areas when the plates catch. The overall motion of the plates does not stop; only the motion beneath the area becomes stopped. Such areas where the plates are hung up are known as "seismic gaps" due to their lack of movement. The forces in these gaps continues to build until finally the built-up tension (or comprehension) is released in a major earthquake and these generate tsunamis. If the sea floor movement is vertical, a tsunami will be generated. Earthquakes of magnitude larger than M 6.5 are critical for tsunami generation.

#### *1.2.3.2 Tsunamis produced by landslides*

Probably the second most common cause of tsunami is landslide. A tsunami may be generated by a landslide starting above sea level and then plunging into the sea, or by a landslide entirely occurring underwater. Landslides occur when slopes or deposits of sediment become too steep and the material falls under the pull of gravity. Once unstable conditions are present, slope failure can be caused by storms, earthquakes, rain, or merely continued deposit of material on the slope. Certain environments are particularly

susceptible to the production of landslide-generated earthquakes. River deltas and steep underwater slopes above sub-marine canyons, for instance, are likely sites for landslide-generated earthquakes.

#### *1.2.3.3 Tsunami produced by Volcanoes*

Sudden geologic activity associated with volcanic eruptions can also generate devastating tsunamis. Although volcanic tsunamis are much less frequent, they are generally highly destructive. These may be due to submarine explosions, pyroclastic flows and collapse of volcanic caldera:

Submarine volcanic explosions occur when cool seawater encounters hot volcanic magma which often reacts violently, producing stream explosions. Underwater eruptions at depths of less than 1500 feet are capable of disturbing the water all the way to the surface and producing tsunamis. Pyroclastic flows are incandescent, ground-hugging clouds, driven by gravity and fluidized by hot gases. These flows can move rapidly off an island and into the ocean, their impact displacing sea water and causing tsunami.

Moreover, the collapse of a volcanic caldera can also generate tsunami. This may happen when the magma beneath a volcano is withdrawn back deeper into the earth, and the sudden subsidence of the volcanic edifice displaces water and produces tsunami waves. The large masses of rock that accumulate on the sides of the volcanoes may suddenly slide down slope into the sea, causing tsunamis. Such landslides may be triggered by earthquakes or simple gravitational collapse. A catastrophic volcanic eruption and its ensuing tsunami waves may actually be behind the legend of the lost island civilization of Atlantis. The largest volcanic tsunami in recent history documented volcanic eruption and tsunami took place in the East Indies eruption of Krakatau Indonesia in 1883 [17].

### *1.3 Research Procedures*

#### *1.3.1 Research motivation*

Reduction of the occurrence of natural phenomena such as tsunamis seems to be impossible, but the disastrous consequence of these events may be lessened by carrying out initial assessment by mapping vulnerable areas and also employing management and

warning systems. Together with the hazard probability, exposure, and capacity measures, vulnerability is one of the parameters used to determine disaster risk [18] [19].

The development of remote sensing technology and its applications enable the use of satellite imagery for mapping the distribution of an area damaged by a disaster and to assess vulnerable areas. Satellite images have the advantage of being able to deliver simultaneous images of wide areas [20]-[22]. In addition, with the aid of the Geographical Information System (GIS), spatial multi criteria analysis helps prioritize the decision-making process using geo-reference data.

Extensively, differ from the conventional Multi Criteria Decision Making (MCDM) techniques, due to the inclusion of an explicit geographic element. In contrast to conventional MCDM analysis, spatial multi criteria analysis uses information on both the criterion values and the geographical positions of alternatives, in addition to the decision maker's preference with respect to a set of evaluation parameters [23][24].

Some of the previous studies on tsunami vulnerability have analyzed remote sensing data, primarily to assess the physical vulnerability and risk of coastal areas. In addition to such studies, the application of remote sensing in hazard and vulnerability assessment related to ecological and socio-economic vulnerability has been analyzed. Previous studies have also applied moderate-resolution optical satellite images and integrated analysis using GIS to identify inundation areas due to tsunamis [25]-[28]. GIS mapping of tsunami vulnerability has also applied using the Shuttle Radar Topography Mission (SRTM) to obtain the topographic data of the study area [29]. Another spatial analysis method has applied soil type, urban form and social type system for the potential natural hazard mapping [30] and has determined the tsunami-vulnerable area by comparing building damage map with the topography data, which is discussed with regard to land elevation, land use, and the distance from the coast [31]. Mapping of the 2011 Tohoku earthquake tsunami inundation and run-up by survey also has been published [32].

A novel approach from the Coastal Risk Analysis for Tsunamis and Environmental Remediation (CRATER) project was applied for assessing tsunami vulnerability on a regional scale using ASTER imagery and SRTM-version 3. This work analyzed the vulnerability of coastal zones and inland areas using the factors of infrastructural, geo-morphological and ecological features for coastal zones, and factors of land use, altimetry and distance from the shoreline for inland areas [33]. The Papathoma Tsunami Vulnerability Assessment (PTVA) model is a useful tool for providing initial assessments

of the vulnerability of buildings [34] [35]. In addition, a critique of previous studies was undertaken to revise the original PTVA model by taking account of newly published data related to attributes affecting building vulnerability to tsunamis, and to introduce the use of multi-criteria analysis and Analytical Hierarchy Process (AHP) [36].

The current research tried to propose the use of some strategies for tsunami susceptibility; tsunami sources, safety measures, and impact assessment that can be apply easily in any part of the world. In this case many studies are dealing with vulnerability mapping using social point of view, many of them propose a numerical model to assess tsunami risk, this study take a part in proposing an integrative analysis of remote sensing data and GIS in the assessment of tsunami vulnerability and impact. For this propose, in general, the dissertation will introduce several methodologies and data processing, starting from Digital Elevation Model (DEM) data for tsunami vulnerability mapping, and followed by the analysis of remote sensing data and multi-criteria analysis through the use of AHP for tsunami vulnerability mapping that applied in Ishinomaki plain coast area in Japan after the 2011 Tohoku earthquake.

### *1.3.2 Research problem*

The research is devoted to provide decisive factors for efficient tsunami vulnerability assessment in order to reduce the damage of tsunami. For this purpose, different research aspects and approaches are examined. The research questions that will be answered are stated below.

Problems were found:

- Due to the intensity of tsunami occurrences in Japan and other Asian countries, tsunami can cause human, physical and economic losses. The study of tsunami vulnerability mapping is important to reduce the impact of disaster.
- Due to the sometimes very limited amount of time between the initial under-sea quake resulting in a tsunami and the speed with which the tsunami reaches the shore, better preliminary mapping in order to define higher risk or higher percentage of vulnerability to specific areas needs to be undertaken in order to reduce tsunami related damage. So the study of tsunami vulnerability mapping is important to reduce the impact of disaster.

- The methods applied to tsunami vulnerability mapping are various, using complex algorithm and numerical modeling. Using integrative remote sensing and GIS is a chance to contribute to one of the methods in tsunami vulnerability assessment.

### *1.3.3 Research Scope and Objectives*

The objectives of this research are:

1. To develop an integrative remote sensing and GIS approach in vulnerability assessment to tsunami hazard.

2. To develop methods for tsunami vulnerability assessment using integration of spatial data and AHP in a concept of spatial data modeling.

3. To identify areas that are vulnerable and could potentially be affected by tsunami hazard.

4. To develop a concept and method for extracting the required information from satellite images for early-disaster observation in the scope of tsunami.

### *1.3.4 Research Structure and Outline*

To create tsunami vulnerability maps, including the distribution of damage area and vulnerable areas, integration of remote sensing technology with spatial analysis applications including GIS is widely employed by the researchers. In the field of disaster management, in particular, remote sensing can help to analyze areas that are prone to natural and man-made hazards and potential damages. Risk and vulnerability assessments are an important part of disaster management and can be supported by remote sensing for pre-disaster analyses.

In this research, we proposed the combined analysis of digital elevation data, very high resolution satellite images, tsunami historical data, with AHP method, proper factors and suitable scores to produce the vulnerability and building damage maps. It is a first attempt for assessing tsunami vulnerability by using the factors of shoreline distance, river distance, elevation, vegetation, and slope though applying the AHP method combined with raster overlay tools through GIS processing in the Ishinomaki plain coast. The AHP has been extensively applied on decision-making problems, and extensive research has been carried out to apply AHP to risk assessment. The input of spatial multi-criteria analysis is a set of maps that are the spatial representation of the criteria, which

are grouped, standardized and weighted. The output is one or more composite index maps, which indicates the realization of the model implemented.

The dissertation is divided into two parts. The first part contains an introduction and overview of general issues in chapter 1. The second part of this dissertation contains a research work at the study area and the analysis of remote sensing data.

The dissertation is organized into eight chapters, as follows:

**Chapter 1** discusses the general introduction and basic motivation of this research, including the research problem and the research objectives. For instance tsunami definition and the origin of a tsunami and vulnerable areas around the world are described.

**Chapter 2** represents literature review of this research. This chapter contains the remote sensing concept explanation, Geographical Information System in disaster observation and vulnerability concept. The definition of vulnerability described in this chapter is related to several factors, mostly in some of previous frameworks are mentioned as physical, economic, social and environmental factors. The Application of GIS for preparation of vulnerability maps are described and the methods of utilizing GIS for remote sensing purposes are reviewed.

**Chapter 3** discusses a more complicated analysis GIS data that used in this research in the Ishinomaki city in the Miyagi Prefecture as a case study. The technical procedures and issues and necessary steps, including factor definition, processing of raw data, and application of remote sensing and GIS in vulnerability assessment are also explained in this chapter concentrating on the case study defined.

**Chapter 4** discusses a simple process and analysis of geospatial image (using GeoEye-1 satellite image) for land use purpose for a given area via Environment for Visualizing Images (ENVI) software. Damage classification and change detection in a study area (Inshinomaki city) is investigated by using ENVI software based on the pixel-based image analysis (PBIA) and Object-based image analysis (OBIA). PBIA and OBIA methods are compared by analyzing the damage classification results. It has been shown that object-based approach to classify imagery is giving much accurate result. In the next step, OBIA approach is selected to classify the damage and change detection in two study areas of Ishinomaki city. It analyses the change detection results and discusses about the accuracy, errors and also the correlation between the results in the study areas.

**Chapter 5** discusses the steps toward creation of the tsunami vulnerability map by using DEM data. Tsunami vulnerability mapping over the coastal area of Ishinomaki city of Miyagi Prefecture is produced by using GSI DEM.

The elevation, slope, coastal proximity, distance from the river and water canal and vegetation were used as the input factors, and weighed raster overlay together with AHP concept was applied to generate the tsunami vulnerability map. Hydrological analysis shows the potential affected area of tsunami wave may spread far into the hinterland by the role of the river of water canal.

Most of the high vulnerability area was spread near coastal area. The output result represented similarity to the historical data of a tsunami event in the research area, where 13.44 $km^2$ inundated areas were reported.

**Chapter 6** discusses the building damage characteristics based on damage levels (in six classes) and inundation depth where buildings are classified according to their structural types (concrete, steel, wooden and others). Several statistical figures are plotted based on the MLIT survey data for the whole Ishinomaki city area and specifically for the plain coast area that gives insight to understand the damage dependency to structural material used in buildings.

Moreover, in order to consider the impact of coastal topography, a suitable method based on GIS is adopted for extracting the required information from satellite images for the purpose of tsunami-affected area observation in the coastal area. Consequently, potentially affected area by the tsunami are extracted among spatial data and raster calculator output.

**Chapter 7** the disaster management and mitigation scopes and framework was described in this chapter. The aim is to reduce the consequences of tsunami event which include saving of lives and capitals. As a prerequisite for this purpose the extent of the damages was obtained from vulnerability studies. Then the quantities to enable us for an appropriate preparedness program can be estimated based on the framework presented. The more exact the data of the vulnerabilities, the more effective the management of its effects. It was shown that which data from vulnerability analysis can more help in disaster management and how we can extract these data for quantifying the needs for disaster management and also planning and preparedness issues.

**Chapter 8** presents the conclusion of this dissertation. It has been shown that remote sensing can be capable to achieve information about the input factors for tsunami

vulnerability mapping and impact assessment. In the study area, several indicators of vulnerability can be achieved using a very high resolution satellite. It is very useful to derive data about the DEM in high spatial resolution so the output of the research will have more accuracy.

It is shown that a suitable set of factors, including elevation, slope, coastal proximity, hydrological feature, vegetation, and land use can be used to obtain an appropriate output, which is close enough to the actual event such as tsunami vulnerability, tsunami disaster management, and tsunami impact assessment. Using very high resolution satellite images and GIS approach, recovery and reconstruction progress can be monitored and studied in future works. The recommendations for the use of the results of this study for disaster management are described and finally the effect of using such methodology on effective management of disasters are discussed.

# Chapter 2

## Literature Review

### *2.1 Vulnerability: a definition*

A disaster can be classified when a significance of expenses damage and disruption to their everyday system of living to such an extent that there is a very high livelihood that recovery shall require aid from more than their local community and possibly also from other countries (Blaikie , 1994) [37]. As for the mesh between people life styles and environmental systems the work Turner and Kasperson (2003) focuses comprehensively on the many faceted links between social and ecological systems [38]. For better understanding of these linkages between human and environment systems, and as a response to continuing global development, a greater exposure of the vulnerabilities has been arised in the ongoing studies of sustainability sciences and global environmental growth.

It is necessary to determine the social and physical vulnerabilities so as to assess the various related hazardous scenarios and to be able to utilize ways and means to minimize the negative impacts (see **Figure 2.1**). Therefore, disaster risk must identify and classify the risks in order to establish the common criteria of potential threats to communities and their environments. The final goal to be better able to administer control of future disaster risk and also just not to act as if upon post disaster response, risk management needs to be brought in to line throughout all phase of any communities development. In order to arrive at disaster risk management which ensures an ongoing and sustainable practical solution there has to be a multi-faceted understanding in total of the most basic root causes of disasters (UN/ISDR, 2004) [39].

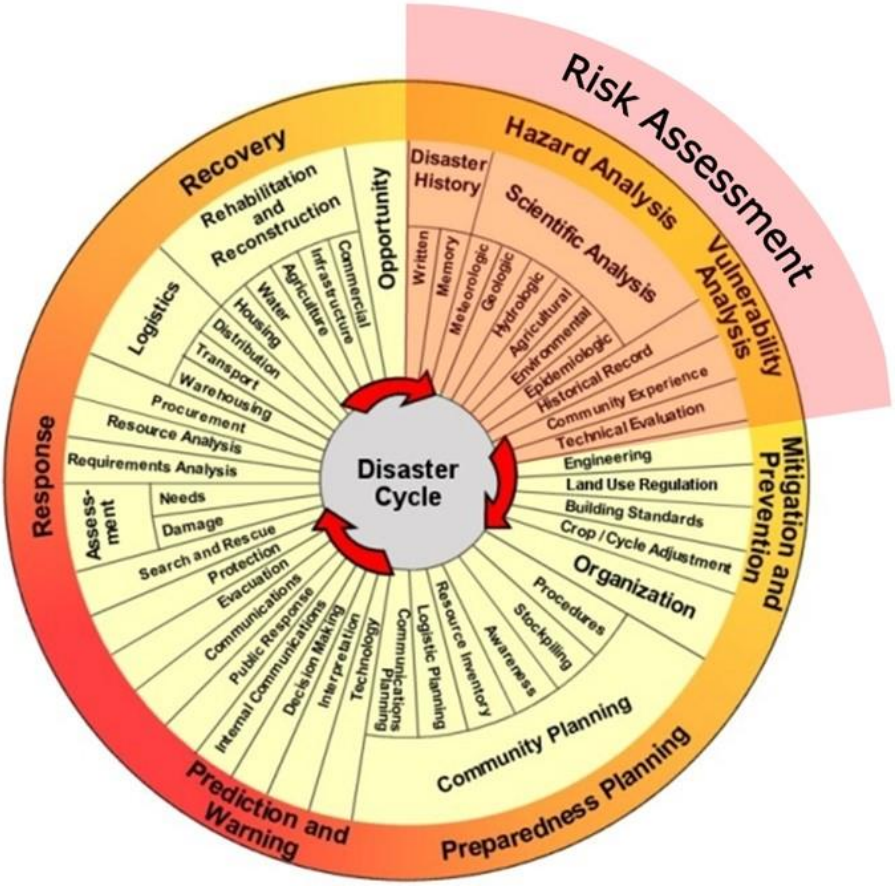


**Figure 2.1** The "traditional" disaster cycle and the role of risk assessment [39].

Since various distinct groups such as, disaster management agencies, development corporations, climatic change organizations are each and all producing their own particular answers as to the fact that vulnerability is a known fact. They have however reached their own and therefore multiple definitions. A complete overview is available in the book on vulnerability edited by Birkmann (2005) as well as on the website of prevention consortium [40] [41].

The first definition is still related only to physical vulnerability while in the other definitions we find that vulnerability is influenced by several factors, mostly mentioned are physical, economic, social and environmental factors. The definitions of vulnerability of Prevention and Blaikie clearly show that besides vulnerability the elements at risk also have capacities. According to the UN, in their report Living with Risk [39] , risk is rooted in conditions of physical, social, economic and environmental vulnerability that need to be assessed and managed on a continuing basis (**Figure 2.2**).

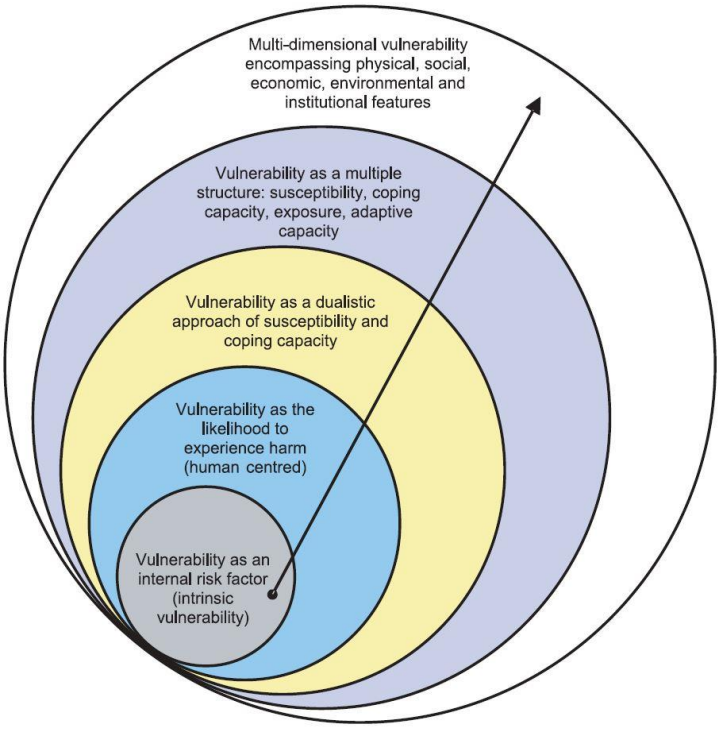


**Figure 2.2** Key spheres of the concept of vulnerability [40].

General definitions of vulnerability:

Vulnerability is:

- "The degree of loss to a given element at risk or set of elements at risk resulting from the occurrence of a natural phenomenon of a given magnitude and expressed on a scale from 0 (no damage) to 1 (total damage)" (UNDRO, 1991) [42].
- "Exposure to risk and an inability to avoid or absorb potential harm (Pelling, 2003) [18]. In this context, he defines physical vulnerability as the vulnerability of the physical environment; social vulnerability as experienced by people and their social, economic, and political systems; and human vulnerability as the combination of physical and social vulnerability" (Vilagrán de León, 2006) [43].
- "The characteristics of a person or group in terms of their capacity to anticipate, cope with, resist and recover from impacts of a hazard" (Blaikie, 1994) [37].
- "A human condition or process resulting from physical, social, economic and environmental factors, which determine the likelihood and scale of damage from the impact of a given hazard" (UNDP, 2004) [44].

- "The conditions determined by physical, social, economic and environmental factors or processes, which increase the susceptibility of a community to the impact of hazards" (UN/ISDR, 1994) [39].
- "The intrinsic and dynamic feature of an element at risk that determines the expected damage/harm resulting from a given hazardous event and is often even affected by the harmful event itself. Vulnerability changes continuously over time and is driven by physical, social, economic and environmental factors" (UNU-EHS, 2006) [45].
- "The potential to suffer harm or loss, related to the capacity to anticipate a hazard, cope with it, resist it and recover from its impact. Both vulnerability and its antithesis, resilience, are determined by physical, environmental, social, economic, political, cultural and institutional factors" [41].

## *2.2 Vulnerability: Conceptual Framework*

Following briefly taken from recent decades and various frame works of vulnerability arrived at in recent decades is a brief description. In the concept arrived by Davidson and adopted by Bollin (2003), risk is seen as the sum of hazard, exposure, vulnerabilities and capacity measures. Hazard is distinguished by probability and severity; exposure elements are structures, population and economy; capacity and measures are concerned with physical planning, management, social and economic capacity [19].

The Risk-Hazard (RH) model Introduced by Turner and Kasperson (2003) shows the impact of a hazard which is seen as a function of the exposure of the system by the hazard event and the response of the system as shown in **Figure 2.3**, where the concept of vulnerability quite often is self-evident [38].


**Figure 2.3** The Risk-Hazard model.

Risk-Hazard assessments incorporating various dimensional scales from world-wide through regional and down to local community sized areas, showing the functional and temporal scales in which varied interactions take place (see **Figure 2.4**). Vulnerability while being registered in the exposure to hazards is also very much apparent in the sensitivity and resilience of the system experiencing such hazards. This sensitivity to exposure is explained by the human-environmental conditions consisting of e.g., social and biophysical capital, which can influence the coping mechanisms as the impact is being experienced and can also influence coping mechanisms causing adjustment, creating newly incorporated changes as the impact is being experienced. In some cases leading ultimately to adaption and changes in the human-environmental conditions.

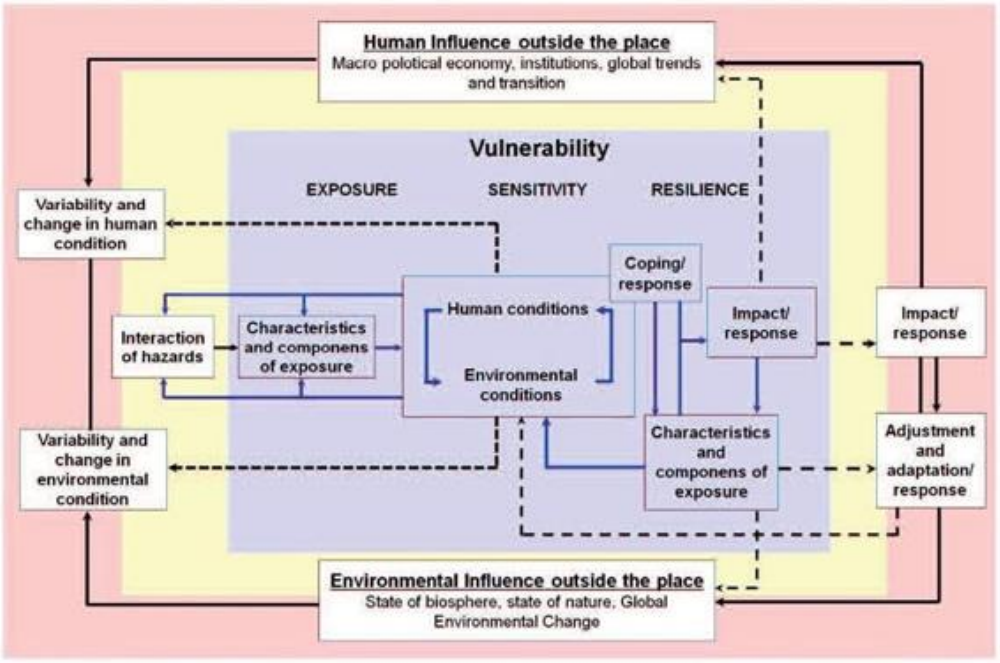


**Figure 2.4** Vulnerability framework; multi-scale (Turner and Kasperson, 2003).

The United Nations University - Institute for Environment and Human Security (UNU-EHS) developed two frameworks for vulnerability. The first one is the onion framework which Bogardi and Birkmann 2004, has a natural event sphere, an economic (monetary) sphere and a social (disutility sphere) crossed by an "opportunity" (probability) axis and a "reality" (certainty) axis [46].

The second one is the BBC (Bogardi and Birkmann (2004) and Cardona (1999)) framework (see **Figure 2.5**) which is a combination of existing models, and is mainly based on their conceptual work. According to the authors, BBC frame work tries to link

vulnerability, human security and sustainable development [47]. The BBC frame work underlines the need to view vulnerability as a dynamic, focusing on vulnerabilities, coping capacities and potential intervention tools to reduce vulnerabilities (feedback-loop system) (Birkmann, 2005). Environmental, social and economic spheres are considered in defining vulnerability, coping capacities, risk and their vulnerability/risk reduction measures [40].

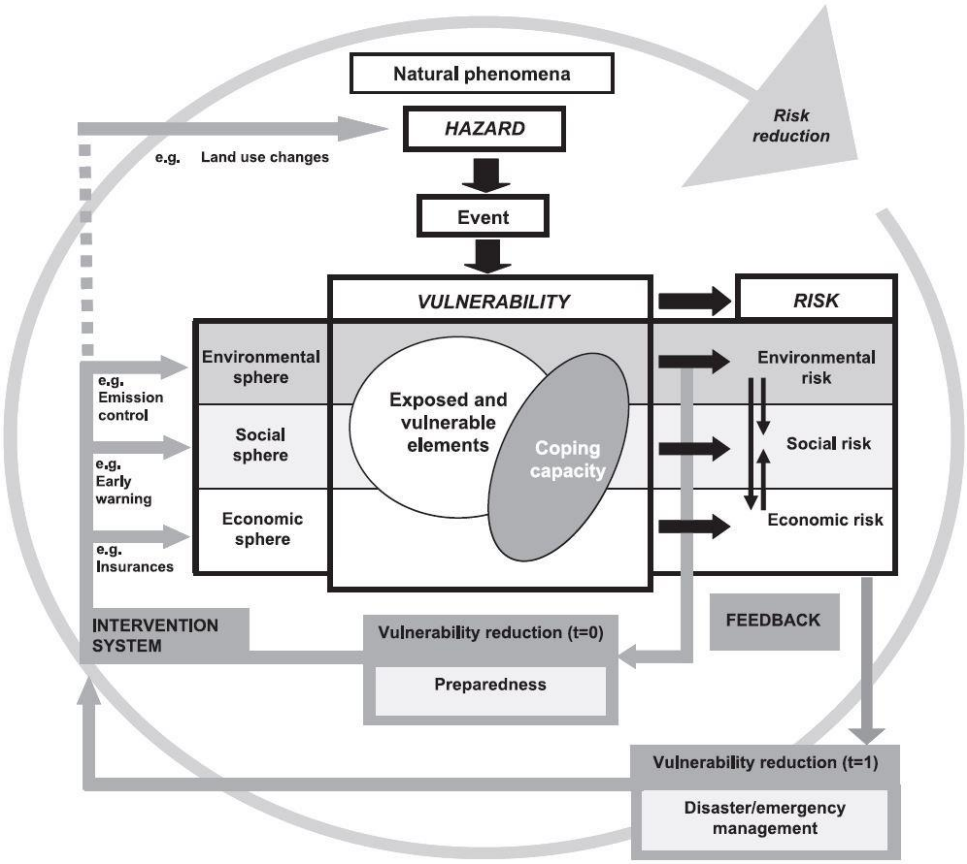


**Figure 2.5** The BBC conceptual framework [46].

## *2.3 Vulnerability Mapping*

A vulnerability map gives the precise location of sites where people, the natural environment or property are at risk due to a potentially catastrophic events that could result in death, injury, pollution or other destruction. Such maps are made in conjunction with information about different types of risks. A vulnerability map can show the housing areas that are vulnerable to a chemical spill at a nearby factory. But they could just as well delineate the commercial, tourist, and residential zones that could be damaged.

Vulnerability maps are most often created with the assistance of computer technology called GIS and digital land survey equipment designed for use in the field. However, vulnerability maps can also be created manually using background maps such as satellite imagery, property boundaries, road maps, or topographic maps. In such cases the municipality's planning office should be consulted in order to take advantage of basic maps that have already been made for other purposes.

Vulnerability maps can be of use in any of the following phases of disaster management: prevention, mitigation, preparedness, operations, relief and recovery. In the prevention stage of risk management planners can use vulnerability maps to avoid high risk zones when developing areas for housing, commercial or industrial use. Technical experts can be alerted about places where the infrastructure can be affected in the event of disaster. Fire departments can plan for rescues before the oncome of any a potentially dangerous event. During an exercise where a predetermined scenario takes place, the rescue crews may use these maps to determine where to respond initially to save human lives, the environment or property. They can also be used to show evacuation routes and to test the effectiveness of these routes for saving large numbers of residents and tourists or moving special groups such as senior citizens, children and those with handicaps. Operations officers can be informed instantly about the disaster situations and the particular needs of specifically sensitive areas.

## *2.4 Spatial Multi Criteria Analysis for Vulnerability Assessment*

The theoretical background for the multi-criteria evaluation is based on the AHP developed by Saaty (1980). The AHP has been extensively applied on decision-making problems (Saaty and Vargas 2001), and extensive research has been carried out to apply AHP to risk assessment. The input of spatial multi-criteria analysis is a set of maps that are the spatial representation of the criteria, which are grouped, standardized and weighted in a 'criteria tree.' The output is one or more 'composite index maps,' which indicates the realization of the model implemented [48] [49].

In 1980, Saaty developed AHP method, in which the hierarchy of components of the decisions was used in decision-making process. The AHP is essentially an interactive one where a decision-maker or group of decision-makers relay their preferences to the analyst and can debate or discuss opinions and outcomes (Proctor, 2000). The AHP is based upon

the construction of a series of Pair-Wise Comparison Matrices (PCMs), which compare all the criteria to one another [50].

Although a variety of techniques exist for the development of weight, one of the most promising would appear to be that of pairwise comparison developed by Saaty (1977) in the context of a decision making process known as AHP. The first introduction of this technique to a GIS application was that Rao (1991) [51] [52]. In the procedure for multi-criteria analysis using weighted linear combination, it is necessary that the weight sum to be 1. In Saaty's technique, weight of the nature can be derived by taking the principal eigenvector of a square reciprocal matrix of pairwise comparisons between the criteria. The comparisons concern the relative importance of the two criteria involved in determining the suitability of a stated objective. Ratings are provided on a nine-point continuous scale (see **Figure 2.6**) for instance, if one felt that elevation was very strongly more important than coastal proximity in determining a vulnerability area due to a possible tsunami, one would enter a 5 or 7 on the scale. If the inverse were the case (coastal proximity was very strongly less important than elevation), one would enter 1/5 or 1/7.

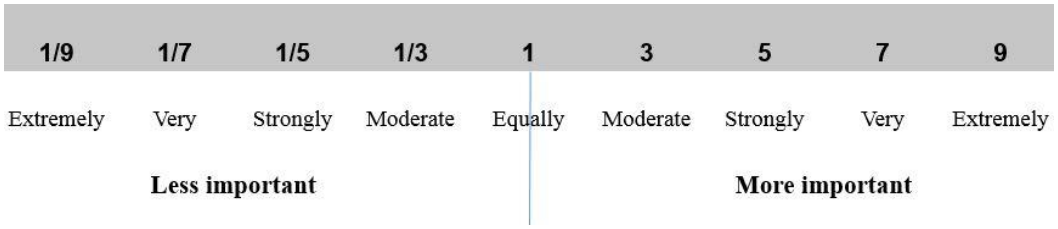


**Figure 2.6** The continuous rating scale used for the pairwise comparison of factors in multi- criteria analysis.

From a decision-making perspective, multi-criteria evaluation can be expressed in a matrix as shown in **Table 2.1** The matrix A contains the criteria in one axis (*C1* to *Cn*), and a list of possible alternatives, from which a decision has to be taken on the other axis (*A1* to *Am*). Each cell in the matrix (*aij*) indicates the performance of a particular alternative in terms of a particular criterion. The value of each cell in the matrix is composed of the multiplication of the standardized value (between 0 and 1) of the criterion for the particular alternative, multiplied by the weight (*W1* to *Wn*) related to the criterion. Once the matrix has been filled, the final value can be obtained by adding up all cell values of the different criteria for the particular alternative.

**Table 2.1** Multi-criteria decision matrix

$$\begin{bmatrix} & C_1 & C_2 & C_3 & C_4 & C_5 & \dots & C_n \\ & W_1 & W_2 & W_3 & W_4 & W_5 & \dots & W_n \\ A_1 & a_{11} & a_{12} & a_{13} & a_{14} & a_{15} & \dots & a_{1n} \\ A_2 & a_{21} & a_{22} & a_{23} & a_{24} & a_{25} & \dots & a_{2n} \\ . & . & . & . & . & . & . & . \\ . & . & . & . & . & . & . & . \\ . & . & . & . & . & . & . & . \\ A_m & a_{m1} & a_{m2} & a_{m3} & a_{m4} & a_{m5} & \dots & a_{mn} \end{bmatrix}$$

For implementing this matrix according to the AHP, three principle steps need to be considered. The first one decomposes the problem (and the weights) into a hierarchical structure. The second one considers the weighting process, employing the pairwise comparisons of the criteria, and the synthesis is related to the multiplications among the hierarchical levels. Additionally, in the three principal steps of spatial implementation of this procedure, every criterion (*Cj*) becomes a raster layer, and every pixel (or set of pixels) of the final composite index map eventually becomes an alternative *Aj*. The goal (risk index) has been decomposed into criteria levels *CL1* and *CL2*. The intermediate levels are often indicated as sub-goals or objectives (e.g. in level 1, the sub-goals are a 'hazard index' and a 'vulnerability index'). Each criterion of each level will also have an assigned weight.

Therefore, the values for the layers of the intermediate levels are obtained through the summation of the performance for the alternative at lower levels. As the criteria consist of raster maps, their spatial performance ($\mathbf{a}_{ij}$) and the alternative (Ai) will be identified for particular raster cells. The composite risk index map (e.g. tsunami risk) is obtained by an assessment rule, which is calculated by adding up the performance of all the cell values of the different criteria ($\mathbf{a}_{ij}$) for the particular alternative. The performance of every element in the matrix ($\mathbf{a}_{ij}$) is applying by **Eq. 2.1**.

$$\mathbf{a}_{ij}\mathbf{v}_j \prod_{L=0}^{h} \mathbf{w}_j^L \qquad \text{(Eq. 2.1)}$$

In this equation, $\mathbf{v}_j$ refers to the standardized value of criterion (Cj) for alternative (Ai), and weight $\mathbf{w}_j^L$ refers to the weight of criterion (Cj) for level L (0–h levels). During

the analysis, it could be desirable to produce the intermediate criteria maps. In this case, **Eq. 2.1** should not be applied because weights need to be multiplied with the standardized values only up to the specific level of the intermediate maps. The intermediate maps might also be combined using different methods. When designing vulnerability indicators, it is necessary to take into account the socio-economic conditions, which may vary from country to country [53]-[55].

## *2.5 Remote Sensing for Tsunami Disaster*

In disaster management field, remote sensing can help to analyze areas that are prone to natural and man-made hazards resulting in potential damage. Risk and vulnerability assessments are important parts of disaster management and can be supported by remote sensing for pre-disaster analyses. Regarding tsunami vulnerability assessment, remote sensing techniques have been used in damage assessment and rapid mapping to support the emergency response phase immediately after a disaster has occurred. Remote sensing also contributes to vulnerability and risk assessment in the pre-disaster phase by deriving relevant information such as land use, settlement areas and buildings, elevation, etc. and monitoring of reconstruction planning in a post-disaster phase.

### *2.5.1 Damage Assessment*

In general, there are two main goals using remote sensing data for analyzing damage: First is rapid mapping assessment and second is mapping the hazard impact affected zones. The latter is very important in risk and vulnerability assessment in order to know the important factors for tsunami hazard mapping. For example, the tsunami run-up is influenced by the topography of a region, the geomorphologic conditions, mangroves, and coral reefs influenced the characteristics of the tsunami inundation in Aceh, and when a landscape analysis was used to model tsunami damage in Aceh Province [56]-[60].

**Figure 2.7** shows damage detection from satellite remote sensing thought comparison images before and after the 2011 Japan tsunami which struck Ishinomaki, Miyagi Prefecture.


**Figure 2.7** Satellite remote sensing (ASTER) images of before and after the 2011 Japan tsunami in Ishinomaki .(The bottom image, acquired by the Advanced Spaceborne Thermal Emission and Reflection Radiometer (ASTER) on NASA's Terra satellite, shows the same area on March 14, 2011) [61].

Satellite images which captured the affected areas before and after the event were fully employed in field investigations and in tsunami damage mapping. Since the affected areas are vast, moderate resolution satellite images are quite effective in change detection due to the tsunami.

### *2.5.2 Satellite Image Analysis for Tsunami-Affected Areas*

Recent advances in remote sensing technologies have expanded the capabilities of detecting the spatial extent of tsunami-affected areas and damage to structures. The highest spatial resolution of optical imageries from commercial satellites is up to 60–70 centimeters (QuickBird owned by DigitalGlobe, Inc.) or 1 meter (IKONOS operated by GeoEye). Since the 2004 Sumatra-Andaman earthquake tsunami, these satellites have captured images of tsunami-affected areas, and the images have been used for disaster management activities, including emergency response and recovery.

To detect the extent of a tsunami inundation zone, NDVI (Normalized Difference Vegetation Index) is the most common index obtained from the post-event imagery, focusing on the vegetation change due to the tsunami penetration on land. In addition to apply the NDVI algorithm to detect the impact of tsunami, the use of soil (NDSI) and water (NDWI) also can apply in tsunami impact prediction [22].

# Chapter 3

## Integrated GIS and RS Vulnerability Assessment Framework

### *3.1 General Procedure*

In order to define the framework for vulnerability assessment by using integrated systems first we should clarify how and in what format the assessment is quantified and what kind of tools and data are needed for that. This should be done considering the purpose of the vulnerability and the type of outputs needed for that. Common findings are that it is adamant to assess vulnerability as an integral part of the causal chain of risk and to appreciate that changing vulnerability is an effective strategy for risk management. For this purpose one should answers to the following questions: Who is vulnerable? To what are they vulnerable? What are the specific reasons for their vulnerability? Where are they vulnerable? How have they come to be vulnerable?

A key research issue in seeking to understand vulnerability is the need to better grasp the causal structures (or maps) of current patterns of vulnerability and how these causal structures that shape immediate attributes of risk and vulnerability are embedded in the basic properties and processes of society, economy, and policy. As yet we know of few explorations, much less modelling efforts, of these causal maps. Such maps will need to be complex enough to allow cross-scale analyses, to evaluate the multiple stresses on vulnerable regions and people which often emanate from higher larger scales as do social forces. The following elements for inclusion in any vulnerability analysis, particularly those aimed at advancing sustainability are identified:

- Multiple interacting perturbations and stressors/stresses and the sequencing of them;
- Exposure beyond the presence of a perturbation and stressor/stress, including the manner in which the coupled system experiences hazards;
- Sensitivity of the coupled system to the exposure;

- The system's capacities to cope or respond (resilience), including the consequences and attendant risks of slow (or poor) recovery;
- The system's restructuring after the responses taken (i.e., adjustments or adaptations);
- Nested scales and scalar dynamics of hazards, coupled systems, and their responses.

In order to manage tsunami disasters and minimize damage in a region, a tsunami disaster vulnerability map is necessary to visualize a graphical presentation of necessary information. A vulnerability map gives the precise location of sites where people, the natural environment or property are at risk due to a potential catastrophic event that could result in death, injury, pollution or other destruction. Such maps are made in conjunction with information about different types of risks. Vulnerability maps are most often created with the assistance of GIS, satellite images and land survey designed for use in the studied area. However, vulnerability maps can also be created manually using background maps such as satellite imagery, property boundaries, road maps, or topographic maps. Vulnerability maps can be of use in all phases of disaster management: prevention, mitigation, preparedness, operations, relief, recovery and lessons-learned.

To create such tsunami vulnerability map, including the distribution of damage area and vulnerable areas, integration of remote sensing technology with spatial analysis applications including Geographical Information System is widely employed. In the field of disaster management, in particular, remote sensing can help to analyze areas that are prone to natural and man-made hazards and potential damages. Risk and vulnerability assessments are an important part of disaster management and can be supported by remote sensing for pre-disaster analyses. Regarding tsunami risk and vulnerability assessment and modeling, remote sensing techniques have been used in damage assessment and rapid mapping to support the emergency response phase immediately after a disaster. Remote sensing also gives a contributes to vulnerability and risk assessment in the pre-disaster phase by collating relevant information such as land use, settlement areas and buildings, elevation, etc. and monitoring of reconstruction and rebuilding in the post-disaster phase.

In this research, we proposed the combined analysis of digital elevation data, very high resolution satellite images, tsunami relevant data, together with an AHP method with proper factors and suitable scores to produce the vulnerability and damage maps. The AHP has been extensively applied to decision-making problems, and extensive research has been carried out to apply AHP to risk assessment. For spatial multi-criteria analysis

by means of GIS, the input data as a set of maps and attribute tables that include the spatial information of the study area, are grouped, standardized and weighed. The output is one or more composite index maps, which indicates the realization of the vulnerable hazardous areas.

### *3.2 Different types of data's*

A lot of datasets are required for the tsunami vulnerability mapping using multi-criteria through AHP technique and analysis of satellite images for tsunami impact observations. These data contains images raster data of satellite (see **Table 3.1**) and vector data of study area map. Besides supporting the analysis, secondary data such as the observation data is used.

#### *3.2.1 Raster Data in GeoEye-1 Satellite images*

The GeoEye-1 is a very high-resolution earth observation satellite which was launched in September 2008. GeoEye-1 will be equipped with the most advanced technology ever used in remote sensing system. The satellite will be able to collect images at 0.41m panchromatic (black & white) and 1.65m multispectral resolution. Just as important, GeoEye-1 will be able to precisely locate an object to within 3 meters of its true location on the surface of the Earth. This degree of inherent geo-location accuracy has never been achieved in any commercial imaging system. The satellite will be able to collect up to 700,000 square kilometers of panchromatic (and up to 350,000 square kilometers of pan-sharpened multispectral) imagery per day. This capability is ideal for large scale mapping projects. GeoEye-1 will be able to revisit any point on Earth once every three days or sooner. The GeoEye-1 satellite is in a sun-synchronous orbit with a nominal equator crossing at 10:30 AM local. It takes approximately 98 minutes to complete one orbit and it makes nearly 15 orbits per day. The relatively high orbit, at 684 km above the Earth's surface, allows for more access time over a particular area of interest resulting in larger collection capacity (see **Table 3.1** for the GeoEye-1 satellite platform technical Information and **Table 3.2** for GeoEye-1 Sensor Specifications) [62]-[65].

**Table 3.1** Satellite platform technical Information

| | |
|---|---|
| **Name of satellite** | GeoEye-1 |
| **Operating country** | United States |
| **Launch Date** | September 6, 2008 |
| **Camera Modes** | 0.41 m Panchromatic (nominal at nadir)<br>1.65 meter multispectral (nominal at nadir) |
| **Imaging Direction** | Capable of imaging in any direction or angle |
| **Collection Capacity** | Up to 700,000 sq km/day of pan area<br>Up to 350,000 sq km/day of pan-sharpened multispectral area |
| **Revisit frequency** | 11 days |
| **Orbital inclination** | 98º |
| **Satellite orbit** | Polar sun-synchronous orbit |
| **Revisit time** | 3 days (in the event that imaging angle is above 60º) |
| **Satellite altitude** | 684 km/ 425 miles |
| **Overpass time (above Japanese skies)** | around 10:30 a.m. to 11:00 a.m. |
| **Satellite Weight** | 1955 kg |
| **Orbital Velocity** | About 7.5 km/sec |
| **Instrument size** | 3 m tall (the volume is 5.3 $m^3$) |

**Table 3.2** GeoEye-1 sensor specifications

| | | | |
|---|---|---|---|
| **Spectral range (band)** | Panchromatic | Pan | 450 to 800 nm |
| | Multispectral (MS) | Blue | 450 to 510 nm |
| | | Green | 510 to 580 nm |
| | | Red | 655 to 690 nm |
| | | Near-infrared | 780 to 920 nm |
| **Spatial resolution at nadir (Ground Sample Distance) (GSD)** | Pan | 0.41 m GSD | |
| | MSS | 1.64 m GSD | |
| **Swath width** | 15.2 km | | |
| **Data quantization** | 11 bits | | |
| **FOV (Field of View)** | > 1.28º | | |

### *3.2.2 Vector Data*

Geospatial Information Authority of Japan (GSI) have provided hardcopy and softcopy of vector maps upon request. A list of vector map is displayed in **Table 3.3**.

**Table 3.3** List of vector maps

| Data type | Scale levels / Resolution | Coordinate system |
|---|---|---|
| Reference point of the survey<br>**Point:**<br>Elevation, shoreline, water, buildings, boundaries of administrative areas.<br>Boundary of the city/ district<br>Point elevation (DEM)<br>**Line:**<br>Elevation, shoreline, water, building center line, boundaries of the area, road. | 1:2,500 | JGD_2000_Japan_ Zone_10<br><br>WGS_1984_UTM_ Zone_54N |
| GSI DEM | 0.2 arc-second (5m) | GSI Japan |

A high spatial resolution of DEM has been provided by the Geospatial Information Authority of Japan (GSI). Based on the surveying methods, a 5m mesh of elevation data is divided into two major types. The first type was created based on the airborne laser, which is the center point grid of mesh on the basis of data equivalent to those published (digital elevation map of 5m mesh) and longitude difference at the surface and separated by interval 0.2 seconds latitude difference. As a sample the method has been applied for the target of metropolitan areas. The second type is based on the photogrammetric. In such methods, the mesh 0.2 seconds difference in latitude (about 5m) interval, the data of the ground surface is created by removing bridge and houses, trees, etc. the target of the methods is urban areas and can also be used for the application of city planning [66].

## *3.3 Spatial Data Analysis in GIS*

As a general rule, GIS have the spatial, graphical, numerical, and textural components. These system components have several important building blocks such as data modeling, data structures, and the types of applications. Basically there are 3 spatial data

components that need to be stored in a GIS format including geometric data, thematic data, and a link identification. Geometric component deals with the location of the data by means, for instance, of a reference coordinate system and the thematic component provides the attribute value of the data [67] [68]. **Figure 3.1** presents design and construction phases for a geo-spatial model in integration with AHP.

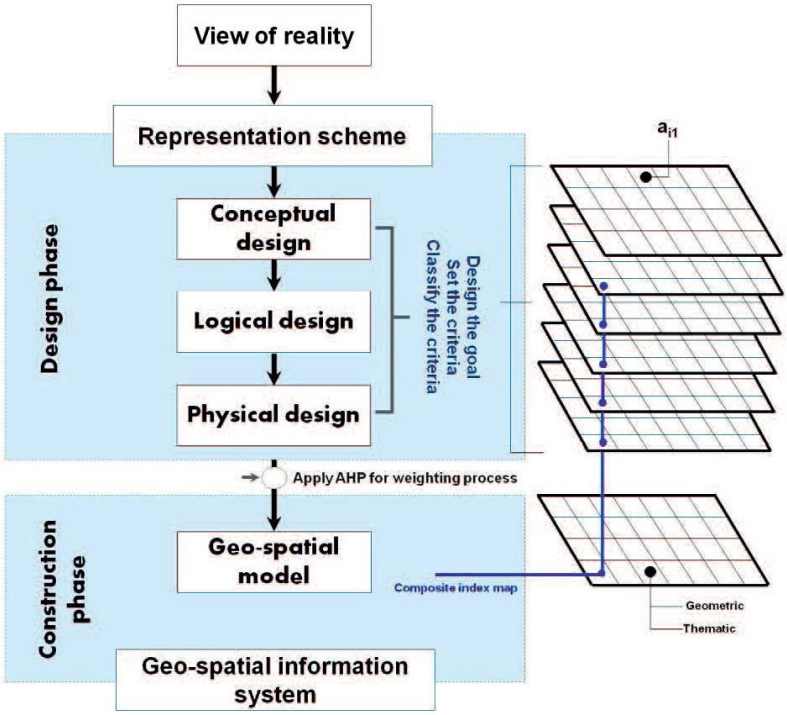


**Figure 3.1** Design and construction phases for a geo-spatial model.

For running a model in multi-criteria analysis, the creation of spatial data will be necessary. The creation of spatial data should follow the design phase (see **Figure 3.2**). Spatial data that is used as input factors for multi-criteria analysis are described as below;

### *3.3.1 Elevation*

Elevation is created by using DEM data which has been derived from both satellite image in raster data type and point data of elevation in vector file.

### *3.3.2 Slope*

For an analytical surface F(x,y), slopes can be defined as the magnitude of the first derivative of the surface function:

$$S=\sqrt{(\frac{\delta F}{\delta x})^2+(\frac{\delta F}{\delta Y})^2} \qquad \text{(Eq. 3.1)}$$

The above formula is not based on a rise-over-run calculation over a fixed interval, but rather it assumes that a plane surface can be placed at any point on the surface F(x,y) in such a way that it only just touches the surface - it is a tangential plane and relies on the notion of infinitesimally small distances. It will be closely related to the formula for the Euclidean distance. It simply shows how much the surface F rises with a small fixed increment in x and y. Surfaces within GIS are rarely even if ever represented by analytic functions - typically they will be modeled as TINs or grids, with a finite resolution. Hence slope calculations can be used as an approximations to the above formula depending on the utilized surface model, which is itself an approximate representation of the true surface. Normally in almost all instances software packages will apply grid-based computation, with TINs being first converted to grid format. Strictly speaking such conversion is not necessary, since TINs can provide interpolated surface values at every point in the grid, and use of a suitable which is generally non-linear function could then provide slope values directly [69].

The output slope raster will be calculated in two types of units, degrees or percent. This percent rise would be better understood if we consider it as the rise divided by the run, multiplied by one hundred. **Figure 3.2** presents the comparison value for slope in degree and percent. Consider triangle *B* below. When the angle is equal to 45, the rise will be equal to the run, and the percent rise is 100 percent. As the slope angle will approaches vertical (90 degrees), as in triangle C, the percent rise begins to approach infinity.

The basic algorithm used for calculation of the slope is:

$$\text{Slope radian} = \tan^{-1}\left(\sqrt{\left[\frac{\delta F}{d_x}\right]^2+\left[\frac{\delta F}{d_y}\right]^2}\right) \qquad \text{(Eq. 3.2)}$$

Slope is commonly measured in units of degrees, which uses the algorithm:

$$\text{Slope degrees} = \tan^{-1}\left(\sqrt{\left[\frac{\delta F}{d_x}\right]^2+\left[\frac{\delta F}{d_y}\right]^2}\right)\times\frac{360}{2\pi} \qquad \text{(Eq. 3.3)}$$

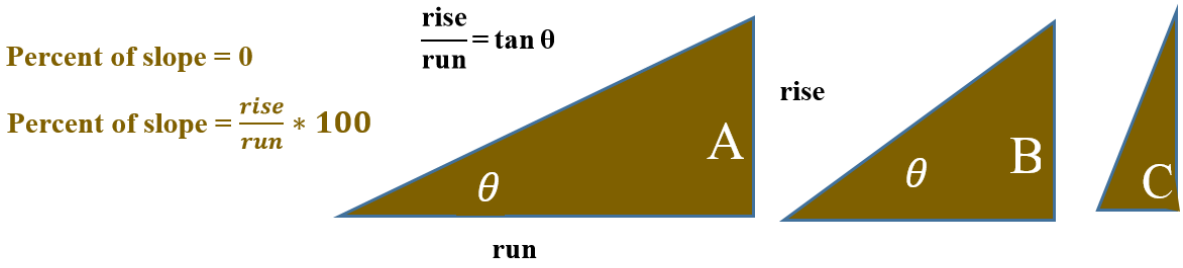


| | | | |
|---|---|---|---|
| Degree of slope = | 30 | 45 | 76 |
| Degree of slope = | 58 | 100 | 373 |

**Figure 3.2** Comparing values for slope in degrees versus percent.

### *3.3.3 Multi Buffering in Proximity Tool*

The distance from the coastal proximity to the land, which has been calculated using multi-buffering, was used as one of the factors in vulnerability mapping, which also used an evaluation of historical reports of the maximum run-up in the area concerned. The algorithm used for the coastal proximity has been based on that of Bretschneider and Wybro (1976) [29]:

$$\text{Log } X_{max} = \log 1400 + \frac{4}{3}\log\left(\frac{Y0}{10}\right) \qquad \text{(Eq. 3.4)}$$

Where $X_{max}$ the maximum reach of the tsunami is over land, and Y0 is the tsunami height at the shore line.

For evaluation of coastal proximity, five classes of distance are used (in meters). The maximum rum-up of the tsunami in the study area from the 2011 Tohoku Earthquake was 8.5 m. Based on the algorithm above: 4.55 m to 7.09 run-up can reach a distance of 489.94m from the coastline; 7.09m to 9.64m of run-up can reach 885.76 m; 9.64-12.18m of run-up can reach 1332.84m; 12.18-14.73m of run-up can reach 1821.46m and 14.73m to 17.27m of run-up can reach more than 2,345.53m.. For the vulnerability assessment, the multi buffering distance from the coastline to an area of land was measured in relation to the impact of a tsunami wave. The five classes of distance used (less than 489.94m, 489.94-1332.84m, 1332.84-1821.46 m, 1821.46-2,345.53m, and more than 2,345.53m) represent: low, slightly low, medium, slightly high, and high vulnerability.

### *3.4 Multi-criteria Analysis*

#### *3.4.1 AHP Methodology*

The philosophy of the AHP was developed by Saaty (1980), whereby the hierarchy of components of the decisions used in the decision-making process was established. The AHP method is essentially an interactive method where a decision-maker or group of decision-makers relay their preferences to the analyst and can debate or discuss opinions and outcomes [50]. The AHP is based on the series of Pair-Wise Comparison Matrices (PCMs) that compare all the criteria to one another. It is suggested that a scale of l to 9 for PCM elements, wherein the value of l suggests that the criteria are equally important and a value of 9 leads one to infer that the criterion under consideration is extremely important in relation to the other criterion with which the comparison is made.

Mathematical expression in AHP, if there are n criteria, then PCM of order n × n may be written as follows:

$$\begin{bmatrix} w_1/w_1 & w_1/w_2 & \cdots & w_1/w_n \\ w_2/w_1 & w_2/w_2 & \cdots & w_2/w_n \\ w_3/w_1 & w_3/w_2 & \cdots & w_3/w_2 \\ \cdots & \cdots & \cdots & \cdots \\ w_n/w_1 & w_n/w_2 & \cdots & w_n/w_n \end{bmatrix} \times \begin{bmatrix} w_1 \\ w_2 \\ w_3 \\ \cdots \\ w_n \end{bmatrix} = \begin{bmatrix} n\ w_1 \\ n\ w_2 \\ n\ w_3 \\ \cdots \\ n\ w_n \end{bmatrix} \qquad \text{(Eq. 3.5)}$$

i.e

$$[A_{(n,n)}] \times [w_{(1,n)}] = [nw_{(1.n)}]$$

Where A is an *n* × *n* PCM in terms of ratio of ratings/weights. The parameter *W* is the ratings or weights (priority rankings/weights) of criteria and n is the order of the PCM matrix. The input matrix is 'A' and the solution for **Eq. 3.5** is similar to the common eigen-value problem. The solution to this set of equations can be found by solving an nth order equation as follows.

Raise the PCM to powers that are successively squared each time. The rows of the PCM and the squared PCM are normalized (i.e. each row element is divided by the sum of the elements in that row) to give the eigenvectors of the PCM and the raised PCM. The difference between these eigenvectors can be checked against a threshold value (i.e. in

this study, a value of 0.0001 is used) and if the difference is less than the threshold value, the eigenvector of the raised PCM will be the estimated rating/weight vector [55].

In order to calculate the consistency of the result Saaty and Vargas (1991) suggested using a preference matrix correction if the CR value exceeds 0.1. CR is defined as the ratio between the consistency index (CI) and the random consistency index (RI), and it can be expressed by the following equation [70]:

$$CR = \frac{CI}{RI} \quad \text{(Eq. 3.6)}$$

in which

$$CI = \frac{(\lambda_{max} - n)}{n - 1}$$

Where $\lambda_{max}$ represents the principal eigen-value and n is the number of comparison matrix (number of factors) and RI is a random index (consistency index for the n row matrixes of randomly generated comparisons in pairs given in **Table 3.4** with calculated values by Saaty.

**Table 3.4** Assignment of the random consistency index [71]

| Random Consistency Index | Matrix Size (N) | | | | | | | | | |
|---|---|---|---|---|---|---|---|---|---|---|
| | 1 | 2 | 3 | 4 | 5 | 6 | 7 | 8 | 9 | 10 |
| RI | 0.00 | 0.00 | 0.52 | 0.89 | 1.11 | 1.25 | 1.35 | 1.40 | 1.45 | 1.49 |

### *3.4.2 Weighted Overlay in Spatial Analyst*

The Weighted Overlay tool as an effective method applies one of the most used approaches for overlay analysis to solve multi-criteria problems such as site selection and suitability models. In a weighted overlay analysis, each of the general overlay analysis steps will be followed.

This tool combines the following steps:

- First one should Reclassify values in the input rasters into a common evaluation scale of suitability or preference, risk, or some similarly unifying scale
- Then multiply the cell values of each input raster by the rasters weight of importance

- Third add the resulting cell values together to produce the output raster

Each value class in each input raster will be assigned a new, reclassified value on an evaluation scale of l to 5, where 1 represents the lowest vulnerability and 5 the highest. In the elevation raster, the lowest elevation is highly vulnerable, while higher elevations are less vulnerable. Areas that are closer to the coast line are more vulnerable than areas of higher elevation. The weight values follow the criteria values that have been established in the AHP process.

## *3.5 Satellite Image Processing*

### *3.5.1 DN to Radiance Conversion*

**Eq. (3.7)** describes the algorithm for converting DN to radiance ($L_\lambda$):

$$L_\lambda = Gain_\lambda \times DN_\lambda + Offset_\lambda \quad \text{(Eq. 3.7)}$$

In which,

$\lambda$ = Specific spectral band of image: Near-IR, Red, Green, Blue or Panchromatic.

$L_\lambda$ =Spectral radiance for band $\lambda$ at the sensor's aperture ($mW/cm^2/\mu m/str$),

$Gain_\lambda$ =Radiometric calibration gain ($mW/cm^2/\mu m/str/DN$) for band $\lambda$.

$DN_\lambda$ =Digital number values for band $\lambda$ of image product.

$Offset_\lambda$ =Radiometric calibration offset ($mW/cm^2/\mu m/str$) for band $\lambda$.

Where both $Gain_\lambda$ and $Offset_\lambda$ are obtained from metadata. The bandwidths for the GeoEye-1 bands are given in **Table 3.5** by integrating over the relative spectral response curve of each band filter,

$$\Delta_\lambda = \int RSR_\lambda d\lambda \quad \text{(Eq. 3.8)}$$

Where,

$\Delta_\lambda$= Bandwidth ($\mu m$) of band $\lambda$.

$RSR_\lambda$= Relative spectral response of band $\lambda$.

Mean solar exoatmospheric irradiance ($Esun_\lambda$) is defined for each of the GeoEye-1 bands by integrating the relative spectral response of each band ($RSR_\lambda$) and the solar irradiance over wavelength,

$$Esun_\lambda = \frac{\int (RSR_\lambda \cdot Irradiance_\lambda) d\lambda}{\Delta_\lambda} \quad \text{(Eq. 3.9)}$$

The solar irradiance used to calculate the $Esun_\lambda$ values presented in **Table 3.5** were obtained from the 2000 American Society for Testing & Materials (ASTM) Standard Extraterrestrial Solar Spectrum:

**Table 3.5** GeoEye-1 Band-dependent Factors

| GeoEye-1 Band (λ) | spectral response for each band | |
|---|---|---|
| | Bandwidth (μm) | Esunλ (mW/cm$^2$/μm) |
| Blue | 0.0584 | 196.0 |
| Green | 0.0646 | 185.3 |
| Red | 0.0316 | 150.5 |
| Near IR | 0.1012 | 103.9 |

### *3.5.2 Radiance to Reflectance Conversion*

**Eq. 3.10** describes the converting from radiance to reflectance.

$$\rho_P = \frac{\pi \cdot L_\lambda \cdot d^2}{Esun_\lambda \cdot \cos\theta_S} \quad \text{(Eq. 3.10)}$$

$\theta_S$ = 90° - Solar Elevation Angle (from metadata).

Where,

$\rho_P$= Unitless planetary reflectance,

d= Earth-Sun distance (astronomical units) from nautical handbook,

$Esun_\lambda$=Mean solar exoatmospheric spectral irradiances (mW/cm$^2$/μm), at an Earth-Sun distance of one astronomical unit (A.U.),

$\theta_S$ = Solar zenith angle in degrees, (The solar zenith angle is calculated from the solar elevation angle,

$L_\lambda$= Spectral radiance for band λ at the sensor's aperture (mW/cm$^2$/μm/str) [72].

### *3.5.3 NDVI and vegetation calculation*

The Normalized Difference Vegetation Index (NDVI) is a common tool for identifying and characterizing vegetation and a measure of the difference in reflectance between these wavelength ranges that takes values between -1 and 1, while vegetated areas produce values starting around 0.4 and approaching 1.0 and values <0 indicating no vegetation.

**Eq. 3.11** was used for NDVI calculation and specification:

$$NDVI=\frac{(NIR-RED)}{(NIR+RED)} \quad \text{(Eq. 3.11)}$$

In which for GeoEye-1 Band 4 is NIR (near infrared band) and Band 3 is red [73].

### *3.5.4 Support Vector Machine Classifier*

Support Vector Machine Classifier (SVMs) have only recently been introduced for remote sensing purposes as an effective and efficient means for classification which was explored textbook of Huang and Davis and Townshend (2002). SVM will be effective because they produce classification with high accuracy values than other classification methods and they will be efficient because they need only small amounts of training data that is located in those areas of feature space that lie near to interclass boundaries. In the two-class case which has been shown in **Figure 3.3** the two classes to be separated are shown as blue circles or green triangles. The margin will be the distance between the two light blue parallel lines.

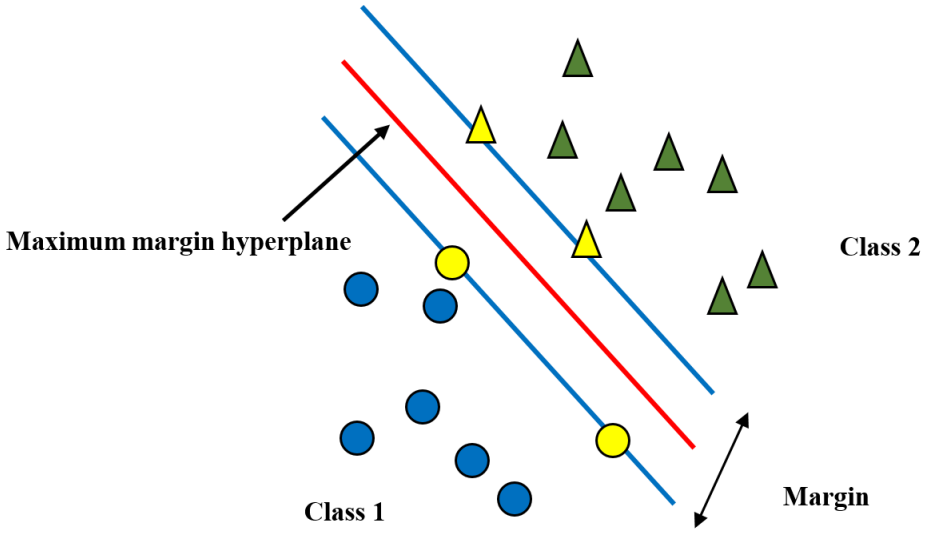


**Figure 3.3** Concept of the support vector [74]

**Figure 3.3** shows the concept of the support vector. The maximum margin hyper plane has been shown in red, and the margin between the support vectors is shown by the parallel light blue lines. The two classes do not overlap on each other. The support vectors (patterns that are on the margin) have been shown as yellow shapes circles for class 1, triangles for class 2.

There is one position of the margins that gives the maximum distance between the closest members of the two classes. Two blue samples and two green samples in **Figure 3.3** have been the closest pairs of data points in the feature space that are the furthest apart and they are shown in yellow. They will be called support vectors. There must be a minimum of two supports but there can normally be more than two. The red running down the center of the margin is the maximum margin hyper plane which is a plane defined in more than three dimensions. Any new point would be identified by reference to the maximum margin hyper plane. If it is above and to the right it is member of the green class. If it is lower than the maximum margin hyper plane and to the left then it will be a member of the blue class. This example will show that only the support vectors are needed and the rest of the training data is irrelevant. Thus, the SVM classification will be stable if the training data are altered provided that the same support vectors emerge. The choice of training data for SVM has been discussed by Foody and Mathur (2004a, 2006).

If the two classes of the data are not linearly separable, then a more complicated approach needs to be adopted. A term can be added to the SVM decision rule which is called a slack variable and it penalizes errors, which has been the assignment of a training

pixel to the wrong class. In fact, the original decision rule was to maximize the margin. The modified rule adds a further requirement, that of penalizing incorrect decisions.

Up to now, the idea underlying SVM appears to be simple. There are instances, especially, where the members of each of the two classes in the training dataset is separated in a nonlinear way for instance by a curved line. The data will then be mapped into a higher-dimensional space that has the property of increasing interclass separability. The mapping function is called a kernel, hence SVM are kernel-based methods. The idea of a kernel is very difficult to explain, and readers wishing to get involved in the mathematics can refer to Shawe-Taylor and Cristianini (2004), who dealt with kernel-based methods of pattern recognition. Another reference on the subject is Abe (2005), while yet another book by Kanevski and Maignan (2004) includes SVM. Tso and Mather (2009) have provided a somewhat dense account of the non-linear mapping procedure. Burges (1998) have provided a tutorial introduction but the level of mathematical sophistication required of the reader is considerable. Those who do not wish to pursue the mathematical details can consider kernel-based methods as analogous to the use of logarithms in manual calculation. Multiplication of large numbers is reduced to addition of smaller numbers resulting in a saving of time and effort. The same accrues to the nonlinear mapping provided by kernel function. This analogy is not strictly true for as noted by Tso and Mather (2009).

The user of SVM should make a selection from a range of available kernel functions, which include homogeneous and also inhomogeneous polynomials, radial basis function and Gaussian radial basis function, and the sigmoid kernel. Currently there is no clear evidence to support the use of one rather than another, though the radial basis function is widely used.

If we compare with Decision Trees (DTs), Maximum Likelihood (ML) methods and even Artificial Neural Networks (ANNs), SVMs appear to be complicated and even, to the mathematically challenged, mysterious and magical. They will have some very significant attractions, particularly their relatively little need for fully-representative training data. SVM requires only one sample per class provided, that sample lies close to the boundary of the class. For training, since data are expensive and time consuming to collect, this is a major advantage. The disadvantages will include the need to specify a kernel function and the relatively slow development of multiclass SVMs. The use of one against all strategies with binary SVMs is a little unaesthetic [74] [75].

### *3.5.5 Accuracy Assessment*

The accuracy of classification can be assessed by comparing the classification with some reference data that is believed to accuracy reflect the rule land-cover. Sources of reference data will include among other things ground truth, higher resolution satellite images, and maps derived from aerial photo interpretation. The result of an accuracy assessment typically will provide us with an overall accuracy of the map and the accuracy for each class in the map. The result of an accuracy assessment can usually be summarized in confusion matrix [76].

# Chapter 4

## Damage Classification and Change Detection (Case study)

In this chapter, the change detection and data classification method is described by using satellite image data and ENVI software. Tsunami disaster data of Ishinomaki city of Japan is used as a case study. Firstly in this chapter, the pixel-based image analysis (PBIA) and object-based image analysis (OBIA) are described and employed to classify and compare the damage classification results. A region of interest near shore namely ROI-1 was chosen from the initial satellite image for this purpose. In sections 4.1 to 4.5, ROI-1 was used to assess the overall accuracy of output obtained from both PBIA and OBIA methods. It was revealed that OBIA analysis to classify the satellite image gives better output accuracies with lower errors than the ones of PBIA. From section 4.6, a change detection application based the OBIA analysis for another region of interest near shore namely ROI-2 was conducted and the results of accuracies are given at the end for both ROI.

### *4.1 Introduction*

On March 11, 2011, a mega thrust earthquake of M 9.0 occurred off the northern Pacific coast of Japan, so-called Tohoku region. The tsunami immediately following caused catastrophic damage to the coastal area in Tohoku. The maximum run-up height has been estimated at 40 m as it swept through Miyako city, Iwate Prefecture. As of September 10, 2011, the National Police Agency have reported that 15,781 people were killed and as a further 4,086 remain are missing. The tsunami while having caused major damage to buildings of all types and all of their connecting infrastructures also caused major erosion of the areas coastline and affected local forests. Because of the varied and wide extent of the effects it will be very difficult to assess in total the impact of this tsunami which is being called the most devastating disaster in recorded history in Japan. Because of the

extremely wide extent of effects and impacts of tsunami, it will be very difficult to comprehend the impact of this disaster.

In addition to immediate relief and reconstruction activities it has also been necessary to assess and determine as fully as possible any and all vulnerabilities of the areas affected.

To meet this requirement, it will be very effective to use remote sensing technology such as image processing or visual inspection of very high spatial resolution (VHR) satellite [77]. The Geoeye-1 satellite images were captured, which include significant information to comprehend the impact of this event.

The primary objective of this chapter is to compare the pixel-based image analysis (PBIA) and object-based image analysis (OBIA) and to study different change detection applications for our case study. In this chapter, we focus on the coastal districts in Ishinomaki City Miyagi Prefecture, Japan, shown in **Figure 4.1** and conduct a visual inspection of satellite image for identifying the local vulnerability with particular regard to structural damage. Furthermore, a proportion of the devastated buildings in inundation zone is estimated in the city. Then the pixel and object-based classification are compared to discuss the local vulnerabilities in the tsunami affected area.

## *4.2 Study area specifications*

The study area is located in Ishinomaki city (**Figure 4.1**) and the data which used in this study is a very high spatial resolution (VHR) Geoeye-1 satellite imagery data taken from Geoeye-1 sensor on the area in 25 June. 2010 (Before) and19 Mar. 2011 (After) the event. The images of Ishinomaki City were obtained 8 months and 15 days before (25 June 2010) and 8 days after (19 Mar. 2011) the event. Base on the reports, the water receded from the areas surrounding the facilities and making access possible on 16 March 2011[78]. **Figure 4.2** and **Figure 4.3** show GeoEye-1 satellite images, pan-sharpened natural colour for Ishinomaki city, Before and After the event.

Ishinomaki is the second biggest city after Sendai the capital of had a population of 160,000 before the event. The total of dead and missing has been recorded at 4,043. The city has a fishery port and an industrial port, both of which were severely damaged by the tsunami. Ishinomaki, suffered the greatest damage of all the tsunami affected areas [79].


**Figure 4.1** Case study site in Ishinomaki, Japan, 2014 Google map [80].

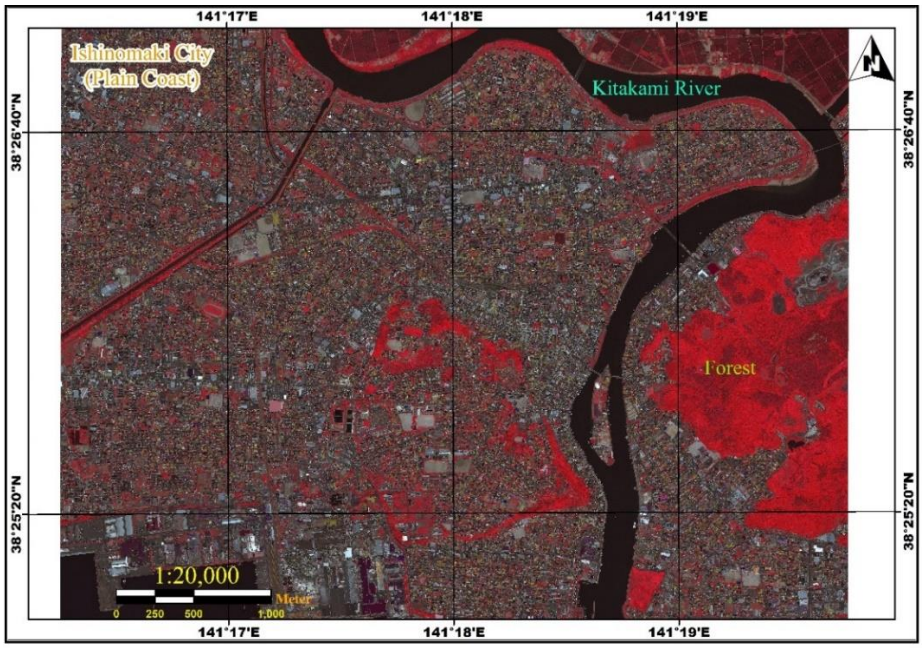


**Figure 4.2** GeoEye-1 satellite image, pan-sharpened false colour, Ishinomaki City, Before (25 June. 2010).

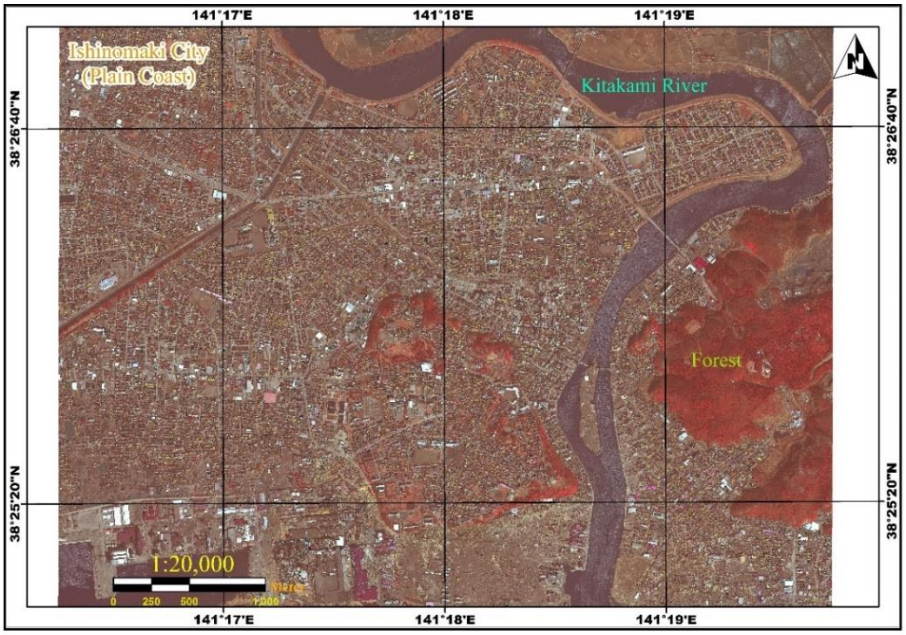


**Figure 4.3** GeoEye-1 satellite image, pan-sharpened natural colour, Ishinomaki City After (19 Mar. 2011).

## *4.3 Data acquisition*

The methodology in this study includes data processing, image classification (using pixel-based and object- based image classification), and post classification using accuracy assessment. Next, two region of interest ROI-1 and ROI-2 were selected as illustrated in the **Figure 4.4** Both regions are located near the shore with similar topographical factors.

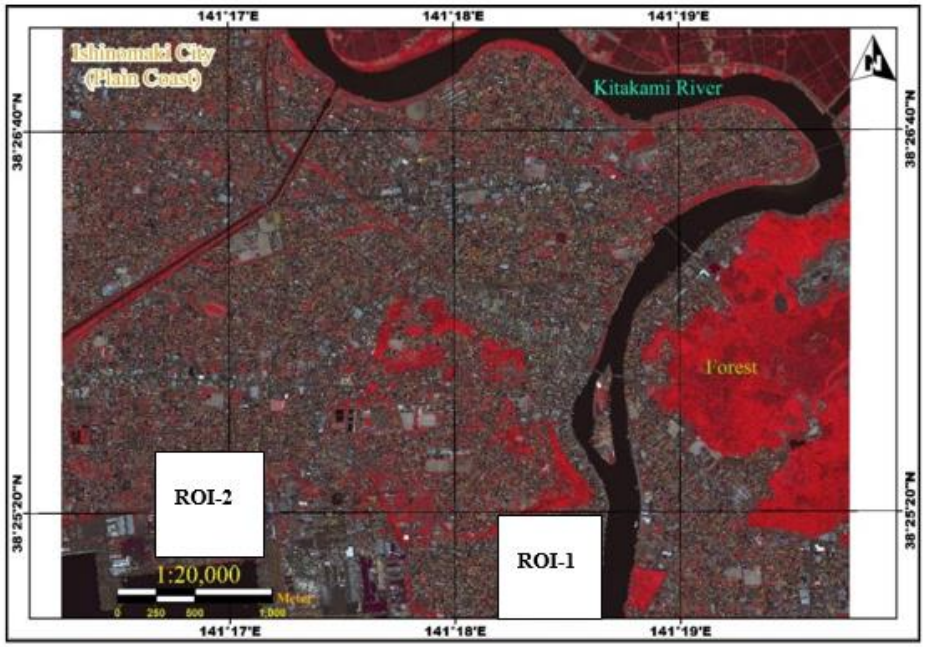


**Figure 4.4** Location of ROI-1 and ROI-2 in GeoEye-1 satellite image.

Then, by using object-based image classification and SVM classifier simultaneously to separate objects automatically followed by post classification and accuracy assessment steps. Finally, from the damage area map obtained by image classification, land cover classification map and change detection statistics are produced. **Figure 4.5** shows the discussed methodology implemented in this study.

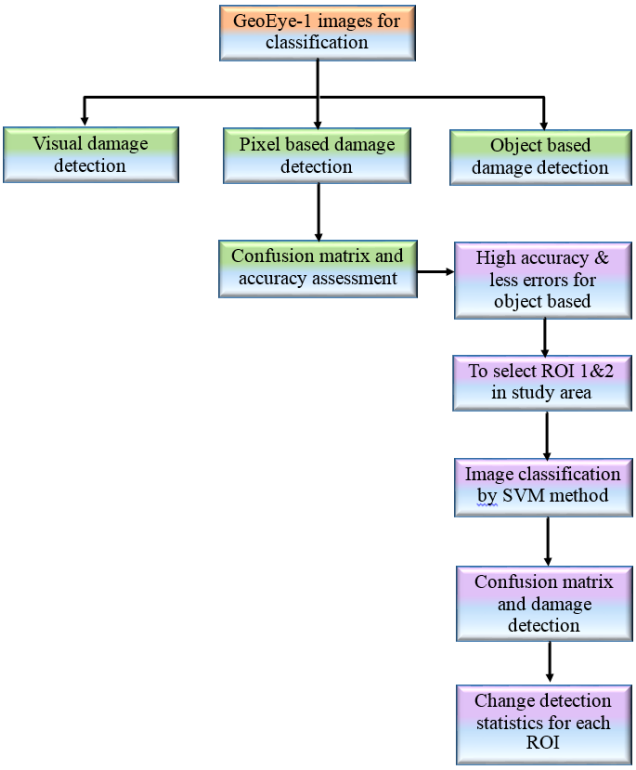


**Figure 4.5** Flowchart of the operations.

Initially we selected a proper region of interest namely ROI-1 from the satellite image in vulnerable area near shore. Then, three processing steps were implemented on ROI-1 to define the ROI's image classifications. Geoeye-1 satellite imagery data taken from Geoeye-1 sensor on the area in 25 June, 2010 (8 months before) and 19 March, 2011 (8 days after) the event. **Figure 4.6** and **Figure 4.7** show GeoEye-1 satellite images ROI-1, False Color Composite (FCC) for the study area, Before and After the event.

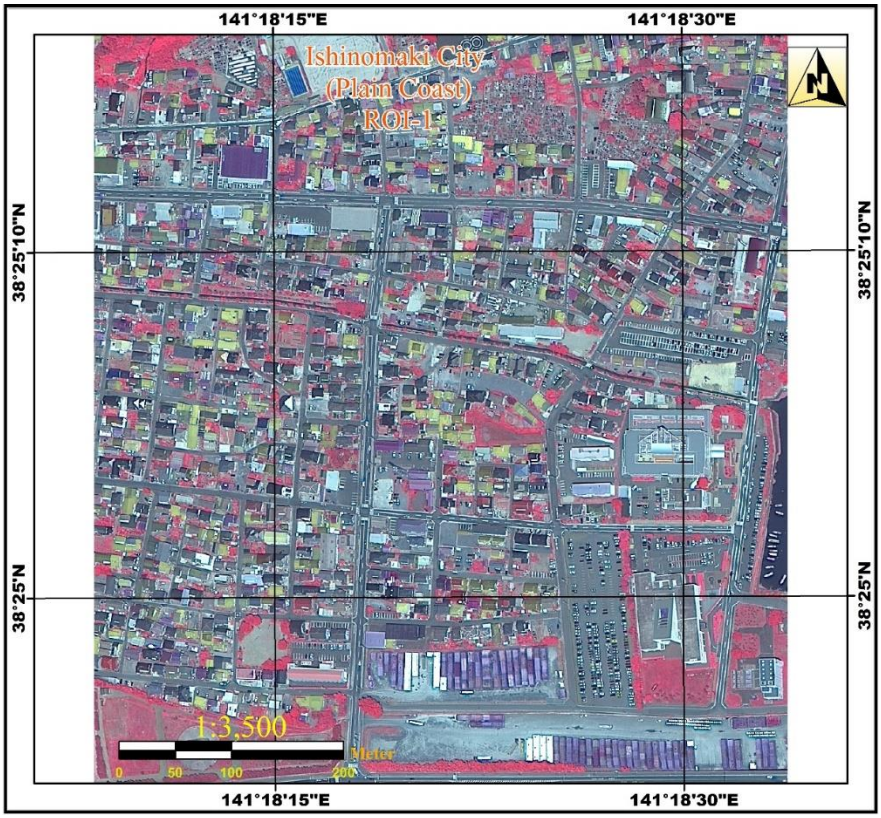


**Figure 4.6** GeoEye-1 satellite images ROI-1, False Color Composite (FCC) for the study area (South), Before, 25 June. 2010.

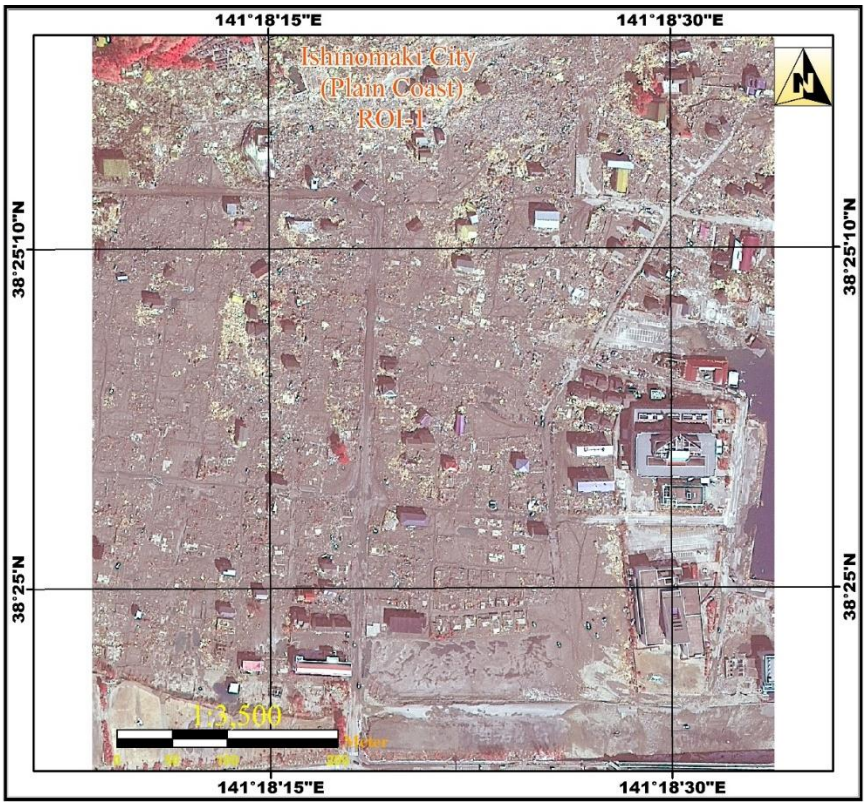


**Figure 4.7** GeoEye-1 satellite images ROI-1, FCC for the study area(South), After (19 Mar. 2011).

First, visual detection of disaster from before and after images were performed, preliminarily. Second, damage areas were extracted using both a pixel-based method and an object-based method. Finally, based on the visual detection result, the accuracies of the two automated detection methodologies were evaluated, which is mentioned in the next section.

### *4.4 Data processing techniques*

The processing techniques applied to the image were pixel-based image classification and object-based image classification in order to compare both methods results.

#### *4.4.1 Pixel-based classification basics*

Classical pixel-based image classification automatically categorizes all pixels in an image into land cover classes or themes in a pixel by pixel manner. Usually, multispectral data are used and the spectral pattern present within the data for each pixel is used as the numerical basis for categorization.

Object-based image analysis comprises two parts: 1) image segmentation and 2) classification based on objects' features in spectral and spatial domains. This kind of processing can be done in three types as texture processing, feature processing and context processing. Image segmentation is a kind of regionalization, which delineates objects according to a certain homogeneity criteria and at the same time requiring spatial contingency. By segmentation, the image is divided into homogeneous, continuous and contiguous objects. Several parameters are used here to guide the segmentation result. The scale parameter determines the maximum allowed heterogeneity for the resulting image objects [81]. **Figure 4.8** shows general comparison of Pixel based (left) and Object based image Classification [82]. Then we use the SVM classifier approach on the image obtained through both pixel based and object based which is explained in the next section.

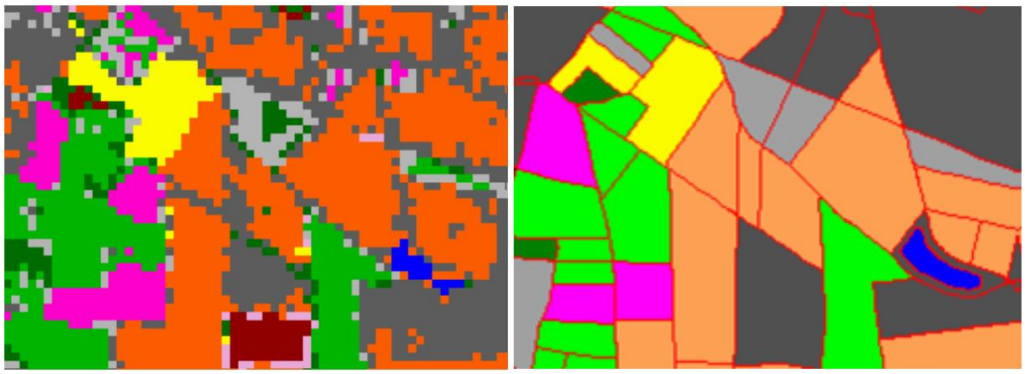

**Figure 4.8** General comparison of Pixel based (left) and Object based image Classification [82].

### *4.4.2 Pixel-based classification by SVM*

Supervised classification algorithms will be applied in pixel-based classification. In the current study, Support Vector Machine (SVM) has been employed. To compare with object-based techniques, the same classes with the same spectral information has been designed in both classification approaches. Recently, particular attention is dedicated to SVM as a classification method. SVMs have most often been found to provide better classification results that those of other widely used pattern recognition methods, such as the maximum likelihood and neural network classifiers (Melgani and Bruzzone 2004, Theodoridis and Koutroumbas 2003). Thus, SVMs will be very attractive for the classification of remotely sensed data [83].

The SVM approach seeks to find the optimal separating hyper-plane between classes by focusing on the training data that are placed at the boundary of the class descriptors. These training data can be called support vectors. Training data other than support vectors have been discarded. This way, not only is an optimal hyper plane fitted, but also less training samples have been effectively used; thus high classification accuracy is achieved with small training sets (Mercier and Lennon 2003). This feature will be very advantageous, especially for remote sensing datasets and more specifically for object-based image analysis, where object samples tend to be less in number than those of a pixel-based approaches [84].

### *4.4.3 Object-based classification basics*

Applying the object based method to image analysis refers to analyzing the image in object space rather than in pixel space, and objects can be used as the primitives for image classification rather than pixels. Segmentation is the process of dividing an image into segments that have similar spectral, spatial, and/or also texture characteristics. The segments in the image ideally correspond to real-world features. Effective segmentation ensures that the classification results are more accurate.

Image segmentation is the primary technique that is used to convert an image into multiple objects. An object, compared to a pixel, inaddition to spectral values has numerous attributes like shape, texture, and morphology that can be used in image analysis. Image segmentation is the process of partisioning an image into segments by grouping neighboring pixels with similar feature values (brightness, texture, color, etc.). These segments ideally correspond to real-world objects. In ENVI 5.1, image segmentation can be performed automatically by employing an edge-based segmentation algorithm that is very fast and requires some input parameters (Scale Level and Merge Level). By suppressing weak edges at different levels, the algorithm can yield multi-scale segmentation results from finer to coarser segmentation. This parameter scale level can ensure that a feature on the image is not divided into too many small segments [85] [86]. **Figure 4.9** shows how pixels group together to form one object through segmentation e.g the streets have become one object.

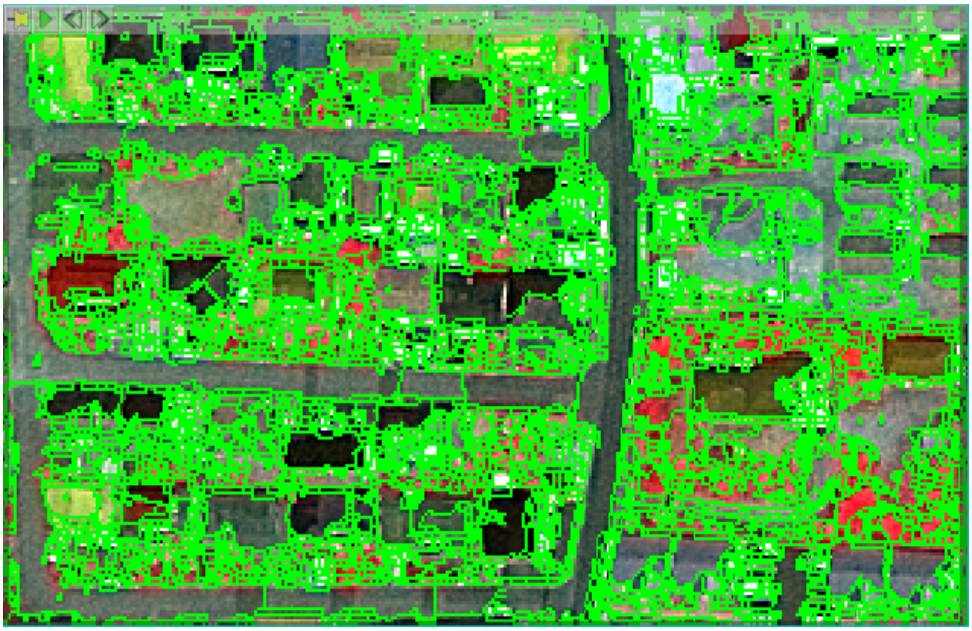

**Figure 4.9** Image segmentation result.

#### *4.4.3.1 Merging segments*

Some features on the image are larger, textured areas such as trees and fields. Merging Segments is employed to aggregate small segments within these areas where over-segmentation may be a problem. If the parameter scale level for merging is 20% it will be a useful option for improving the delineation of roads, buildings and farms boundaries as it is clearly shown in **Figure 4.10**.

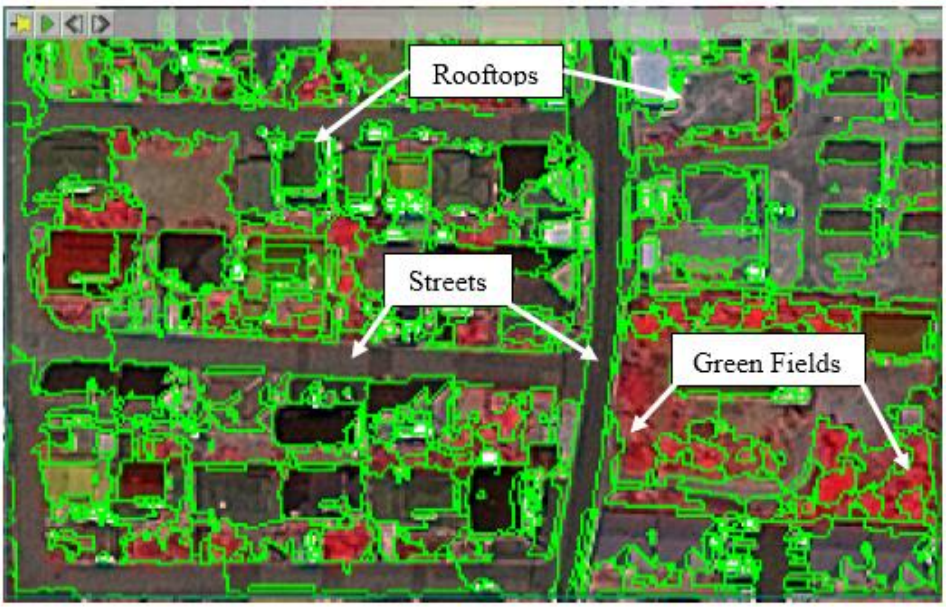


**Figure 4.10** Merging segments.

#### *4.4.3.2 Supervised classification*

The classification procedure starts with an image segmentation based on the single intensity band. After segmentation a supervised classification is performed, using samples for the different classes (Roof, Asphalt, Green field, artificial grass, Water and Soil). Using a SVM classifier the defined set of classes can be separated automatically.

Since in reality most problems will not be linearly separable, the data is often transformed into a higher-dimensional space, where a hyperplane will be computed. The drawback of this methodology is the high computational load of the transformation. This load may be reduced by using the so called kernel-trick: All inner products are defined as convenient kernel-functions which allow classifying in the higher-dimensional space without having to do any actual computing in it [87].

Multiplication of large numbers could be reduced to addition of smaller numbers resulting in saving of the time and effort. The same thing accrues to the nonlinear mapping provided by the kernel function. The purpose of this kernel function is to enable operations to be performed in the current domain rather than the potentially high dimensional feature space of the kernel. This will provide a smart means of resolving the computational issue caused by high dimensionality.

#### *4.4.3.3 Post-classification*

Pixel-based and object-based image analysis approaches have been performed by classifying the remote sensing image. Accuracy assessment of the classification result using these two approaches has also been done by creating the error matrix.

#### *4.4.3.4 Accuracy assessment*

The most common method of accuracy assessment is the Confusion Error Matrix. Confusion Matrix shows the accuracy of a classification result by comparing a classification result with ground truth information. In this study, ENVI 5.0 software was used to calculate a confusion matrix using ground truth for regions of interest (ROIs).

In order to compare the accuracy of the classification results created by the two approaches, pixel-based and object-based, the same set of ground truth was used. Then confusion matrixes were produced. **Tables 4.1, 4.2, 4.3** and **4.4** below illustrate confusion matrix based on errors of omission and commission, user's accuracy (user. acc.), producer's accuracy (prod. acc.) and overall accuracy for both classification methods.

**Table 4.1** Confusion matrix of pixel-based image classification for ROI-1 (Before event)

**Overall Accuracy:** 76.0%

| Pixel Number | Roof | Asphalt | Green Field | Artificial Grass | Water | Soil & Sand | Total | Commission Error (%) | User. Acc. (%) |
|---|---|---|---|---|---|---|---|---|---|
| **Roof** | 27353 | 4752 | 767 | 4 | 9 | 110 | 32995 | 25.2 | 82.9 |
| **Asphalt** | 7159 | 7680 | 0 | 4 | 0 | 16 | 14859 | 49.1 | 51.7 |
| **Green Field** | 507 | 0 | 13922 | 0 | 0 | 0 | 14429 | 5.3 | 96.5 |
| **Artificial Grass** | 631 | 1390 | 0 | 4958 | 0 | 0 | 6979 | 0.2 | 71.0 |
| **Water** | 225 | 5 | 14 | 0 | 542 | 0 | 786 | 1.6 | 68.9 |
| **Soil & Sand** | 686 | 1271 | 0 | 0 | 0 | 1160 | 3117 | 9.8 | 37.2 |
| **Total** | 36561 | 15098 | 14703 | 4966 | 551 | 1286 | 73165 | - | - |
| **Omission Error (%)** | 17.1 | 48.3 | 3.5 | 29.0 | 31.0 | 62.8 | - | - | - |
| **Prod. Acc. (%)** | 74.8 | 50.9 | 94.7 | 99.9 | 98.4 | 90.2 | - | - | - |

**Table 4.2** Confusion matrix of object-based image classification for ROI-1 (Before event)

**Overall Accuracy:** 74.5%

| Pixel Number | Roof | Asphalt | Green Field | Artificial Grass | Water | Soil & Sand | Total | Commission Error (%) | User. Acc. (%) |
|---|---|---|---|---|---|---|---|---|---|
| **Roof** | 733514 | 183432 | 18626 | 441 | 0 | 2708 | 938721 | 21.9 | 78.1 |
| **Asphalt** | 203271 | 487136 | 11534 | 0 | 143 | 103 | 702187 | 30.6 | 69.3 |
| **Green Field** | 35880 | 17217 | 191016 | 55 | 236 | 166 | 244570 | 21.9 | 78.1 |
| **Artificial Grass** | 676 | 1077 | 0 | 15985 | 0 | 0 | 17738 | 9.9 | 90.1 |
| **Water** | 132 | 0 | 22 | 0 | 9552 | 0 | 9706 | 1.6 | 98.4 |
| **Soil & Sand** | 4590 | 5565 | 8499 | 0 | 0 | 7374 | 26028 | 71.7 | 28.3 |
| **Total** | 978063 | 694427 | 229697 | 16481 | 9931 | 10351 | 1938950 | - | - |
| **Omission Error (%)** | 25.0 | 29.8 | 16.8 | 13.0 | 3.8 | 28.8 | | - | |
| **Prod. Acc. (%)** | 75.0 | 70.1 | 83.2 | 97.0 | 96.2 | 71.2 | - | - | - |

**Table 4.3** Confusion matrix of pixel-based image classification for ROI-1 (After event)

**Overall Accuracy:** 61.0%

| Pixel Number | Survived Roof | Washed away | Debris | Asphalt | Green Field | Water | Soil & Mud | Total | Commission Error (%) | User. Acc. (%) |
|---|---|---|---|---|---|---|---|---|---|---|
| **Roof** | 13033 | 3243 | 307 | 1056 | 138 | 448 | 2801 | 21026 | 38.0 | 62.0 |
| **Washed away** | 2316 | 10572 | 3574 | 824 | 1 | 0 | 3740 | 21027 | 49.72 | 50.3 |
| **Debris** | 756 | 1003 | 2137 | 0 | 0 | 0 | 15 | 3911 | 45.4 | 54.7 |
| **Asphalt** | 171 | 456 | 20 | 3457 | 0 | 0 | 2 | 4106 | 15.8 | 84.2 |
| **Green Field** | 539 | 1 | 0 | 0 | 3229 | 0 | 0 | 3769 | 14.3 | 85.7 |
| **Water** | 291 | 3 | 0 | 0 | 0 | 1406 | 0 | 1700 | 17.3 | 82.7 |
| **Soil & Mud** | 5 | 44 | 13 | 0 | 0 | 0 | 10 | 72 | 86.1 | 13.9 |
| **Total** | 17111 | 15322 | 6051 | 5337 | 3368 | 1854 | 6568 | 55611 | . | - |
| **Omission Error (%)** | 23.8 | 31.0 | 64.7 | 35.2 | 4.1 | 24.2 | 99.9 | - | - | - |
| **Prod. Acc. (%)** | 76.2 | 69.0 | 35.3 | 64.8 | 95.9 | 75.8 | 0.15 | - | | - |

**Table 4.4** Confusion matrix of object-based image classification for ROI-1 (After)

**Overall Accuracy:** 70.2%

| Pixel Number | Survived Roof | Washed away | Debris | Asphalt | Green Field | Water | Soil & Mud | Total | Commission Error (%) | User. Acc. (%) |
|---|---|---|---|---|---|---|---|---|---|---|
| **Survived Roof** | 101312 | 29077 | 8714 | 6564 | 1084 | 11883 | 8185 | 166819 | 39.3 | 60.7 |
| **Washed away** | 37246 | 821449 | 123088 | 5558 | 1128 | 4534 | 108031 | 1101034 | 25.4 | 74.6 |
| **Debris** | 3204 | 22189 | 136678 | 246 | 269 | 1948 | 1001 | 165535 | 17.4 | 82.6 |
| **Asphalt** | 17562 | 7159 | 1017 | 30036 | 0 | 2166 | 26693 | 84633 | 64.5 | 35.5 |
| **Green Field** | 12487 | 13009 | 3889 | 26 | 38373 | 1091 | 1034 | 69909 | 45.1 | 54.9 |
| **Water** | 166 | 297 | 19 | 254 | 0 | 19921 | 0 | 20657 | 3.6 | 96.4 |
| **Soil & Mud** | 6601 | 77963 | 1738 | 1778 | 0 | 807 | 147933 | 236820 | 37.5 | 62.5 |
| **Total** | 178578 | 971143 | 275143 | 44462 | 40854 | 42350 | 292877 | 1845407 | - | - |
| **Omission Error (%)** | 43.3 | 15.4 | 50.3 | 32.5 | 6.1 | 523.0 | 49.5 | - | - | - |
| **Prod. Acc. (%)** | 56.7 | 84.46 | 49.7 | 67.5 | 94.0 | 47.0 | 50.45 | - | | - |

## *4.5 Results comparison of PBIA and OBIA*

The classification by pixel-based image analysis approach failed in differentiating between soil, sand and asphalt classes or between asphalt and buildings. The boundaries between green fields are not very clear. But it shows the green field, artificial grass and water classes very well. **Figure 4.11** shows the result of pixel-based classification before the disaster for ROI-1.

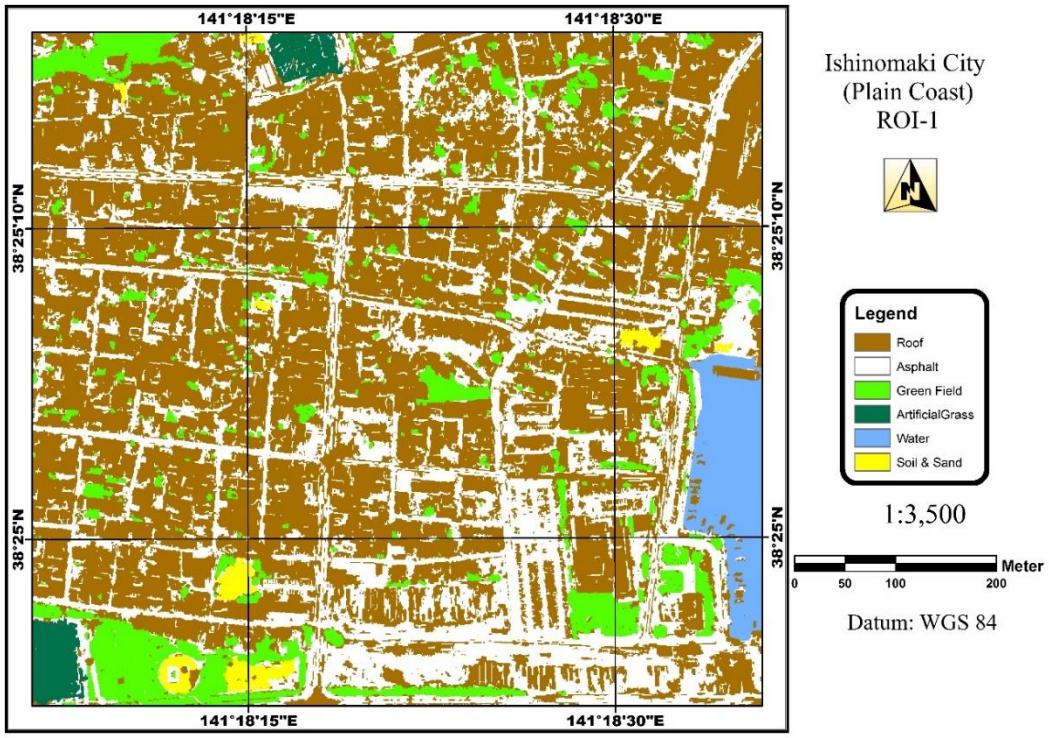


**Figure 4.11** The result of pixel-based image classification for ROI-1(Before).

The classified image of object-based image classification shows more clear boundaries between objects. Washed away buildings are selected as objects in the image. All the features are illustrated with almost exact shape as it is in the ground truth. The classes of green field, asphalt all can be seen without mix classification as can be shown in **Figure 4.12** for ROI-1.

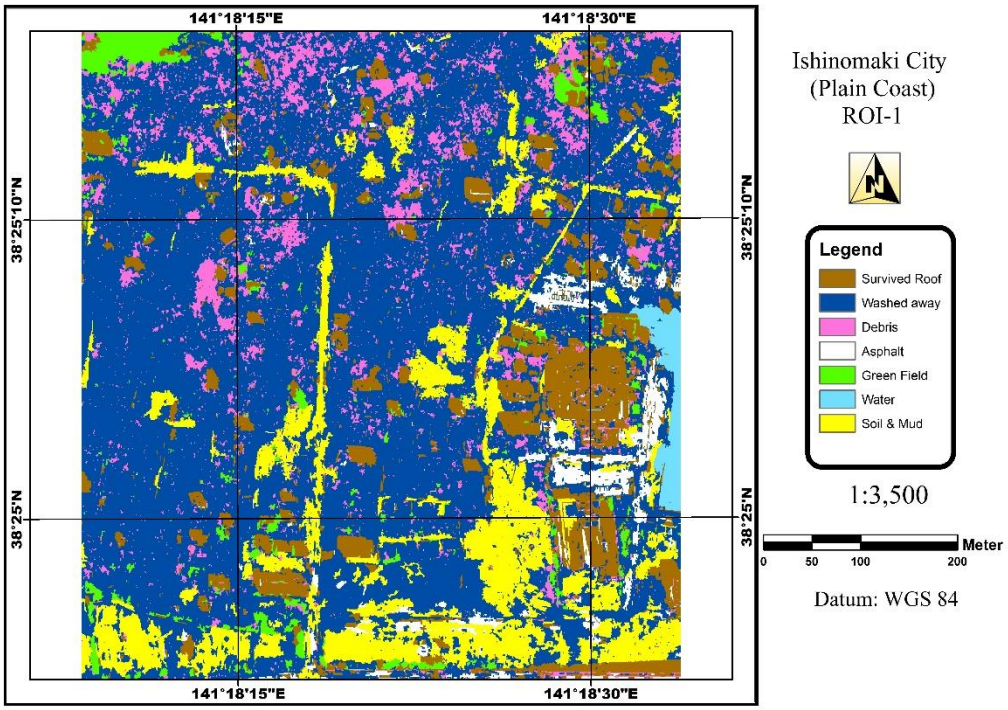


**Figure 4.12** The result of object-based image classification for ROI-1 (After).

In pixel-based image classification method, classes are defined according to the software operator's visual interpretation by selecting pixels representing geometrical shapes. When the classes are not clear, the operation is repeated by defining another geometrical shape around the class that was misclassified in the earlier stage of classification.

When the results of accuracy assessment were compared, it is shown that in before disaster stage, pixel-based attain more overall accuracy (76%) but in after disaster stage, object oriented image analysis attain higher overall accuracy (70%) comparing with (61%) to pixel-based classification approach. Also higher individual producer's and user's accuracy for each classified class is shown by object-based image classification. **Tables 4.5**, **4.6**, **4.7** and **4.8** show the accuracy assessment results of the classification with pixel-based and object-based image analysis for each class in ROI-1.

**Table 4.5** Accuracy assessment results of pixel-based classification for ROI-1 (Before)

| classes | Roof | Asphalt | Green Field | Artificial Grass | Water | Soil & Sand |
|---|---|---|---|---|---|---|
| **User's accuracy (%)** | 82.90 | 51.69 | 96.49 | 71.04 | 68.96 | 37.22 |
| **Producer's accuracy (%)** | 74.81 | 50.87 | 94.69 | 99.84 | 98.37 | 90.20 |
| **overall accuracy** | **76.0 %** | | | | | |

**Table 4.6** Accuracy assessment results object-based classification for ROI-1 (Before)

| classes | Roof | Asphalt | Green Field | Artificial Grass | Water | Soil & Sand |
|---|---|---|---|---|---|---|
| **User's accuracy (%)** | 78.14 | 69.37 | 78.10 | 90.12 | 98.41 | 28.33 |
| **Producer's accuracy (%)** | 75.00 | 70.15 | 83.16 | 96.99 | 96.18 | 71.24 |
| **overall accuracy** | **74.5 %** | | | | | |

**Table 4.7** Accuracy assessment results of pixel-based classification for ROI-1 (After)

| classes | Survived Roof | Washed away | Debris | Asphalt | Green Field | Water | Soil & Mud |
|---|---|---|---|---|---|---|---|
| **User's accuracy (%)** | 62.0 | 50.3 | 54.7 | 84.2 | 85.7 | 82.7 | 13.9 |
| **Producer's accuracy (%)** | 76.2 | 69.0 | 35.3 | 64.8 | 95.9 | 75.8 | 0.12 |
| **overall accuracy** | **60.9 %** | | | | | | |

**Table 4.8** Accuracy assessment results of object-based classification for ROI-1. (After)

| classes | Survived Roof | Washed away | Debris | Asphalt | Green Field | Water | Soil & Mud |
|---|---|---|---|---|---|---|---|
| **User's accuracy (%)** | 60.7 | 74.6 | 82.6 | 35.5 | 54.9 | 96.4 | 62.5 |
| **Producer's accuracy (%)** | 56.7 | 84.6 | 49.7 | 67.5 | 93.9 | 47.0 | 50.5 |
| **overall accuracy** | **70.2 %** | | | | | | |

The method of object-based classification is supported by rule-based classification. The rules can be defined based on the spectral statistics, spatial data and patterns. It was generally concluded that the results obtained from object-based classification can present better overall accuracy and less errors. It should be noted that for the comparison, it was tried to reduce the human errors in pixel-based classification in the case of visual interpretation. It is recommended to develop better rule-based models that can be used to identify remote sensed data to obtain more accurate classification results.

## *4.6 Change detection application using OBIA*

In this section, change detection applications are studied for another similar region of interest (ROI) from the satellite image called ROI-2. Geoeye-1 satellite imagery data taken from Geoeye-1 sensor on the area in 25 June, 2010 and 19 March, 2011. **Figure 4.13** and **Figure 4.14** show GeoEye-1 satellite images, False Color Composite (FCC) for the study area, before and after the event.

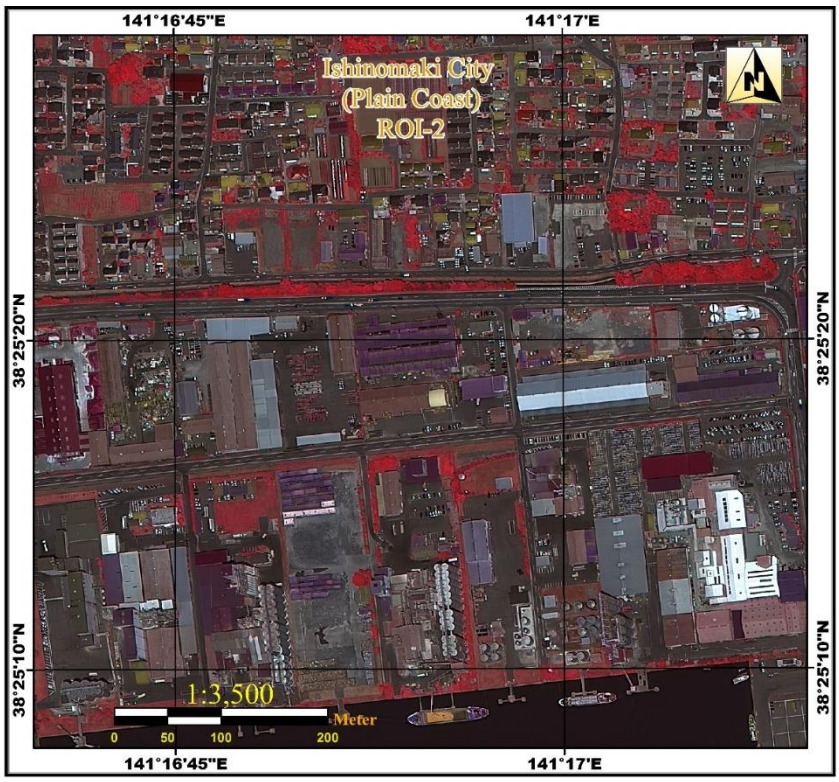


**Figure 4.13** GeoEye-1 Satellite Images of ROI-2, False Color Composite (FCC) images, Ishinomaki City (South West), 25 June. 2010.

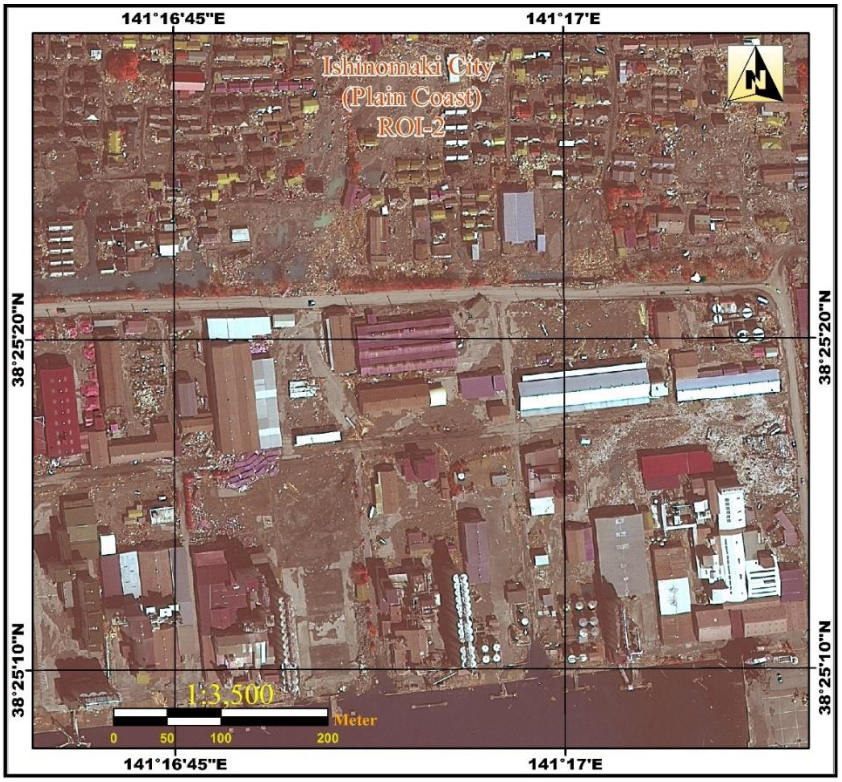


**Figure 4.14** GeoEye-1 Satellite Image of ROI-2, FCC image, Ishinomaki City (South West), After (19 Mar. 2011)

The methodology in this study includes data processing, using object-based image classification and SVM classifier simultaneously to separate objects automatically followed by post classification and accuracy assessment steps. Next, from the damage area map obtained by the image classification the land cover classification map and change detection statistics are produced. **Figure 4.5** shows the discussed methodology implemented in this study.

Initially we selected a proper region of interest namely ROI-2 from the satellite image in vulnerable area near shore similarly to ROI-1 in previous study. Then, four processing steps were implemented on ROI-2 to define the ROI's image classifications. Firstly, visual detection of disaster from pre and post-event images was performed, preliminarily. Secondly, damage areas were extracted using an object-based method. Then, based on the visual detection result and supervised image classification the accuracies of the automated detection methodology were evaluated, which is mentioned in the next section. Finally by comparing the two images and damaged area classified on the map will be possible to find statistical change detection after the event in the study area.

## 4.7 Object-based classification techniques

The processing techniques applied to the images were object-based image classification and change detection statistics in order to compare the results.

### 4.7.1 Supervised image classification by SVM

As described in the above sections, a Support Vector Machine (SVM) is a discriminative classifier formally defined by a separating hyper plane. Given labeled training data (supervised learning), the algorithm outputs an optimal hyper plane which categorizes new examples. In which sense is the hyper plane defined as optimal? For a linearly separable set of 2D-points that belong to one of two classes, find a separating straight line which is shown in **Figure 4.15**.

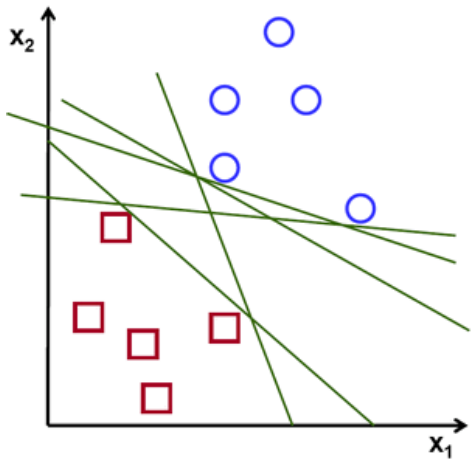


**Figure 4.15** Discriminative classifier formally defined for a set of 2D-points

In the current example we deal with lines and points in a Cartesian plane instead of hyper planes and vectors in a high dimensional space. This is a simplification of the problem. This simplified method is used because our intuition is better built from easier to imagine examples. However, these same classifications ore necessary and the dimensions will be higher than two.

In **Figure 4.16** there are multiple lines that offer a solution to the problem which ones are better than the others. We may define a criterion to estimate the worth of the lines. Because of noise sensitivity any line that passes too close to any of the points will not generalize correctly. Therefore, the use of the SVM algorithm to find the hyper plane needs

to find the greatest maximum distance between the sets of 2D points to ascertain the hyper plane margin lines by using the SVM's theory, as per **Figure 4.16**.

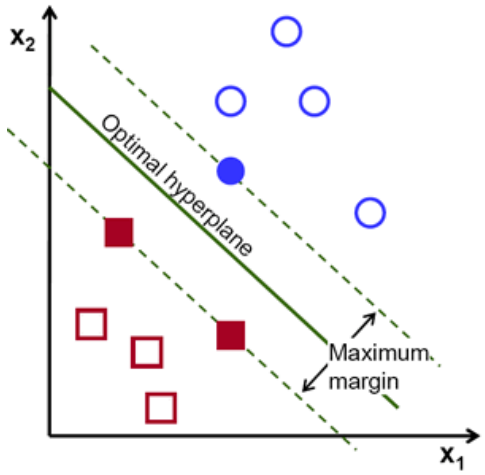


**Figure 4.16** Hyper plane obtained for a linearly separable set of 2D-points

Let's present the notation used to define formally a hyper plane:

$$f(x)= \beta_0+\beta^T x, \qquad \text{(Eq. 4.1)}$$

Where the parameter β is known as the weight vector and $\beta_0$ as the bias. The optimal hyperplane can be represented in an infinite number of different methods by scaling of β and $\beta_0$. As a matter of convention, among all possible representations of the hyper plane, the one chosen will be:

$$|\beta_0+\beta^T x|=1 \qquad \text{(Eq. 4.2)}$$

Where x symbolizes the training examples closest to the hyper plane. In general, the training samples that are the closest to the hyper plane are called support vectors. This representation is known as the canonical hyper plane.

Now, we use the result of geometry that will give the distance between a point $\mathbf{x}$ and a hyperplane $\beta, \beta_0$:

$$\text{distance}=\frac{|\beta_0+\beta^T x|}{\|\beta\|} \qquad \text{(Eq. 4.3)}$$

In fact, for the canonical hyper plane, the numerator is equal to one and the distance to the support vectors is:

$$\text{distance}_{\text{support vectors}} = \frac{|\beta_0 + \beta^T x|}{\|\beta\|} = \frac{1}{\|\beta\|} \quad \text{(Eq. 4.4)}$$

Recalling that the margin introduced in the previous section, here denoted as M, is twice the distance to the closest examples:

$$M = \frac{2}{\|\beta\|} \quad \text{(Eq. 4.5)}$$

Finally, the problem of maximizing *M* will be equivalent to the problem of minimizing a function $L(\beta)$subject to some constraints. The constraints model the requirement for the hyper plane to classify correctly all the training examples $x_i$ . Formally,

$$\min_{\beta,\beta_0} L(\beta) = \frac{1}{2}\|\beta\|^2 \quad \text{subject to} \quad y_i(\beta^T x_i + \beta_0) \geq 1 \ \forall i, \quad \text{(Eq. 4.6)}$$

Where $y_i$ shows each of the labels of the training examples. This is a problem of Lagrangian optimization which can be solved using Lagrange multipliers to obtain the weight vector $\beta$ and the bias $\beta_0$ of the optimal hyper plane [88].

### *4.7.2 Object-based results*

Based on the discussion so far for ROI-1, the object-based classification gives higher accuracy. The classified image of object-based image classification shows more clear boundaries between objects. Consequently in this section OBIA is used to classify the satellite image ROI-2. Classes performed in object-based before and after event by SVM Classifier shown in **Table 4.9**.

**Table 4.9** Classes performed in object-based for before and after event by SVM Classifier

| **Satellite Image** | **Classification** |
|---|---|
| Before | Rooftop, Asphalt, Green field, Water and Soil |
| After | Survived Roof, Washed away, Debris, Asphalt, Green field, Water and Soil & Mud |

The classified images of ROI-2 for Before and After event are shown in **Figure 4.17** and **Figure 4.18** with classes given in **Table 4.9**. From these figures one can recognize that water, green field, survived roof and asphalt classes present less misclassification than others.

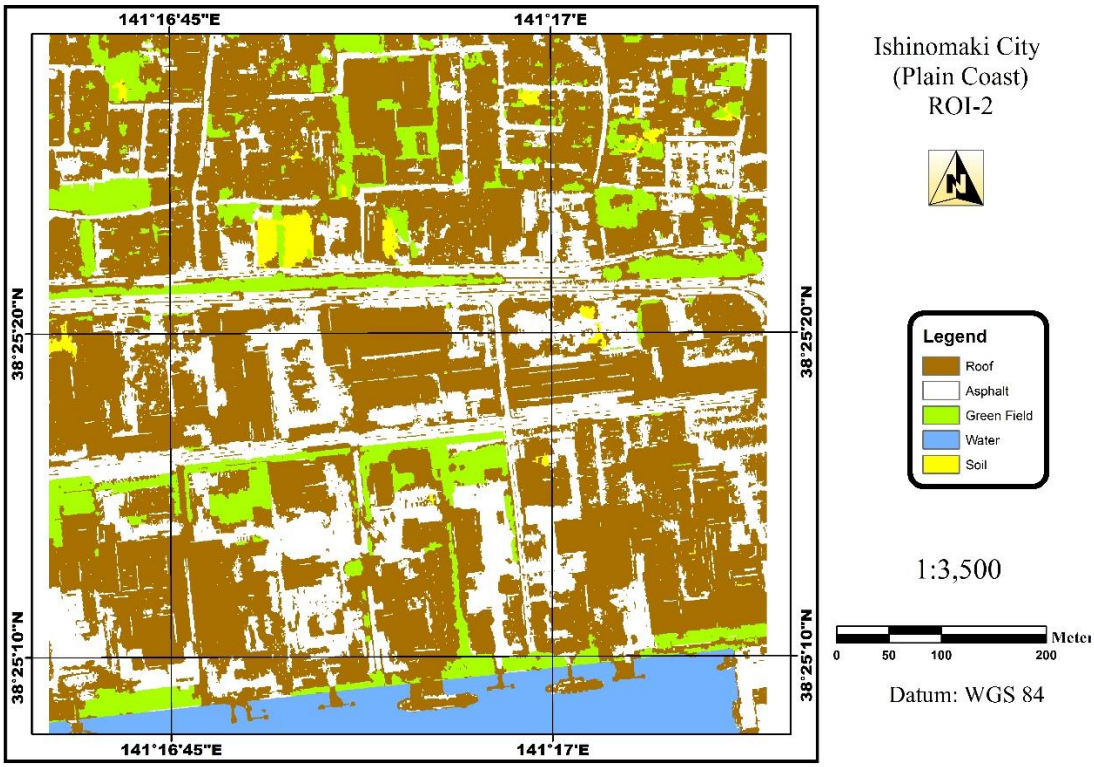


**Figure 4.17** The result of object-based image classification (Before event).

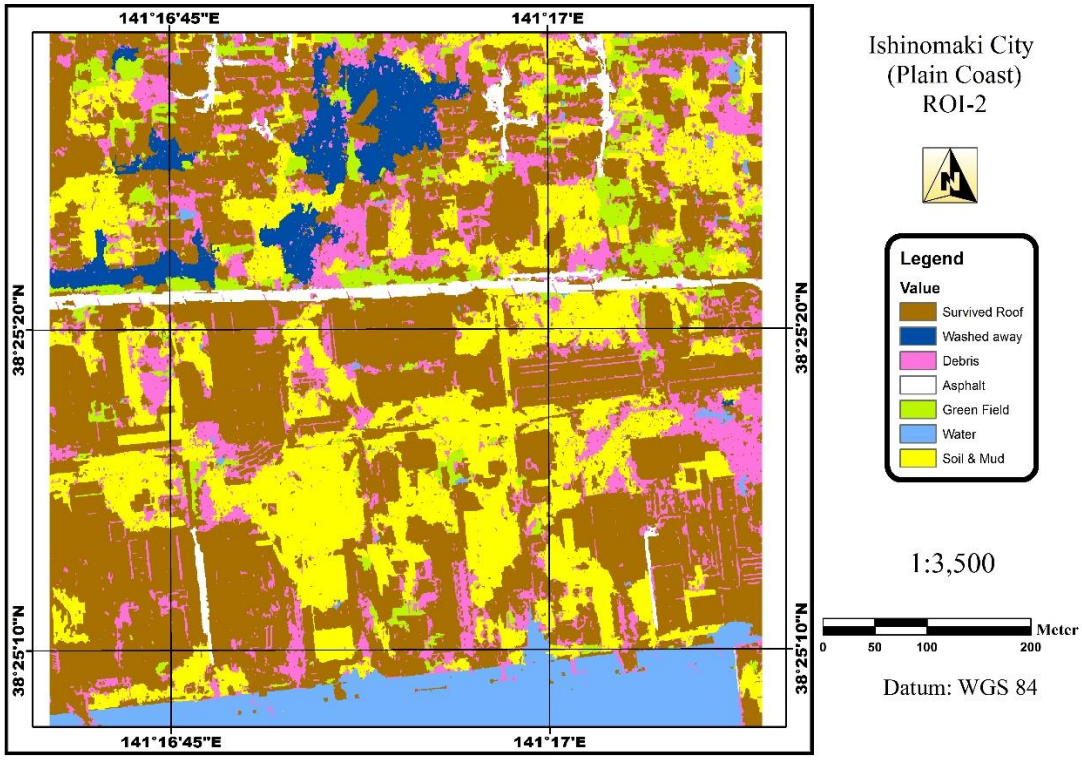


**Figure 4.18** The result of object-based image classification (After event).

## *4.8 Accuracy assessment of OBIA*

Accuracy assessment of the classification result using the approach has also been done by creating the error matrix. The most common method of accuracy assessment is the Confusion Error Matrix which shows the accuracy of a classification result by comparing with ground truth information. In this study, we used to calculate a confusion matrix using ground truth for regions of interest (ROIs).

In order to compare the accuracy of the classification results created by object-based, the same set of ground truth was used. Then confusion matrixes were produced. **Tables 4.10** and **Table 4.11** below illustrate error matrix, user's accuracy, producer's accuracy and overall accuracy for object-based classification method.

**Table 4.10** Confusion matrix of image classification, Before-Disaster, (Pixels Number)

Overall Accuracy: 77.5%

| Classification | Rooftop | Asphalt | Green Field | Water | Soil | Total | User. Accuracy (%) | Commission Error (%) |
|---|---|---|---|---|---|---|---|---|
| **Rooftop** | 775541 | 295372 | 34761 | 686 | 2765 | 1109125 | 69.92 | 30.08 |
| **Asphalt** | 68731 | 441003 | 8026 | 47 | 1945 | 519752 | 84.85 | 15.15 |
| **Green Field** | 14703 | 14875 | 159086 | 8 | 908 | 189580 | 83.91 | 16.09 |
| **Water** | 0 | 0 | 0 | 203231 | 0 | 203231 | 100.00 | 0.00 |
| **Soil** | 888 | 15016 | 756 | 0 | 2952 | 19612 | 15.05 | 84.95 |
| **Total** | 859863 | 766266 | 202629 | 203972 | 8570 | 2041300 | - | - |
| **Prod. Accuracy (%)** | 90.19 | 57.55 | 78.51 | 99.64 | 34.45 | - | - | - |
| **Omission Error (%)** | 9.81 | 42.45 | 21.49 | 0.36 | 65.55 | - | - | - |

**Table 4.11** Confusion matrix of image classification, After-Disaster, (Pixels Number)

Overall Accuracy: 72.97%

| Classification | Survived Roof | Washed away | Debris | Asphalt | Green Field | Water | Soil & Mud | Total | User. Accuracy (%) | Com. Error (%) |
|---|---|---|---|---|---|---|---|---|---|---|
| **Survived Roof** | 711137 | 58900 | 28328 | 8413 | 4914 | 0 | 85736 | 897428 | 79.24 | 20.76 |
| **Washed away** | 1295 | 49892 | 526 | 0 | 0 | 0 | 21100 | 72813 | 68.52 | 31.48 |
| **Debris** | 45409 | 40452 | 160369 | 2641 | 1136 | 0 | 1152 | 251159 | 63.85 | 36.15 |
| **Asphalt** | 4331 | 0 | 0 | 44309 | 0 | 0 | 2549 | 51189 | 86.56 | 13.44 |
| **Green Field** | 32090 | 15464 | 3223 | 152 | 36356 | 0 | 2930 | 90215 | 40.30 | 59.70 |
| **Water** | 1530 | 1377 | 4651 | 0 | 74 | 221576 | 0 | 229208 | 96.67 | 3.33 |
| **Soil & Mud** | 67592 | 80714 | 16353 | 18781 | 0 | 0 | 265848 | 449288 | 59.17 | 40.83 |
| **Total** | 863384 | 246799 | 213450 | 74296 | 42840 | 221576 | 379315 | 2041300 | - | - |
| **Prod. Accuracy (%)** | 82.37 | 20.22 | 75.13 | 59.64 | 85.58 | 100.00 | 70.09 | - | - | - |
| **Omission Error (%)** | 17.63 | 79.78 | 24.87 | 40.36 | 14.42 | 0.00 | 29.91 | - | - | - |

To increase the accuracy when the classes are not clear, the operation is repeated by defining another geometrical shape around the class that was misclassified in the earlier stage of classification. Errors of commission occurs when incorrectly we identify pixels associated with a class as other classes, or when we improperly separate a single class into two or more classes. Errors of omission happen whenever we simply don't recognize pixels that we should have identified as belonging to a particular class.

Table **4.12** shows the errors and accuracies assessment results of the object-based image classification analysis in each stage by using F-measure to explain a harmonic mean of precision and test's accuracy which is defined as: [89]

$$\text{F-measure} = 2.\frac{\text{Accuracy}_{\text{producer}} * \text{Accuracy}_{\text{user}}}{\text{Accuracy}_{\text{producer}} + \text{Accuracy}_{\text{user}}} \qquad \text{(Eq. 4.1)}$$

Where the values of factors and the obtained F-measurements for both Before event and After event are given in **Table 4.12**.

**Table 4.12** Errors and accuracies of automated damage detection

| Accuracy / Images | Errors (%) | | Accuracy (%) | | F. measure % |
|---|---|---|---|---|---|
| | Commission | Omission | Producer | User | |
| **Before** | 29.25 | 27.93 | 72.07 | 70.75 | 71.40 |
| **After** | 29.38 | 29.57 | 70.43 | 70.62 | 70.52 |

Next, the change detection is performed by comparing the initial state (Before event) and final state (after event). It involves the use of multi temporal data sets to discriminate areas of land cover change between dates of imaging. The types of changes that might be of interest can range from short and term phenomena such as vegetation cover or urban fringe development. Ideally, change detection procedures should involve data acquired by the same or similar sensor and be reordered using the same spatial resolution, viewing geometry, spectral bands, radiometric resolution and time of day. In this study the GeoEye-1 satellite offers unprecedented spatial resolution by acquiring 0.41 m panchromatic images (black and white) with multispectral images (color) of 1.64 m resolution to create 0.41 m pan-sharpened images (colored images) [90]. One way to discriminate changes between two dates of images is to employ post classification comparison. In this approach, two images are independently classified and registered. Then an algorithm can be employed to determine those pixels with changes in classification between dates.

A variance from the mean will be chosen and tested empirically to find, if it represents a reasonable threshold. The threshold can also be changed interactively in most image analysis system so the analyst can obtain immediate visual feedback on the suitability of a given threshold [91]. The procedures for change detection are based on post classification

to compare the Before-disaster image as initial state image and After-disaster as final state image. Finally it is possible to have change detection statistics based on the pixels number and areas ($m^2$). **Table 4.13**, **Figure 4.19** and **Figure 4.120** represent the change detection statistics for ROI-1 and **Table 4.14**, **Figure 4.21** and **Figure 4.22** represent the change detection statistics for ROI-2.

**Table 4.13** Change detection statistics between Before and After the disaster for ROI-1

| After (Final State) | | Before (Initial State) | | | | | | | | | | | |
|---|---|---|---|---|---|---|---|---|---|---|---|---|---|
| | | Roof | | Asphalt | | Green Field | | Water | | Soil | | Artificial Grass | |
| | | Area ($m^2$) | % | Area ($m^2$) | % | Area ($m^2$) | % | Area ($m^2$) | % | Area ($m^2$) | % | Area ($m^2$) | % |
| | Survived Roof | 26,851 | 11.9 | 15,930 | 9.3 | 4,189 | 7.0 | 74 | 3.0 | 579 | 9.1 | 59.0 | 1.3 |
| | Washed away | 149,483 | 66.0 | 92,355 | 54.0 | 29,066 | 48.4 | 183 | 7.5 | 3,679 | 57.6 | 2461.0 | 55.6 |
| | Debris | 25,380 | 11.2 | 9,194 | 5.4 | 4,731 | 7.9 | 4 | 0.2 | 343 | 5.4 | 1897.0 | 42.8 |
| | Asphalt | 4,614 | 2.0 | 15,382 | 9.0 | 1,133 | 1.9 | 0 | 0 | 40 | 0.6 | 0.0 | 0.0 |
| | Green Field | 6,490 | 2.9 | 2,216 | 1.3 | 9,614 | 16.0 | 0 | 0 | 256 | 4.0 | 15.0 | 0.3 |
| | Water | 454 | 0.2 | 1,799 | 1.1 | 994 | 1.7 | 2128 | 87.7 | 0 | 0.0 | 0.0 | 0.0 |
| | Soil & Mud | 13,153 | 5.8 | 34,273 | 20.0 | 10,367 | 17.3 | 38 | 1.6 | 1,495 | 23.4 | 0.0 | 0.0 |
| | Class Total | 226,425 | 100.0 | 171,149 | 100.0 | 60,095 | 100.0 | 2,427 | 100.0 | 6,391 | 100.0 | 4432.0 | 100.0 |
| | Class Changes | 199,574 | 88.14 | 155,767 | 91.1 | 50,481 | 84.0 | 298 | 12.3 | 4,897 | 76.6 | 2534.0 | 57.2 |
| | Image Difference | -154,378 | -79.7 | -149,979 | -87.9 | -41,505 | -69.5 | 2948 | 121.5 | 52,934 | 811.7 | 37.116 | 837.0 |

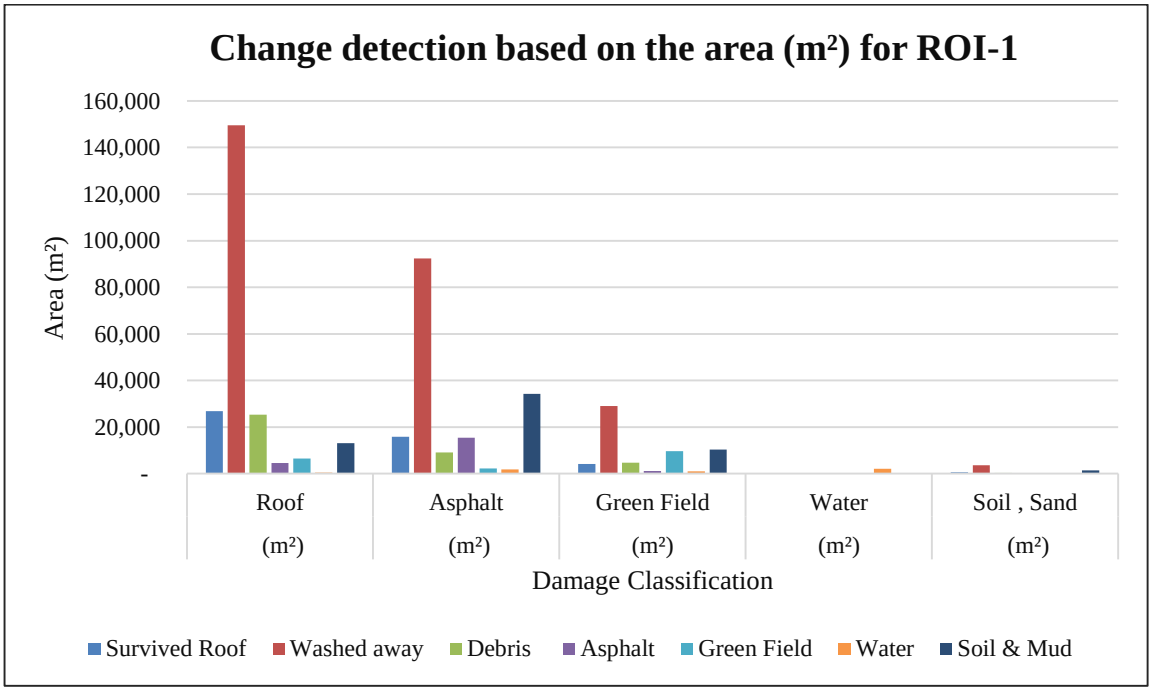


**Figure 4.19** Change detection statistics area with comparing initial and final state in ROI-1

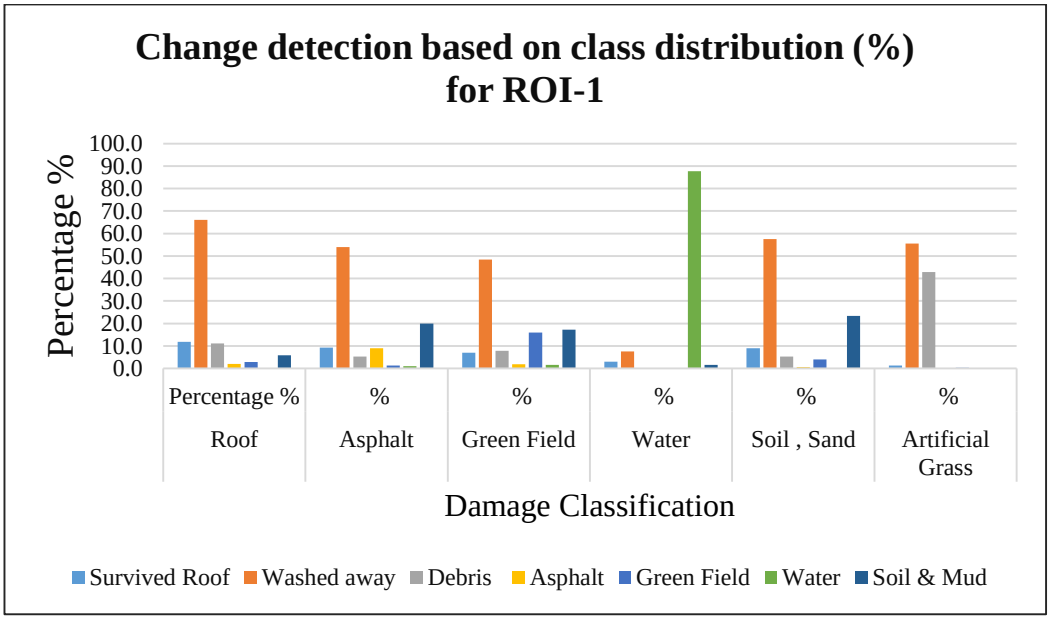


**Figure 4. 20** Percentage of change detection statistics area for ROI-1

**Table 4.14** Change detection statistics between before and after the disaster for ROI-2

| After (Final State) | | Before (Initial State) | | | | | | | | | |
|---|---|---|---|---|---|---|---|---|---|---|---|
| | | Roof | | Asphalt | | Green Field | | Water | | Soil | |
| | | Area ($m^2$) | % | Area ($m^2$) | % | Area ($m^2$) | % | Area ($m^2$) | % | Area ($m^2$) | % |
| | Survived Roof | 157,150 | 56.7 | 51,068 | 39.3 | 14,633 | 30.9 | 455 | 0.9 | 1,051 | 21.4 |
| | Washed away | 10,930 | 3.9 | 2,770 | 2.1 | 3,049 | 6.4 | 0 | 0 | 1,453 | 29.7 |
| | Debris | 38,347 | 13.8 | 17,475 | 13.4 | 6,232 | 13.1 | 365 | 0.7 | 369 | 7.5 |
| | Asphalt | 5,304 | 1.9 | 7,272 | 5.6 | 220 | 0.5 | 0 | 0 | 2 | 0 |
| | Green Field | 11,296 | 4.1 | 3,769 | 2.9 | 7,367 | 15.5 | 6 | 0 | 116 | 2.4 |
| | Water | 4,691 | 1.7 | 1,190 | 0.9 | 1,455 | 3.1 | 49,961 | 98.3 | 5 | 0.1 |
| | Soil & Mud | 49,563 | 17.9 | 46,393 | 35.7 | 14,438 | 30.5 | 21 | 0.1 | 1,907 | 38.9 |
| | Class Total | 277,281 | 100.0 | 129,938 | 100.0 | 47,395 | 100.0 | 50,808 | 100.0 | 4,903 | 100.0 |
| | Class Changes | 120,131 | 43.3 | 122,666 | 94.4 | 40,027 | 84.5 | 847 | 1.7 | 2,996 | 61.1 |
| | Image Difference | -52,924 | -19.1 | -117,140 | -90.1 | -24,841 | -52.4 | 6494 | 12.8 | 107,419 | 2190.9 |

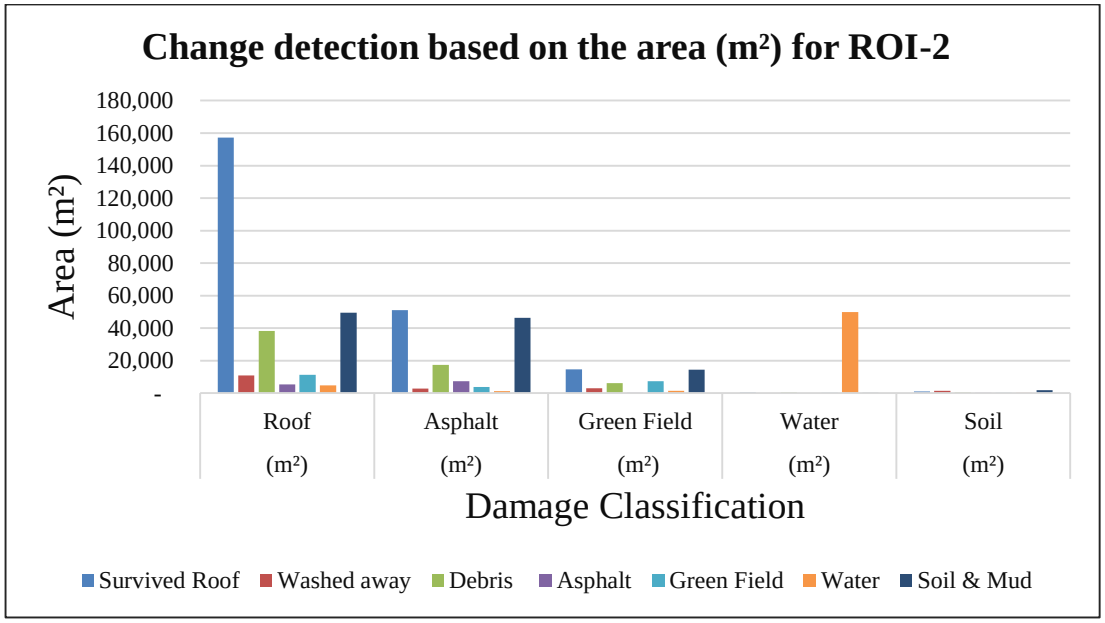


**Figure 4.21** Change detection statistics area with comparing initial and final state in ROI -2

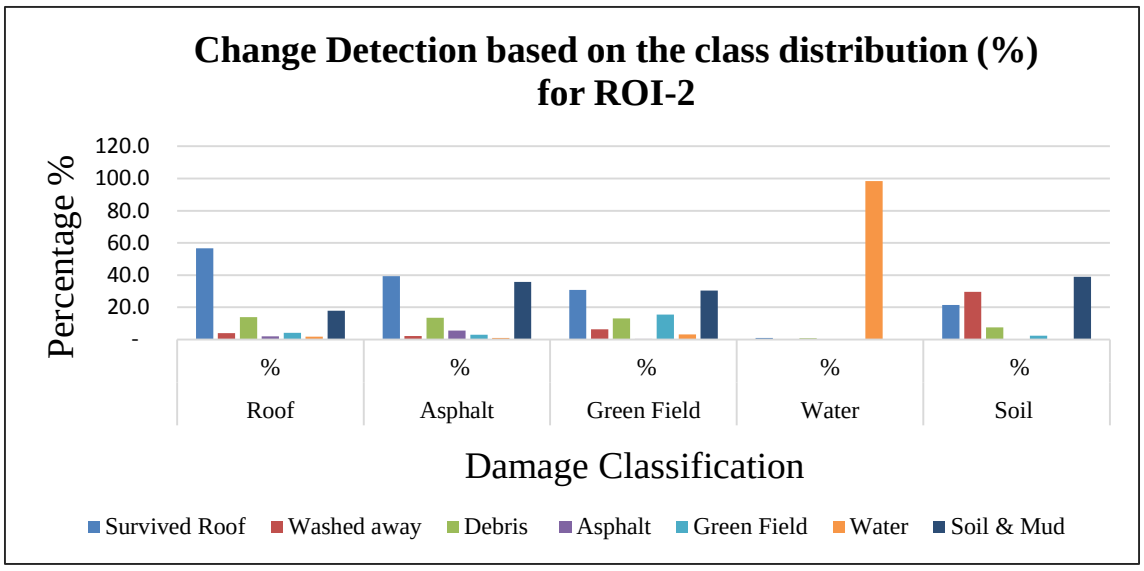


**Figure 4.22** Percentage of change detection statistics area for ROI-2

## *4.9 Summary*

It was generally shown in this chapter that the results obtained from OBIA method can present better overall accuracy and less errors compared to PBIA one . For a selected area in Ishinomaki city during 2011 Tohoku earthquake, several number of classifications for the change detection purpose were adopted. It was observed that the amount of changes strongly depends on the selected ROI which was investigated by using two ROIs through

comparing their change detections before and after the tsunami. It is worth noting that although the selected near shore ROI-1 and ROI-2 had similar topographical factors but the detected destruction indicated the stimulated influence of the river carrying tsunami waves on building damages which will be discussed in the next chapters.

Based on the classification results obtained from object based method, each class gives some information which can be used for disaster management. For instance, bare lands can be used to accumulate debris, asphalt routs for transportation.

# Chapter 5

## Application of integrated GIS and RS in tsunami vulnerability assessment (Case Study)

In accordance with the previous chapter, in this chapter another software application for analyzing the satellite images of Ishinomaki city as a case study is explored. As a result, the vulnerability map is produced. Vulnerable areas due to tsunami disaster have been studied by means of GIS application on satellite images and AHP method used in multi-criteria analysis. Initially with considering five main geographical factors, for each factor one vulnerability map is produced. In next step, by means of an appropriate AHP method with pair-wise comparisons between factors and a Weighted Linear Combination (WLC) analysis, the final tsunami vulnerability map is created.

### *5.1 Introduction*

Tsunami is a hazardous event as a natural phenomenon when happens in a populated area causing unacceptably large numbers of fatalities or property damages. By means of the vulnerable areas map and performing a primary assessment, minimizing the impact of tsunami event is possible. Vulnerability is defined as an element to estimate the disaster risk within the context of hazard and risk. Since vulnerability is a result of capacity lack, increasing in capacity means reducing vulnerability, and high vulnerability means low capacity [92]-[94].

The evolution of remote sensing technology and its applications have enabled us to use satellite imagery data for mapping the damage area due to a natural disaster and also for assessing the vulnerable areas and damage distribution. As a further matter, introduction of Geographic Information System (GIS) as a database system have allowed us to analyze and display spatial data by using digitized maps for planning, mitigation and decision making [95] [96].

GIS software with its powerful set of tools is widely employed by decision-makers and planners for analyzing the spatial information through spatial multi-criteria analysis. Spatial multi-criteria analysis of GIS requires standard values and geographical locations of features, weighted topographical factors, according to users' preferences [97]-[101]. GIS is also applicable to evaluate the strategies required for creation of coastal vegetation belts against tsunami risk and to analyze tsunami risk using a multi-scenario approach [101] [102].

Previous studies have developed and analyzed integrative remote sensing techniques in assessing building vulnerability to tsunami hazard. GIS approaches and a set of building vulnerability classification rule have been developed and successfully applied to categorize building vulnerability classes. Another study developed the Papathoma Tsunami Vulnerability Assessment (PTVA) to provide first-order assessments of building vulnerability to tsunami. In another study to undertake assessments of coastal vulnerability analysis data are gathered from available ASTER satellite images (Advanced Space born Thermal Emission and Reflection Radiometer) and 3s-SRTM-v3 (3 arc-seconds Shuttle Radar Topography Mission, version 3) digital elevation models which the vulnerability assessment can be displayed via GIS as a series of thematic maps. The use of multiple geospatial variables of topographic elevation, relation to tsunami direction, coastal proximity, and coastal shape are incorporated by the Analytic Hierarchy Process (AHP) to construct a weighting scheme for the geospatial variables and assessing tsunami vulnerability [104] [36] [33] [29].

## *5.2 Spatial data gathering and analysis*

In this study, remote sensing data captured by very high resolution (VHR) optical satellites with a pixel size about 0.5 meter is used to identify critical geographical elements such as buildings, transport infrastructure and the inundation area due to the tsunami event in order to estimate the vulnerability and risk in coastal areas. Specifically in this study, the area of Ishinomaki City in Miyagi Prefecture, Japan was studied (**Figure 5.1**) and the general steps used in this study are shown in **Figure 5.2**.

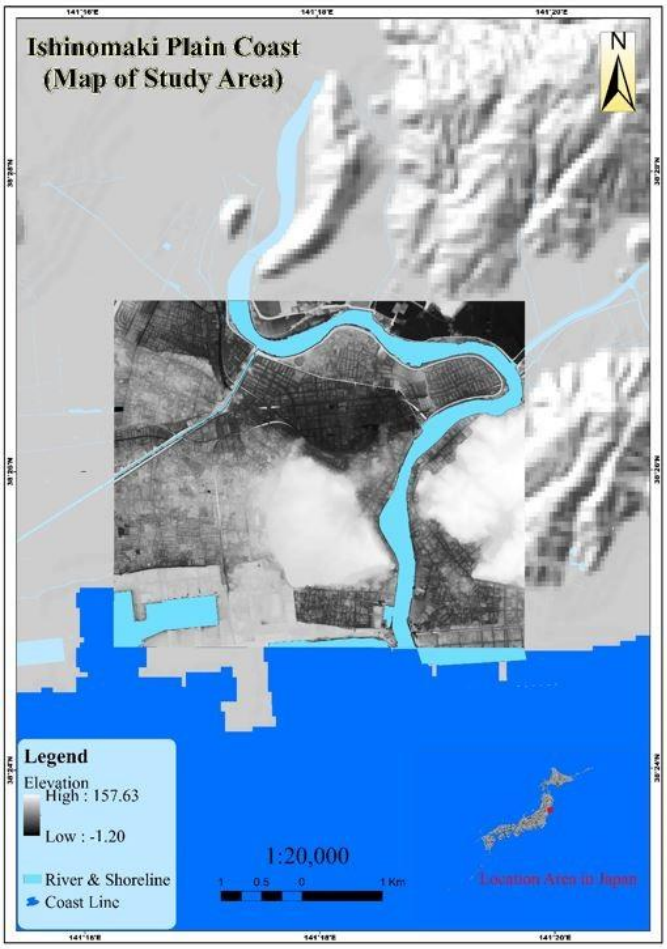


**Figure 5.1** Case study site in Ishinomaki, Japan.

We extracted the factors of elevation and slope from a digital elevation model (DEM) obtained from the Geospatial Information Authority of Japan (here after referred to as GSI DEM), while the NDVI for vegetation density is extracted from Geoeye-1 image and Image Analysis toolbar in ArcGIS 10.2.1 The shoreline distance and river distance were measured from the vector maps of the study area.

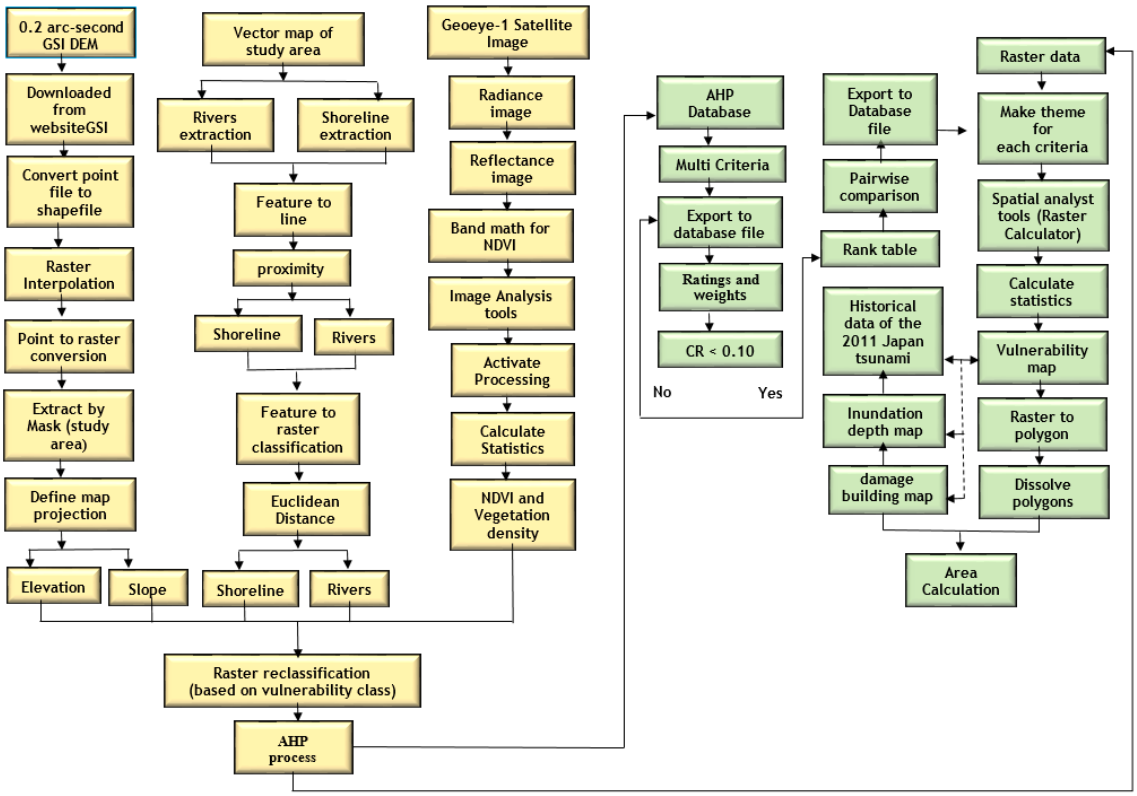


**Figure 5.2** Framework for the study
GSI: Geospatial information authority of Japan, DEM: Digital Elevation Model, Geoeye-1: Very high resolution optical satellite image, NDVI: Normalized Difference Vegetation Index, AHP: Analytical Hierarchy Process, CR: Consistency Ratio.

The vulnerability by tsunami is then estimated by applying AHP to factors of elevation, slope, shoreline distance, river distance and vegetation. The vulnerability assessment can be displayed via GIS in terms of spatial multi - criteria analysis on a map of the tsunami vulnerability area.

### *5.2.1 Elevation*

A digital elevation model was created from elevation data obtained from GSI. GSI DEM was downloaded from http://fgd.gsi.go.jp/download/GsiDLSelFileServlet. The mesh elevation data created by interpolating to the elevation point at center point in 0.2 seconds (about 5 meter) mesh that is from the value of elevation (ground data) measured by airborne laser. The height accuracy of the 5m mesh elevation from the airborne laser is less than 0.3m and the standard deviation of the altitude acquisition position (from the photogrammetry) is less than 1.0 meter. The data was in JPGIS (format) converted to

shapefile in point format using base map viewer converter software version 4.00 (FGDV) provided by GSI [66].

Finally, this point format was converted to raster for creating the digital elevation model via Arc GIS 10.2.1 software and raster interpolation toolset function. The steps are shown in **Figure 5.3**.

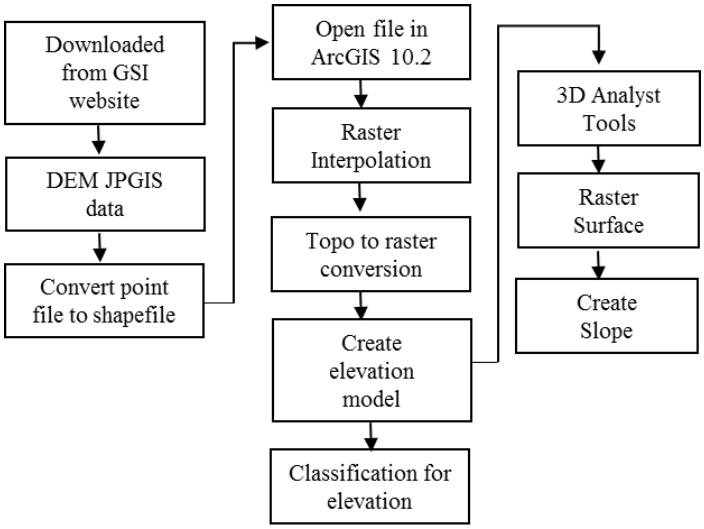


**Figure 5.3** Elevation and Slope data process.

### *5.2.2 Slope*

The slope was determined as the rate of maximum change in z value from each cell of the satellite image. The use of a z-factor is essential for correct slope calculations when the surface z units are expressed in units different from the ground x,y units. The range of values in the output depends on the type of measurement units. The range of slope values is 0 to 90 for degrees and 0 to essentially infinity for percent rise. We created a slope map using the surface creation and analysis tools of the ArcGIS 10.2.1 software to use a third-order finite difference method for calculating the slope [105] [106].

### *5.2.2 Distance from shoreline*

The distance from the shoreline was created in a polyline file for buffering the distance from the shoreline to the land. We computed the distance using the proximity and the Euclidean distance analyst tool in the ArcGIS 10.2.1 software. The distance is based on

the historical report of the maximum run-up in the area of study. We used the **Eq. 3.4** to classify coastal proximity and shoreline distance buffering from Bretschneider and Wybro (1976) [29].

The maximum run-up of the tsunami in the study area was 8.6 m according to the 2011 Tohoku Earthquake Tsunami Joint Survey Group, 2011 at Ayukawa in Ishinomaki City, Miyagi Prefecture. We classified distance buffers in five classes based on the **Eq 3.4** in order to create a tsunami vulnerability map. It explains that 4.55m to 8.90m of run-up can reach a distance of 489.94m from the shoreline, 8.9m to 11.6m of run-up can reach 1,198.53m, 11.6m to14.0m of run-up can reach 1,700.48m, 14.0m to 15.4m of run-up can reach 2,184.28m and 15.4m to 18.0m of run-up can reach more than 2,491.91m.

For the vulnerability assessment, the multi buffering distance from the coastline to an area of land was measured in relation to the impact of a tsunami wave. The five classes of distance used (less than 489.94m, 489.94-1,198.53m, 1,198.53-1,700.48 m, 1,700.48-2,184.28m, and 2,184.28m-2,491.91) represent to low vulnerability, slightly low vulnerability, medium vulnerability, slightly high vulnerability, and high vulnerability.

### *5.2.4 Distance from the (Kita kami) river and (Unga) Water canal*

We know the tsunami propagation in the rivers has higher speed than the tsunami propagation over land and it may maintain and propagate the wave energy further upstream and may cause damages in area far from the shoreline. The Kita kami River, the fourth largest river in Japan and the downstream branches into two water canal, Old-Kita kami river and Kita kami river. Old-Kita kami River flows on a fertile plain which has been highly developed for agriculture and industries and this water canal passes through the study area, while Kita kami river flows through a narrow valley into a small bay faced to the Pacific Ocean. The Old-Kita kami river mouth had parallel jetties. The bed slope was 0.00017, which is the average bed slope from the river mouth up to the intrusion limit. On the contrary, the Kita kami river mouth was mostly sandy soil with 0.0001 bed slope and not as deep as the Old-Kita kami River mouth. It can be seen that the tsunami had reached 8 to 10 km or more off the coastline towards inland around Kita kami River and Old Kita kami River and the elevation in this region was extremely low,

ranging between 0 and 2 m. while the devastated damages to the building were seen till the 3 km of the river area while the inundation area was about 8 km in the study area [107]-[109].

Kita kami-unga or Kita kami Canal is an artificial watercourse (canal) with an average elevation of -9 meter below sea level along 15.8km. The soil in the area is high in andosols (an), soils composed of volcanic materials, usually dark colored. Kita kami Canal that ran across the city and then inundated the inland area [110]. Similarly to the river study, based on the historical report of the inundation area and inundation depth maps, we evaluated the inundated area along the water canal. Accordingly the influence of water canal width on the inundation flows was classified into three classes which are shown in **Figure 5.8**.

The elevation, river distance and shoreline distance were classified into five classes of vulnerability using the Jenks natural breaks method. This classification method indicates by picking the class breaks in best group similar values, maximize the differences between classes and minimize value differences between data within the same class and emphasize the differences between the reclassified classes [111]. The tsunami vulnerability map based on the elevation, slope, shoreline distance, river distance and Unga canal distance are shown in **Figure 5.4**, **Figure 5.5**, **Figure 5.6**, **Figure 5.7** and **Figure 5.8**.

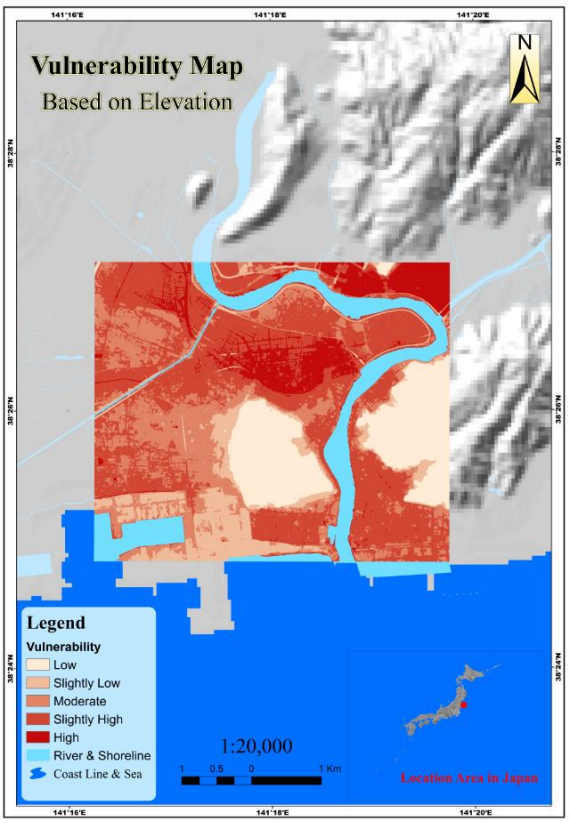


**Figure 5.4** Vulnerability map based on Elevation.

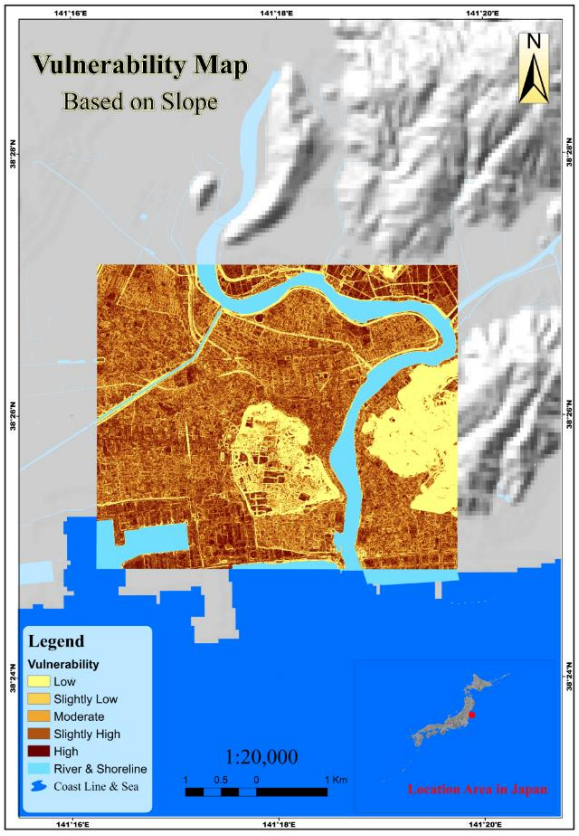


**Figure 5.5** Vulnerability map based on Slope**.**

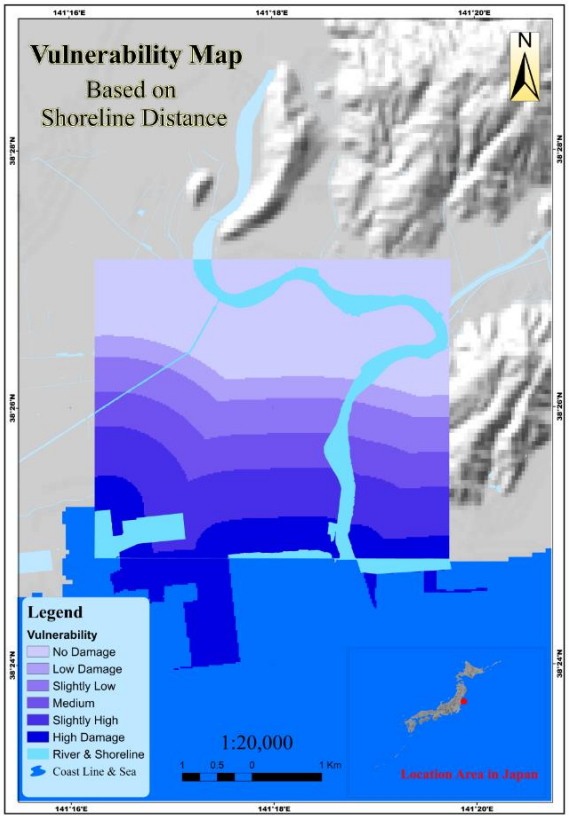


**Figure 5.6** Vulnerability map based on Shoreline distance.

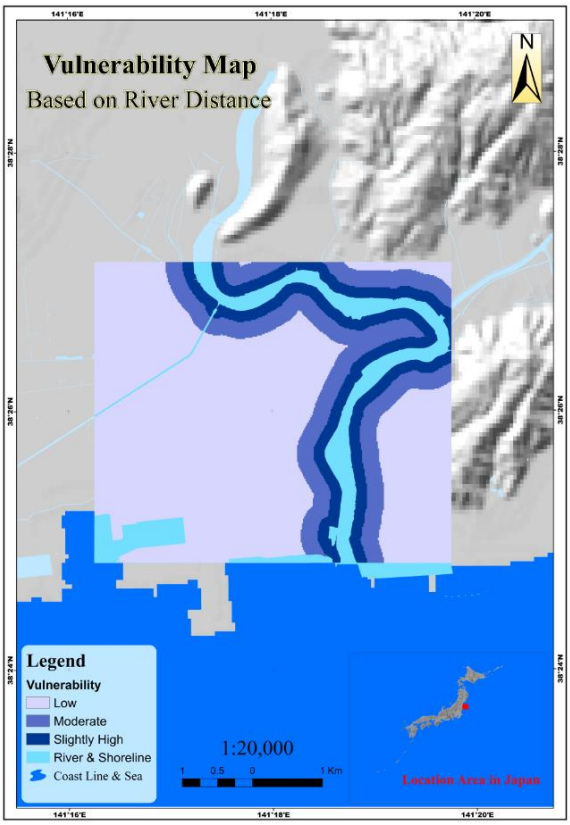


**Figure 5.7** Vulnerability map based on River distance.

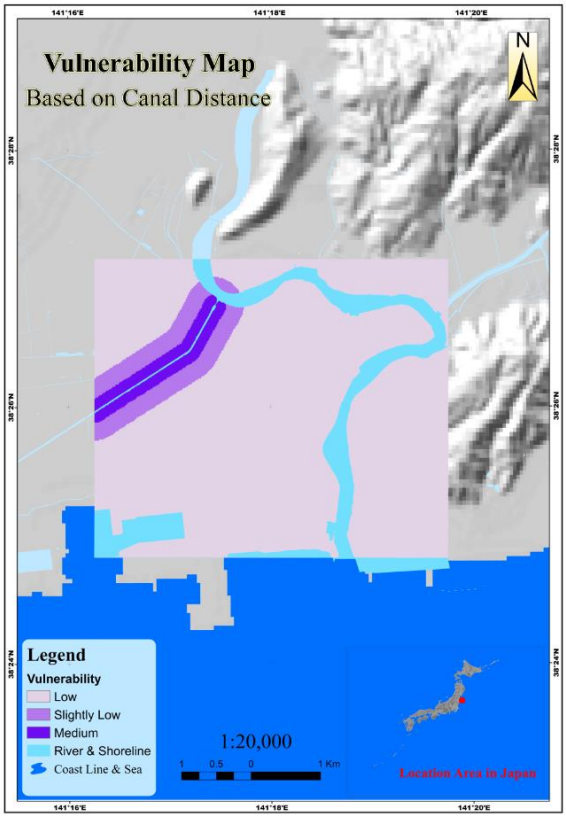


**Figure 5.8** Vulnerability map based on the Canal distance.

## *5.3 GeoEYE-1 Processing*

We calculated normalized difference vegetation index (NDVI), and vegetation density by using GeoEye-1 satellite image. The spectral radiance can be calculated from the digital number (DN) values in the GeoEye-1 image product using the radiometric gain and offset values in the product metadata by the **Eq 3.7**, **Eq 3.8** and **Eq 3.9** to create vegetation density map and the steps to create vegetation density map are described in the following subsection:

The Normalized Difference Vegetation Index (NDVI) is a common tool for identifying and characterizing vegetation and a measure of the difference in reflectance between these wavelength ranges that takes values between -1 and 1, while vegetated areas produce values starting around 0.4 and approaching 1.0 and values < 0 indicating no vegetation [73][73].

Regarding elevation, it is classified in five categories of the distance for river, canal and shoreline based on the values described in **Table 5.1**.

**Table 5.1** Tsunami Vulnerability Classes based on elevation, Shoreline distance, river distance and vegetation

| Vulnerability | Factors Name | | | | | | |
|---|---|---|---|---|---|---|---|
| | Elevation (m) | Shoreline Distance (m) | River distance (m) | | Slope (%) | Vegetation | |
| | | | Kitakami | Unga Canal | | Index | Density |
| High (5) | -4 - 3 | 0-489.94 | - | - | 0-1 | -0.99-0.151 | Low dense |
| Slightly high (4) | 3 - 4 | 489.94-1,198.53 | - | - | 1-3 | 0.151-0.164 | Slightly dense |
| Medium (3) | 4 - 5 | 1,198.53-1,700.48 | 0-160 | 0-150 | 3-6 | 0.164-0.188 | Medium dense |
| Slightly low (2) | 5 - 6 | 1,700.48-2,184.28 | 160-400 | 150-400 | 6-8 | 0.188-0.218 | Slightly dense |
| Low (1) | > 6 | 2,184.28-2,491.91 | > 400 | > 400 | > 8 | 0.218-0.556 | Highly dense |

As shown in **Figure 5.9** a vulnerability map based on vegetation density, explained that most of high-vulnerability areas were located in the coastal areas where the vegetation is less.

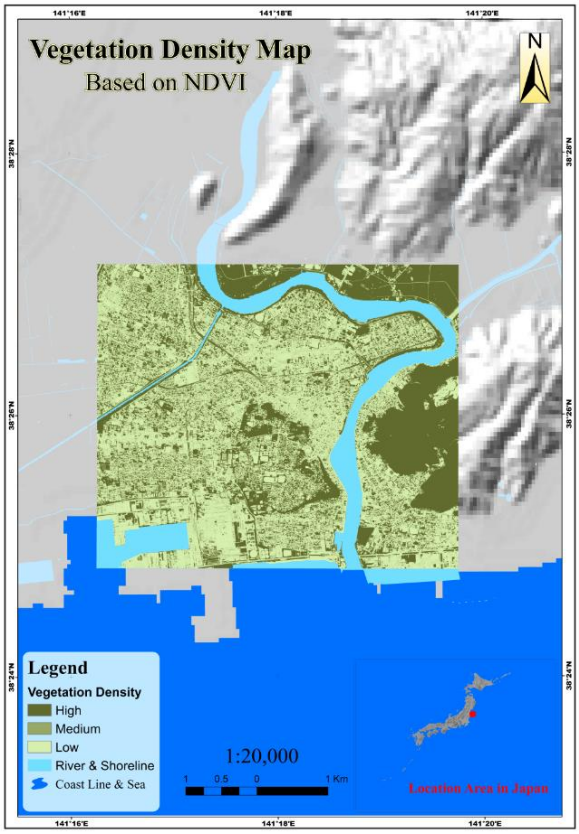


**Figure 5.9** Vulnerability map based on vegetation density.

## 5.4 GIS and AHP for Vulnerability Mapping

Cell-based modeling in spatial analysis was used to specify the vulnerability area due to tsunami hazard. Cells are classified into five classes of vulnerability in the numbers of 1, 2, 3, 4 and 5, which represent low, slightly low, medium, slightly high, and high vulnerability classes.

AHP is a multi-criteria decision-making analysis (MCDA) approach introduced by Saaty (1977, 1980), which is developed by a series of pair-wise comparisons between each factor relative to other factors to make a scaled set of preferences. By the AHP measurement theory, pairwise comparisons and relies on the judgements of experts to conclude priority scales that measure intangibles in relative terms. The AHP is an Eigen value technique to the pair-wise comparisons approach and a numerical fundamental scale, which ranges from 1 to 9 to calibrate the quantitative and qualitative performances of priorities to score the importance of each factor (Saaty, 2008). **Table 5.2** describes the fundamental scale of absolute numbers which is named the Saaty nine-point comparison scale. As we mentioned each number depends on the relative importance of each factor [112] [113].

**Table 5.2** The Saaty Nine-Point Comparison Scale [114]

| Intensity of importance (Score) | Definition and Explanation | |
|---|---|---|
| | Definition | Explanation |
| 1 | Equal importance | Two factors contribute equally to the objective. |
| 3 | Weak importance of one over another | The judgment is slightly favor one factor over another. |
| 5 | Essential or strong importance | The judgment is to strongly favor one factor over another. |
| 7 | Demonstrated importance | A factor is strongly favored and its dominance is demonstrated in practice. |
| 9 | Absolute importance | The evidence favoring one factor over another is of the highest possible order of affirmation. |
| 2, 4, 6, 8 | Intermediate values between the two adjacent judgments | When compromise is needed. |

All of tsunami vulnerability factors are overlaid and weighted based on their dominant influences in determining the class of tsunami vulnerability. The relative

importance of each factor within the hierarchy is determined by their weights (Saaty, 1977 & 1980). The hierarchical interactions based on the respective importance of each factor were computed by estimating the numerical score. When there are evaluation criteria/ objectives, decision makers must carry out a pairwise comparison. The scores are made by the subjective definition of the investigator in determining the importance of each factor [115]-[117].

In order to assign appropriate AHP comparative factors for different criteria, it is required to use expert choices. As it is discussed already, at each node of the hierarchy, a matrix will collect the pairwise comparisons of the decision-maker. Psychologists argue that it is easier and more accurate to express one's opinion on only two alternatives than simultaneously on all the alternatives. It also allows consistency and cross checking between the different pairwise comparisons (see Consistency part under the section the original AHP method). AHP uses a ratio scale, which, contrary to methods using interval scales, requires no units in the comparison. The judgement is a relative value or a quotient $a/b$ of two quantities $a$ and $b$ having the same units (intensity, meters, utility and so on). The decision-maker does not need to provide a numerical judgement; instead a relative verbal appreciation, more familiar in our daily lives, is sufficient. For each problem these pairwise comparison should be done by well experienced people so as more precision in the results of next steps can be obtained. We have requested several experts in the field if earthquake engineering and tsunami studies to fill out the matrices with a pairwise comparison prepared for our specific problem which is shown in **Table 5.3**.

**Table 5.3** Pair-wise Comparison

| Pairwise Comparison | Factors Name | | | | |
|---|---|---|---|---|---|
| | Elevation | Slope | Shoreline Distance | River Distance | Vegetation |
| Elevation | 1.00 | 2.00 | 0.33 | 0.50 | 2.00 |
| Slope | 0.50 | 1.00 | 0.25 | 0.33 | 1.00 |
| Shore-line Distance | 3.00 | 4.00 | 1.00 | 2.00 | 5.00 |
| River Distance | 2.00 | 3.00 | 0.50 | 1.00 | 4.00 |
| Vegetation | 0.50 | 1.00 | 0.20 | 0.25 | 1.00 |

The first eigenvector was computed based on the pairwise comparison matrix. The normalized principal eigenvector explains that shoreline distance has the highest weight (42.16%), followed by elevation (14.92%), slope (8.57%), river distance (26.60%) and vegetation density (7.74%) as shown in **Figure 5.10**.

$$\begin{array}{c} \text{Eevation} \\ \text{Slope} \\ \text{Shoreline Dis.} \\ \text{River Dis.} \\ \text{Vegetation} \end{array} \begin{bmatrix} 0.1429 & 0.1818 & 0.1460 & 0.1224 & 0.1538 \\ 0.0714 & 0.0909 & 0.1095 & 0.0816 & 0.0769 \\ 0.4286 & 0.3636 & 0.4380 & 0.4898 & 0.3846 \\ 0.2857 & 0.2727 & 0.2190 & 0.2449 & 0.3077 \\ 0.0714 & 0.0909 & 0.0876 & 0.0612 & 0.0769 \end{bmatrix}$$

**Figure 5.10** Normalized matrix and eigenvector calculation.

AHP is subjective and tolerates inconsistency through the amount of redundancy by providing a measure of inconsistency assessment, which is shown by Consistency Ratio (CR). If the value of CR is smaller or equal to 10%, the inconsistency is acceptable. CR indicates the probability that the matrix judgments were randomly generated and it is defined as the ratio of the Consistency Index (CI), which is the degree of logical consistency among pair-wise comparisons, to the Random consistency Index (RI) which is the average CI value of randomly-generated comparison matrices.

**Eq. 3.6** describes the algorithms for CR and CI calculation where $\lambda_{max}$ is the maximum eigenvalue of the judgement matrix and calculated from the sum of all factors and it is multiplied by its eigenvector which is 42.16%. The RI value is based on the random consistency index as shown in **Table 3.4** for comparison matrix of size 5, thus the RI of 1.11 was chosen. Accordingly the consistency index, CI, is calculated 0.093 and CR is 8.37%.

We calculated each raster cell-by-cell basis of the factor to its weight using GIS system with overlay capabilities. A Weighted Linear Combination (WLC) analysis is very straightforward in a raster GIS, and each factors are combined by applying a weight, to each followed by a summation of the results to proceed a suitability map. **Eq. 5.1** describes the suitability calculation [118]:

$$S = \Sigma W_i \cdot X_i \qquad \text{(Eq. 5.1)}$$

Where:

$S$ = Suitability,

$W_i$ = Weight of factor i

$X_i$ = the criterion score of factor *i* (potential rating of the factor).

We estimated raster calculator in map algebra menu using the spatial analyst tools of ArcGIS 10.2.1 to produce vulnerability map by applying **Eq. 5.1**.

**Figure 5.11** shows the tsunami vulnerability map in the Ishinomaki area as output of this calculation. We estimated the statistics of the vulnerability map based on the vulnerability classification of five factors used in this study is shown in **Table 5.4** while the vulnerability index of 91,437.35 grid cells ranged between 1to 5, with a standard deviation of 0.792. The GIS produced tsunami vulnerability map is shown in **Figure 5.11** which is in good agreement with the historical data recorded by "GSI" and "2011 Earthquake Tsunami Joint Survey Group". Based on the comparison most of the inundation areas are located in high and slightly high vulnerability areas.

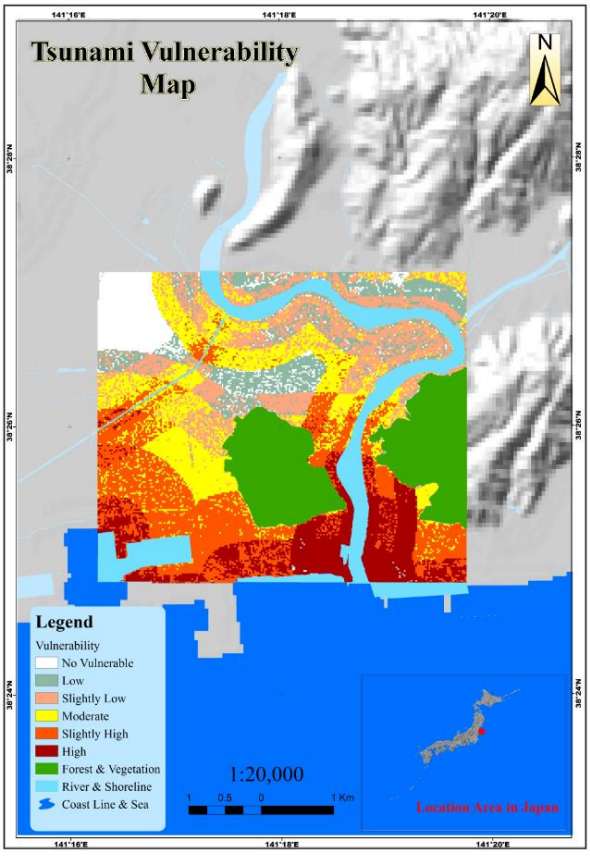


**Figure 5.11.** Tsunami vulnerability map of Ishinomaki Study area.

**Table 5.4** Vulnerability Classification and Tsunami inundated Area

| Damage Index | Vulnerable Area Classification | | | |
|---|---|---|---|---|
| | Vulnerability class | Vulnerability Value in Tsunami Map | Area ($km^2$) | Area (%) |
| 1 | Low | 1.57 – 1.84 | 2.17 | 14.74 |
| 2 | Slightly low | 1.84 – 2.28 | 3.23 | 21.96 |
| 3 | Medium | 2.28 – 2.85 | 3.15 | 21.35 |
| 4 | Slightly high | 2.85 – 3.45 | 3.75 | 25.44 |
| 5 | High | 3.45 – 4.73 | 2.43 | 16.51 |

Based on the result of our study, which is shown in **Figure 5.12** the inundation area was 14.73$km^2$, while GSI reported that the inundation area in Ishinomaki in the 2011 Japan tsunami was 13.45 $km^2$. On the study area the maximum inundation height (run-up) based on the 2011 Earthquake Tsunami Joint Survey Group was 8.6 m and found at Ayukawa in Ishinomaki City, Miyagi Prefecture (in the latitude of 39.021 and longitude of 141.647).

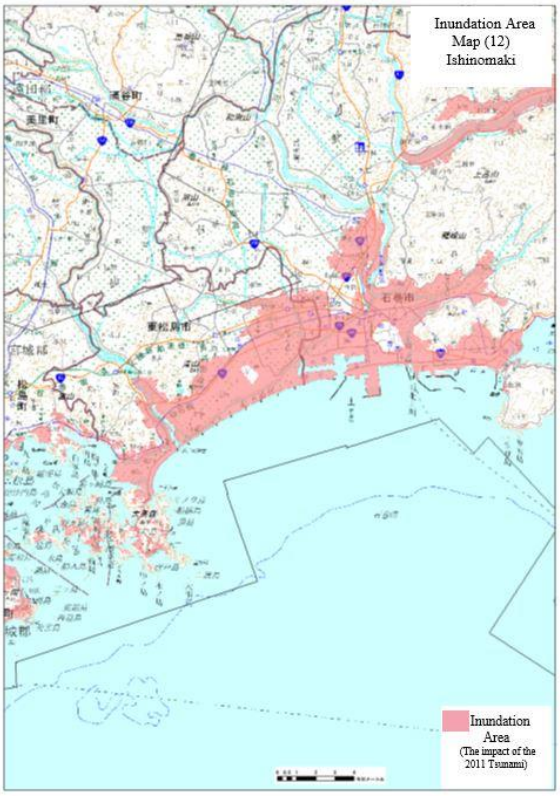


**Figure 5.12.** Tsunami Impact Map in Ishinomaki (published by GSI) [119]

### *5.5 Discussion*

Vulnerability is defined as the potential area that can be damaged by natural hazards. Physical vulnerability is often defined as the loss degree to a given factor or set of factors within the area affected by a hazard like tsunami. Physical factors, such as elevation, slope, shoreline distance, river distance and vegetation density could be used for vulnerability classification. Moreover, we know "Inundation" is the result of a tsunami travelling a long distance inland and is a horizontal measurement of the path of the tsunami. A tsunami effect is defined by several factors like height, run-up height and run-up distance [120]-[123].

In this research, we used and analyzed satellite remote sensing (data), elevation data and field survey data followed by multi-criteria analysis through AHP raster overlay tools in GIS processing can be used as the basic operation for vulnerability mapping and inundation assessment due to tsunami hazard.

In this study a first attempt for assessing tsunami vulnerability was performed by using the factor of river distance besides elevation, vegetation, shoreline distance and slope and applying the AHP method combined with raster overlay tools through GIS processing in the Ishinomaki area. It is valuable step to estimate inundation area via this method and primary tsunami vulnerability mapping for impact assessment and output.

Remote sensing can be capable to achieve information about the input factors for tsunami vulnerability mapping and impact assessment. In the study area, several indicators of vulnerability can be achieved using a very high resolution satellite. It is very useful to derive data about the DEM in high spatial resolution so the output of the research will more accuracy. Although obtaining the digital elevation model from GSI DEM needs some processing and ArcGIS is a powerful software for processing and combining spatial data of each factor and analyzing the result of AHP in order to generate a vulnerability map.

In this study, we used five classes of vulnerability for tsunami vulnerability map. Based on this, 2.43km$^2$ of the study area was in high vulnerability, 3.75km$^2$ was in slightly high vulnerability, 3.15km$^2$ was in medium vulnerability, 3.23km$^2$ was in slightly low vulnerability and 2.17km$^2$ of the area was in low vulnerability. The high-vulnerability areas were located in the coastal areas in low slopes. In high-vulnerability area and slightly high vulnerability inundation areas were predicted. In addition, the Kitakami River and water canal have the role to act as a flooding strip that transports

inundation into the hinterland. The tsunami run-up comes up to the hinterland through the flat surface, urban areas and rivers. In this research we created the tsunami vulnerability map and inundation map which can be used for determining the priority for land-use planning related to tsunami hazard risk management.

In this chapter, we proposed the combined analysis of digital elevation data, very high resolution satellite images, tsunami historical data, AHP, and spatial multi-criteria processing via GIS to provide a tsunami vulnerability map and inundation map. Using the reflectance value of Geoeye-1 image before and after 2011 Japan, Tohoku tsunami was calculated as a preliminary study. In the next research, the height of the buildings and their materials in the inundation area can be considered in classifying the damaged buildings.

## *5.6 Summary*

By means of GIS application, it is possible to manage hazards due to tsunami disasters. In the case of data limitation, very high resolution of the DEM and other factors, such as coastal type, relative direction of tsunami, coastal bathymetry and river morphological consideration is needed to achieve a better tsunami vulnerability mapping. This chapter used high resolution of DEM for the input factors for elevation and slope. For evaluation of vegetation factor, the normalized difference vegetation index (NDVI) is calculated to precisely assess vegetation density on GeoEye-1 satellite image.

Importantly, an appropriate AHP method with considering five geographical factors was proposed in order to create a valuable tsunami vulnerability map. The produced vulnerability map was in good accordance with the inundation area map of tsunami in Ishinomaki area of Miagi Prefecture in Japan. As a result of this vulnerability map, although the importance of the shoreline areas in the creation of whole inundation pattern is observed but also our results indicate an important role of rivers in inundation pattern far from the coast line. Furthermore, low level land areas far from the coast line are observed to be in inundated areas. The simulated tsunami pattern shows over eighty percent compatible with the inundation map. Same approach can be employed to evaluate the assessment of the other vulnerable areas that could be affected by tsunami hazard in future natural disasters.

# Chapter 6

## Updating GIS and RS vulnerability assessment using survey data (Case Study)

In accordance with the previous chapter, in this chapter another software application for analyzing the satellite images of Ishinomaki city as a case study is explored. As a result, the tsunami damage map is produced. Moreover, an initiative approach to classify the survey damage data was proposed to obtain key material factors controlling the amount of destruction. Damage behavior of different construction materials were compared in different inundation depth and the corresponding inundation threshold for each material was extracted. The results emphasis that the damage is not only controlled by the tsunami height which is dependent highly to coastal topography, but also highly dependent on the building material.

### *6.1 Introduction*

A natural disaster event occurs in a populated area is a hazardous event that causes huge amount of destruction and fatalities. Tsunami is one of these natural hazards which can harm human and properties vastly since it happens in an inhabitant area. The 2011 Great east Japan tsunami that attacked east coast of Japan causes more than 400,000 buildings damaged or destroyed [124]. Unfortunately, in different human society that are in danger of such natural disasters people are engaging in developing infrastructure and building constructions seemingly without vulnerability assessment of hazards impact. Therefore, it is essential to improve our understanding of building damage characteristics and coastal topography due to a tsunami event. Then it will be possible to prepare an initial vulnerability assessment of a disaster event as a tool to reduce its damage to the community for an effective hazard mitigation [93]-[95]. Such mitigation of natural disasters becomes successful only with accurate and reliable information through building damage surveyed

databank of previous hazardous events in an area together with spatial data of vulnerable areas.

Early studies provides discussions about the influence of building construction material and the number of stories on the building resistance to tsunami inundation in several case studies using surveyed building damage data [125]-[127]. Moreover, several threshold depths as damage criteria for each different construction material against a range of tsunami inundation depths are accordingly suggested [128] [129].

It is shown by these studies that the Reinforced Concrete (RC) or steel based constructions are stronger than wood or masonry based constructions for different inundation depth ranges through plotting of fragility curves in many case studies [130]-[136]. These results reflected the tsunami damage probability related to the building construction material, height and number of stories under different tsunami inundation depths. Instead of plotting fragility curves, we adopted a way to classify by the Ministry of Land, Infrastructure and Transportation of Japan (MLIT) surveyed damage data of Ishinomaki city for each building material and six damage levels based on their percentage amount under inundation depth range of 0-8.5m with simple graphical schematics. These graphical illustrations are suitable for quick assessment of building damage based on the tsunami inundation map produced through a field survey and a GIS software. Results not only shows a better resistant performance of RC and steel buildings over wood or other buildings for all inundation depth ranges, but also can explain clearly the inundation-induced damage behavior for each building material as well as the threshold depth for each damage level.

In addition to this field survey data classification, the effect of coastal topography, geographical features and buildings locations has been treated by means of an analysis of satellite imagery in the plain coast of Ishinomaki city by creating tsunami damage map. Previous studies have developed and analyzed integrative remote sensing techniques in assessing building vulnerability to tsunami hazard. High resolution satellite imagery, which has become available in the last few years, made satellite remote sensing more useful in disaster management since even the damage status of individual buildings can be identified without visiting the sites of disasters [92][97]. Recent advancements in the field of the management of the databases and the computer information systems made the GIS as an ideal instrument for analyzing satellite maps in the disaster management field by using a multi-scenario approach [103][104][36]. Several topographic factors of elevation, slope,

coastal proximity, vegetation, river and water canals are incorporated by the AHP to construct a weighting scheme for the geospatial variables and assessing tsunami vulnerability [113]-[117] and [119][120].

In our case study, the satellite image of Ishinomaki plain coast, which is shown in **Figure 6.1** is analyzed through GIS with appropriate geographical factors to produce the vulnerability map in five classifications. The impact of Kitakami river and water canals floods in the creation of the tsunami building damage map are one of the main distinctive aspect of this coastal topography analysis over similar studies.


**Figure 6.1** Area map of Ishinomaki city showing the plain coast and ria coast [137].

Experiencing to historical hazardous events through field surveys together with obtaining information through GIS, management authorities pre-plans appropriate response activities in order to minimize the damages of a future similar event. These disaster risk management includes activities such as providing better evacuation routs and

safe places or shelters, educations for public, construction of tsunami barriers and new regulations for building construction.

## *6.2 Data and method*

The first part of this study dedicated to evaluate the building materials behavior and damage because of tsunami inundation according to the field survey conducted by the MLIT provided in database format. In the second part the costal topography impact is treated through damage map produced through GIS incorporated with AHP methodology for the plain coast area. The coastal topography effect on inundation based building damage is investigated by defining shore line, elevation, slope, river and vegetation by means of GIS as a tool to analyze Ishinomaki plain coast satellite image. The analysis results aim to reflect potential differences in dam-age probabilities related to the tsunami inundation, construction materials and the buildings' location according to the damage map.

### *6.2.1 Building damage classification method*

According to MLIT survey the damage levels were categorized in six classes: (1) Low damage, (some part of building damage and water between ground and first floor), (2) Slightly low damage (half damage and water between ground and first floor), (3) Moderate damage (half damage), (4) High damage (water over than first floor and completely destroyed), (5) collapse and (6) Washed away. Moreover, the main building characteristics, including building construction material, number of stories and buildings locations were included. An example of such building damage data for affected area in Ishinomaki city is represented in **Table 6. 1** for RC. In this table, building damages are classified based on the measure of tsunami inundation depth. Similar files were available for steel, wood and lightweight building materials named as others in our classifications.

**Table 6.1** Example of building damage data for whole affected area in Ishinomaki city of Japan.

| Inundation depth (m) | Damage level of RC for inundated buildings in Ishinomaki | | | | | | |
|---|---|---|---|---|---|---|---|
| | Low | Slightly low | Moderate | High | Collapse | Washed away | Total |
| ～0.5m | 46 | 29 | 7 | | | | 82 |
| 0.5～1.0 | 39 | 160 | 32 | | 1 | 1 | 233 |
| 1.0～1.5 | 8 | 94 | 38 | 4 | 2 | | 146 |
| 1.5～2.0 | 1 | 15 | 23 | 10 | 7 | 2 | 58 |
| 2.0～2.5 | | 7 | 14 | 29 | 22 | 2 | 74 |
| 2.5～3.0 | | 2 | 16 | 19 | 20 | 1 | 58 |
| 3.0～3.5 | | | 11 | 28 | 24 | | 63 |
| 3.5～4.0 | | | 12 | 15 | 22 | 4 | 53 |
| 4.0～4.5 | | | 6 | 13 | 13 | 1 | 33 |
| 4.5～5.0 | | | | 10 | 4 | | 14 |
| 5.0～5.5 | | | | 11 | 10 | 4 | 25 |
| 5.5～6.0 | | | 7 | 12 | 4 | 1 | 24 |
| 6.0～6.5 | | | 1 | 1 | 9 | | 11 |
| 6.5～7.0 | | | | 1 | 13 | | 14 |
| 7.0～7.5 | | | | | 1 | | 1 |
| 7.5～8.0 | | | | | | | 0 |
| 8.0～8.5 | | | | 2 | 1 | 1 | 4 |
| 8.5～9.0 | | | | 1 | 5 | 2 | 8 |
| 9.0～9.5 | | | | 2 | 6 | | 8 |
| 9.5～10.0 | | | | 1 | 2 | 5 | 8 |
| 10.0～10.5 | | | | | 2 | | 2 |
| 10.5～11.0 | | | | | 4 | 3 | 7 |
| 11.0～11.5 | | | | 1 | | | 1 |
| 11.5～12.0 | | | 1 | 2 | 2 | | 5 |
| 12.0～12.5 | | | | | | | 0 |
| 12.5～13.0 | | | | | | | 0 |
| 13.0～13.5 | | | | 1 | | | 1 |
| 13.5～14.0 | | | | | | | 0 |
| 14.0～14.5 | | | | | | | 0 |
| 14.5～15.0 | | | | | | | 0 |
| 15.0～15.5 | | | | | | | 0 |
| 15.5～16.0 | | | | | | | 0 |
| 16.0～16.5 | | | | | | | 0 |
| 16.5～17.0 | | | | | | | 0 |
| 17.0～17.5 | | | | | | | 0 |
| 17.5～18.0 | | | | | | | 0 |
| 18.0～18.5 | | | | | | | 0 |
| 18.5～19.0 | | | | | | | 0 |
| 19.0～19.5 | | | | | | | 0 |
| 19.5～20.0 | | | | | | | 0 |
| 20.0m～ | | | | | | | 0 |
| **Total** | | | | | | | **933** |

The data were provided for 63,157 buildings where the number of buildings in inundated area of Ishinomaki city and ones in the plain coast area (look to **Figure 6.1**), for different construction types are listed in **Table 6.2** Also the percentage distribution of different building types in Ishinomaki city and Ishinomaki-plain coast area shown in **Figure 6.2**.

**Table 6.2** Number of buildings with different construction materials

| Building materials | Ishinomaki city | Ishinomaki-Plain Coast |
|---|---|---|
| Concrete | 933 | 692 |
| Steel | 2,450 | 1526 |
| Wooden | 45,976 | 24997 |
| Others | 13,798 | 6258 |
| Total | 63,157 | 33473 |

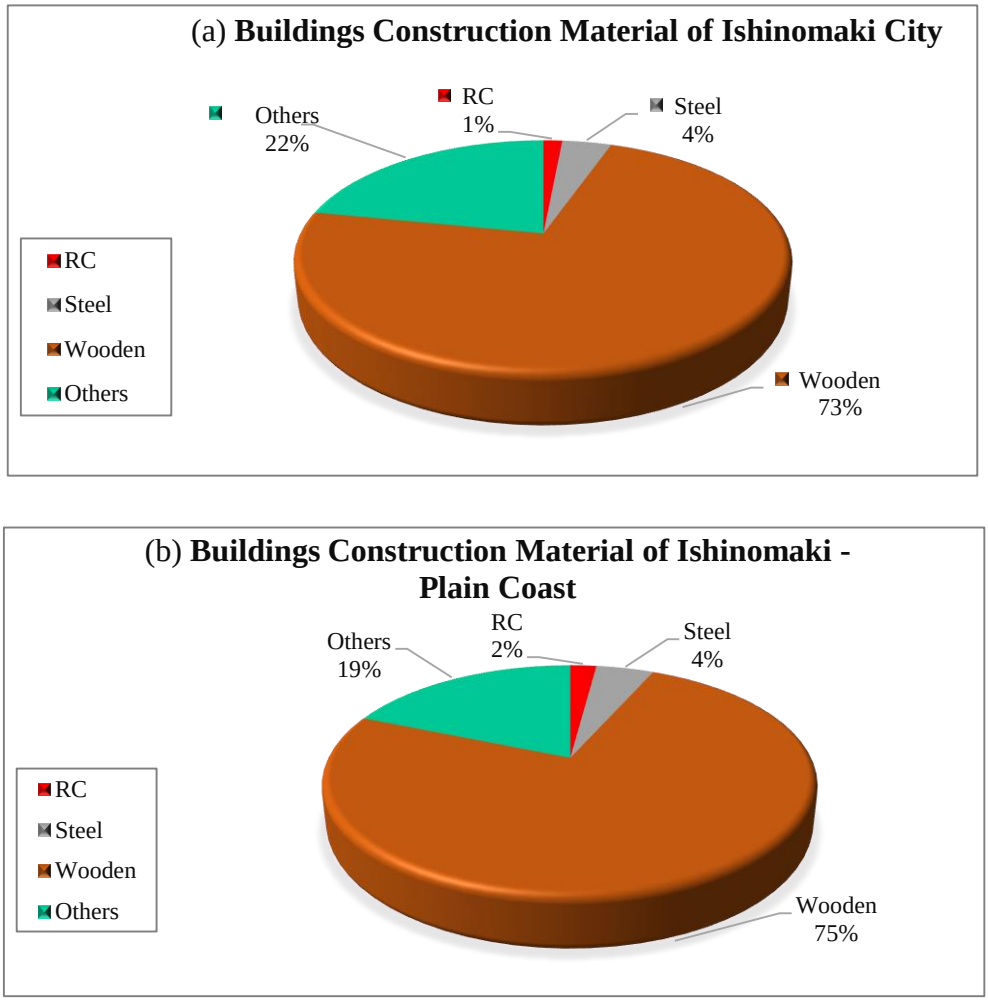


**Figure 6.2.** Percentage distribution of different building types a)Ishinomaki city, b) Ishinomaki plain coast area.

As illustrated in the **Figure 6.2** nearly 95% of buildings in Ishinomaki city can be classified either wooden or other lightweight building materials.

Other important buildings characteristic provided by MLIT was number of stories. It has been explained in some previous studies that the more number of stories per building the stronger the building construction because of their structural design to support heavier loads. Since based on MLIT database about 98% of buildings found to be two floors with few multi stories buildings that are located mostly in safe areas, building damage due to the number of stories are neglected in this study.

The MLIT survey analysis method in this study covers an investigation on damage level distribution based on inundation depth, building damage distribution with considering both construction material and inundation depth in Ishinomaki city. For necessary occasions, the similar data analysis is applied for buildings located in the plain coast area for comparison. Several data classification were performed to extract valuable charts to assess the impact of construction material in amount of damage. Finally an analysis of the impact of the coastal topography in amount of building damage for 33,473 buildings of Ishinomaki city plain coast (shown in **Figure 6.2** (b)) is provided. For this purpose, Arc GIS software tool based on AHP method is used to analyze the satellite image and to classify the vulnerable areas.

### *6.2.2 Damage building map method*

In this study, remote sensing data captured by GeoEye-1 a Very High Resolution (VHR) optical satellite with a pixel size about 0.41m was used to identify critical geographical elements such as buildings, transport infrastructure and the inundation area due to the tsunami event in order to estimate the vulnerability and risk in coastal areas in the area of Ishinomaki City in Miyagi Prefecture**.**

We extracted the factors of elevation and slope from a Digital Elevation Model (DEM) obtained from the Geospatial Information Authority of Japan while the Normalized Difference Vegetation Index (NDVI) for vegetation density is extracted from Geoeye-1 image and Image Analysis toolbar in ArcGIS 10.2.1 software. The shoreline distance and river distance were measured from the vector maps of the study area.

The damage by tsunami is then estimated by applying AHP to all the mentioned factors. The damage assessment can be displayed via GIS in terms of spatial multi - criteria analysis on a map of the tsunami damage area.

### *6.2.2.1 Tsunami damage map critical factors*

The steps to create the tsunami damage map is similar to ones for vulnerability map explored in section **5.2** for elevation, slope, distance from shoreline, distance from the Kitakami river and Unga water canal and vegetation. The major difference comes with the distance range for each class since the damage degree and inundation depths are slightly different. Accordingly, we classified distance buffers in five classes based on the **Eq. 3.4** in order to create a tsunami damage map. It explains that 4.55m to 7.09m of run-up can reach a distance of 489.94m from the shoreline, 7.09m to 9.64m of run-up can reach 885.76m, 9.64m to12.18m of run-up can reach 1,332.84, 12.18m to 14.73m of run-up can reach 1,821.46m and 14.73m to 17.27m of run-up can reach more than 2,345.53m.

For the damage assessment, the multi buffering distance from the coastline to an area of land was measured in relation to the impact of a tsunami wave. The five classes of distance used (less than 489.94m, 489.94-885.76m, 885.76-1,332.84m, 1,332.84-1,821.46m, and 1,821.46-2,345.53m) represent to low damage, slightly low damage, medium damage, slightly high damage, and high damage.

Furthermore, we classified elevation and the distance for river, canal and shoreline based on the values described in **Table 6.3**.

**Table 6.3** Tsunami damage classes based on Elevation, Slope, Shoreline distance, River distance and Vegetation

| Damage class | Factors name | | | | | | |
|---|---|---|---|---|---|---|---|
| | Elevation (m) | Slope (%) | Shoreline distance (m) | River distance (m) | | Vegetation | |
| | | | | Kitakami | Unga canal | Index | Density |
| High (5) | -4 - -1 | 0-1 | 0 - 489.94 | - | - | -0.998 - 0.151 | Low |
| Slightly high (4) | -1 - 0 | 1 - 3 | 489.94–885.76 | - | - | 0.151 - 0.164 | Slightly low |
| Medium (3) | 0 - 2 | 3 - 6 | 885.76 – 1,332.84 | 0-160 | - | 0.164 - 0.188 | Medium |
| Slightly low (2) | 2 - 8 | 6 - 8 | 1,332.84–1,821.46 | 160-680 | 0-300 | 0.188 - 0.218 | Slightly high |
| Low (1) | > 8 | > 8 | 1,821.46 – 2,345.53 | >680 | > 300 | 0.218 - 0.556 | High |

As shown in **Figure 5.9** a vulnerability map based on vegetation density, explained that most of high-damage areas were located in the coastal areas where the vegetation is less.

#### *6.2.2.2 GIS and AHP for tsunami damage mapping*

Cell-based modeling in spatial analysis was used to specify the damage area due to tsunami hazard. Map's cells are classified into five classes of damage in the numbers of 1, 2, 3, 4 and 5, which represent low, slightly low, medium, slightly high, and high damage classes for different inundation depth.

As we mentioned in previous chapter, the AHP is an eigen value technique to the pair-wise comparisons approach and a numerical fundamental scale, which ranges from 1 to 9 to calibrate the quantitative and qualitative performances of priorities to score the importance of each factor (Saaty, 2008). **Table 5.3** illustrates the Saaty nine-point comparison scale that indicate the relative importance of each factor [112] [113].

All of tsunami damage factors are overlaid and weighted based on their dominant influences in determining the class of tsunami induced damage. The relative importance of each factor within the hierarchy is determined by their weights (Saaty, 1977 & 1980) with a pairwise comparison as shown in **Table 6.4**.

**Table 6.4** Pair-wise comparison

| Pairwise comparison | Factors name | | | | |
|---|---|---|---|---|---|
| | Elevation | Slope | Shoreline distance | River distance | Vegetation |
| Elevation | 1.00 | 2.00 | 0.33 | 0.50 | 2.00 |
| Slope | 0.50 | 1.00 | 0.25 | 0.33 | 1.00 |
| Shoreline distance | 3.00 | 4.00 | 1.00 | 2.00 | 5.00 |
| River distance | 2.00 | 3.00 | 0.50 | 1.00 | 4.00 |
| Vegetation | 0.50 | 1.00 | 0.20 | 0.25 | 1.00 |

The first eigenvector was computed based on the pair-wise comparison matrix. An approximation of eigen vector and eigen value of a reciprocal matrix can be obtained by through the following method: 1) sum of each column of the reciprocal matrix 2) Then we divide each element of the matrix with the sum of its column, we have normalized relative

weight where the sum of each column is 1 as shown in **Figure 6.3** The normalized principal eigen vector can be obtained by averaging across the rows. The obtained normalized principal eigenvector explains that shoreline distance has the highest weight (42.16%), followed by elevation (14.92%), slope (8.57%), river distance (26.60%) and vegetation density (7.74%) as shown in **Figure 6.3**.

$$
\begin{array}{c}
Eevation \\
\text{Slope} \\
\text{Shoreline distance} \\
River\ distance \\
\text{Vegetation}
\end{array}
\begin{bmatrix}
0.1429 & 0.1818 & 0.1460 & 0.1224 & 0.1538 \\
0.0714 & 0.0909 & 0.1095 & 0.0816 & 0.0769 \\
0.4286 & 0.3636 & 0.4380 & 0.4898 & 0.3846 \\
0.2857 & 0.2727 & 0.2190 & 0.2449 & 0.3077 \\
0.0714 & 0.0909 & 0.0876 & 0.0612 & 0.0769
\end{bmatrix}
$$

**Figure 6.3** Normalized matrix and eigenvector calculation

RI value was chosen 1.1 according to **Table 3.4** for n=5 and $\lambda_{max}$ which is the maximum eigenvalue of the judgement matrix and calculated from the sum of all factors is multiplied by its eigenvector which is 42.16%. Consequently the CR is calculated based on **Eq. 3.6** which is 8.37%.

We estimated raster calculator in map algebra menu using the spatial analyst tools of ArcGIS 10.2.1 to produce damage building map by applying Eq. 5.1.

## *6.3 Results and discussion*

The first part is representing results of building damage for different construction materials. Second part shows the result of GIS for building tsunami damage map.

### *6.3.1 Building damage classification*

In this section, based on surveyed data several statistical analysis results of building damage for different construction materials are provided and discussed. The damage level percentage distribution of different building materials are plotted for different inundation depth ranges in several sets of figures: (1) Tsunami inundation depth only (2) Construction material only, (3) Construction material and inundation depths together.

### *6.3.2 Building damage based on tsunami inundation depth*

The tsunami inundation depth for each building was obtained by MLIT survey database format and Geoeye1 satellite image. According to this data, we classified and summarized the distribution of damage levels based on tsunami inundation depth on an interval of 0.5 m for whole city which is graphically represented in **Figure 6.4**.

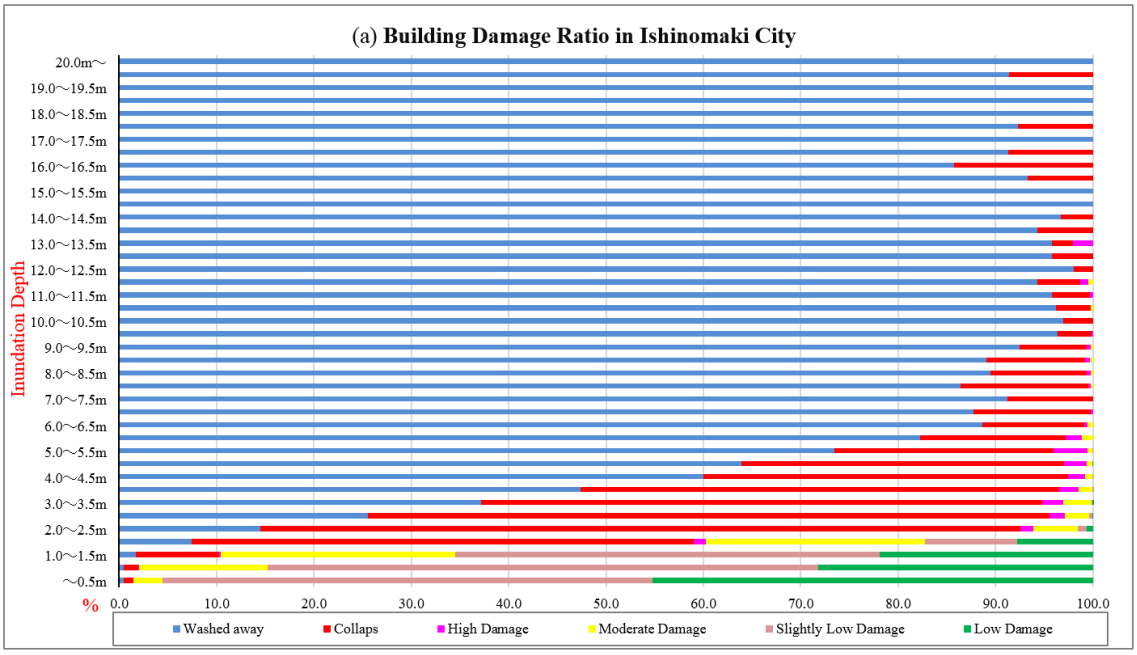

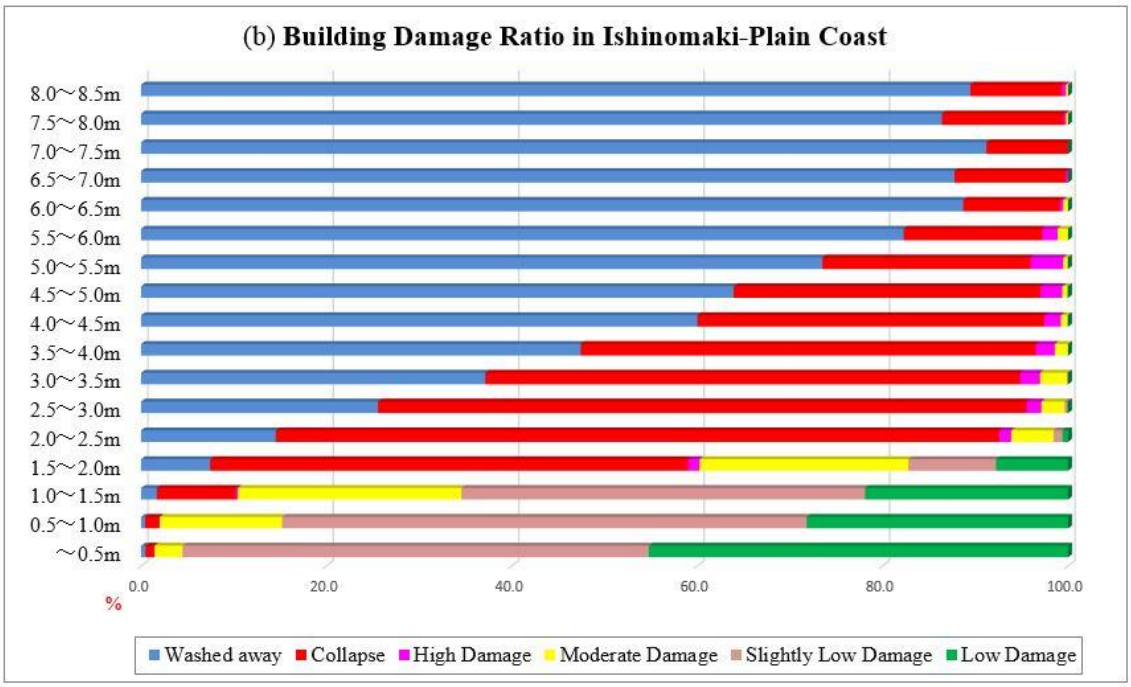


**Figure 6.4** Distribution of the total 52,904 building data surveyed by MLIT in Ishinomaki city a) inundation depth 0-20m b) Ishinomaki-plain coast inundation depth (0-8.5m).

According to **Figure 6.4** for higher inundation depth the amount of damages is increased. For instance, for an inundation depth interval below 0.5m low damage and slightly low damage are the most dominant. The inundation depth in the range of 0.5-1.5m about half of the buildings are slightly low damage while the rest building damages are mostly distributed between low damage and moderate damage. The range between 1.5-4.0m most buildings are collapse and for inundation depths over 4m most of the buildings are washed away. Since for inundation depth over 8m, more than 90% of buildings are washed away as shown in **Figure 6.4** (b).

### *6.3.3 Construction material*

The wave forces brought by a tsunami cause great damages to fragile buildings. Standing buildings in the path of the waves tend to block the water, and thus the pressure on them increases. The water force can be calculated by using the wave pressure distribution by Tanimoto formula. Water just 2m deep will impose pressure of approximately 20 kN per square meter, much more than any normal construction can remain undamaged. The deeper the water, the greater the pressure [138] [139]. Thus, one of the key factors to minimizing damage caused by tsunamis is to build constructions with basic requirements that can

withstand the damage of such storms. When comparing building materials, it was found that RC constructions were more likely to survive the wave forces brought by a tsunami, as compared to masonry and wood constructions, which did not survive well [128][136].

This part is dedicated to comparing statistically different building material damage during the east Japan great tsunami 2011 for Ishinomaki city with 63,157 buildings for the whole city and with 33,473 buildings for Ishinomaki plain coast as a case study. Each damaged building was measured and classified according to its damage level (six levels were defined by MLIT), construction material (RC, steel, wooden and other light weight construction such as clay or brick mentioned in text as others).

### *6.3.4 Damage levels distribution*

The damage data are classified according to the building material as shown in **Figure 6 .5** and **Figure 6.6** As it is expected, RC buildings could withstand best against tsunami waves with showing the lowest amount of damage and no RC building is recorded to be washed away. On the other hand, half of the wooden and other fragile structures are either washed away or collapsed. As for steel buildings expressed with over 50% either collapsed or high damaged.

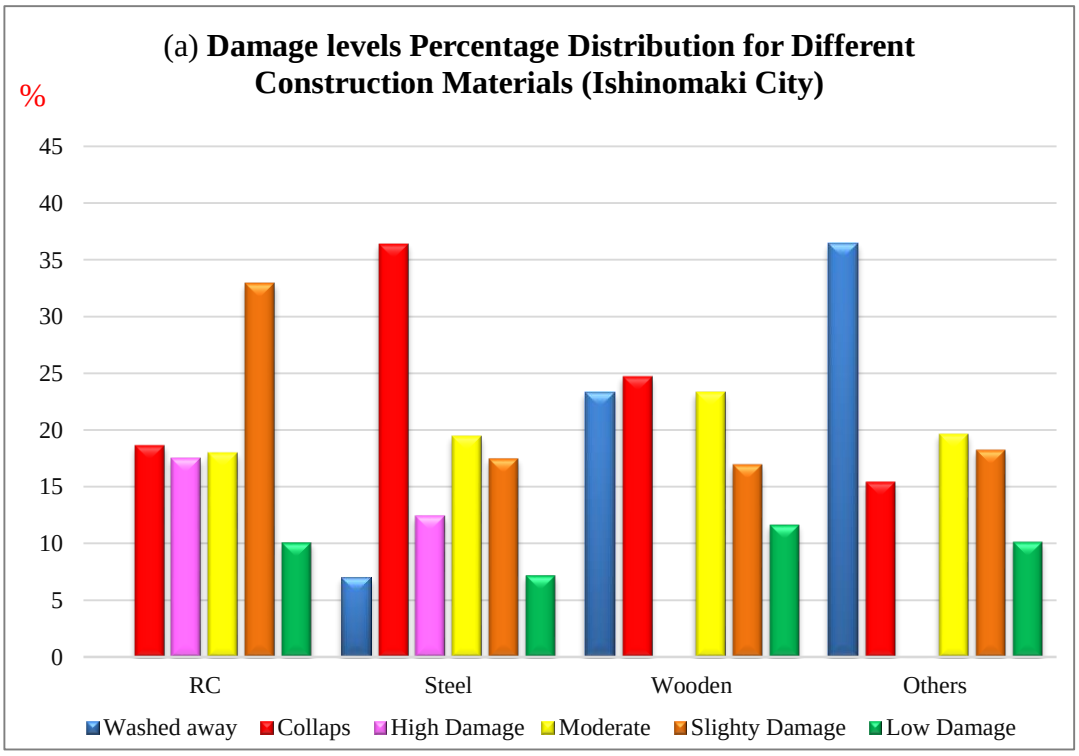

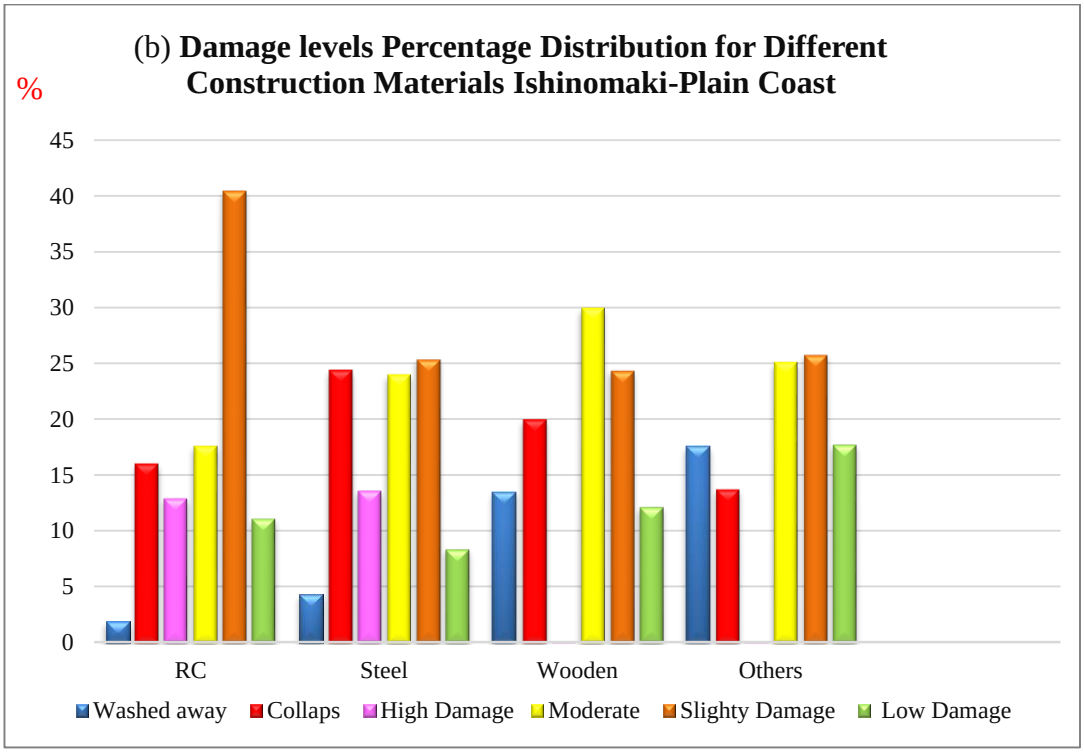


**Figure 6.5** Comparison of damage levels a) Ishinomaki city b) Ishinomaki-plain coast for different construction materials RC, Steel, Wood and Others.

In **Figure 6.6** for each different damage levels the percentage distribution of building materials are depicted and are compared in whole city via plain coast area. In **Figure 6.6** By considering collapsed and washed away buildings via slightly damaged ones, it can be recognized that the plain coast was less affected than whole city. The absence of wooden and others material in high damage levels is another result from this figure. Moreover, by looking at the slightly damaged buildings distribution, it can be concluded that with the same probability, wooden, steel and others material buildings are distributed.

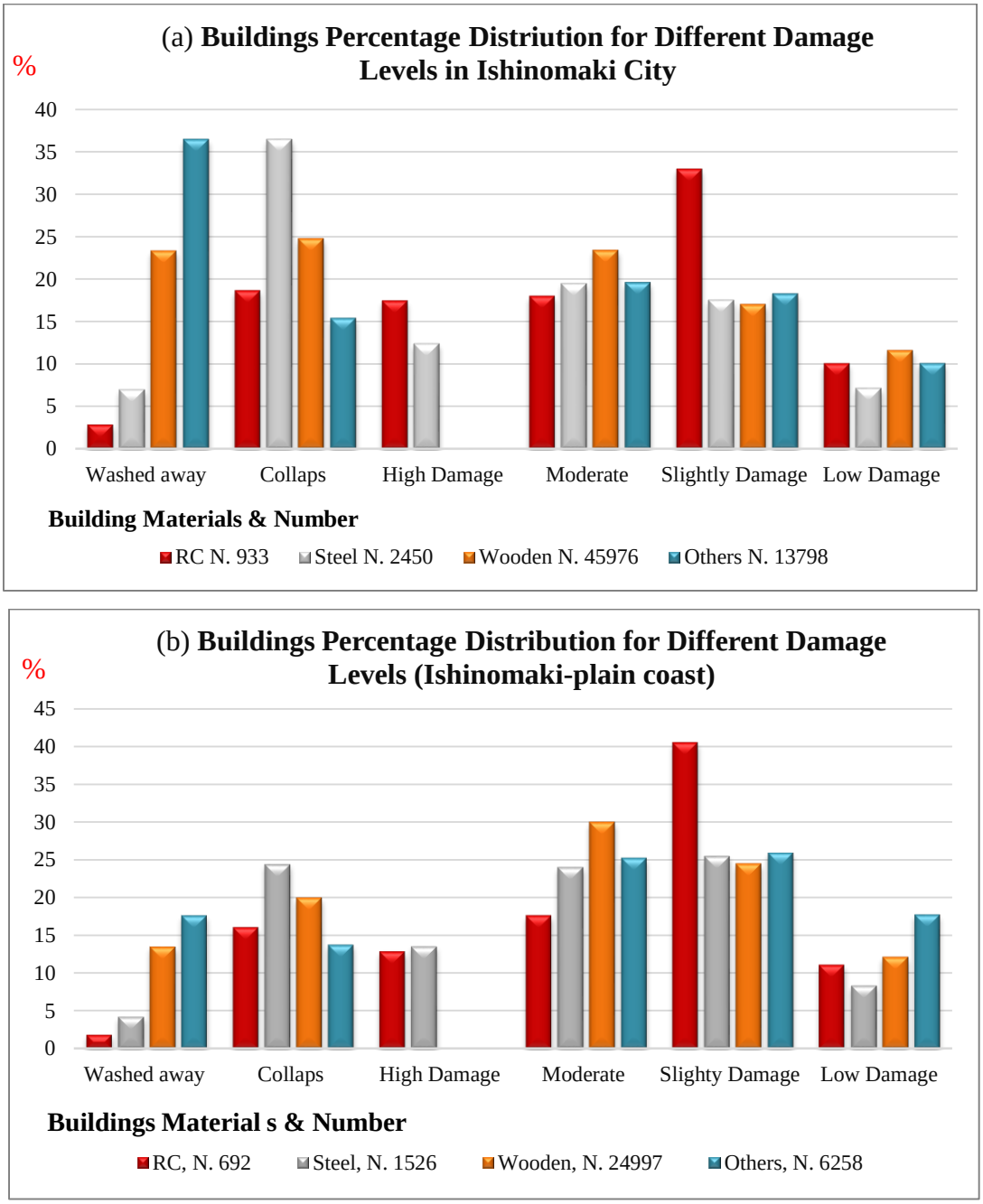


**Figure 6.6** Comparison of damage levels with construction material consideration a) Ishinomaki city b) Ishinomaki-plain coast.

### *6.3.5 Construction material and tsunami inundation*

As it is mentioned earlier the deeper the water, the greater the pressure and the greater the amount of damage is expected. With considering the inundation depth on an interval of 0.5-8.5m, the damage data for whole ishinomaki city is classified according to the type of

construction materials. For a given inundation depth interval, the percentage distribution of each damage level is calculated. The results are shown graphically in **Figure 6.7** for different constructions**.** According to **Figure 6.7** (a), the percentage damage distribution for RC material for the inundation depth range less than 2.0m only low and slightly damages are expected. For the inundation depth of 2.5-6.0m RC buildings are mostly high damaged since buildings located in inundation depth over 6m are all collapsed. For steel buildings as depicted in **Figure 6.7** (b), for inundation depth less than 2.0m low, slightly and moderate damages are observed. For inundation depth range of 2.0-6.5m most of steel buildings are collapsed (over 40%) and for over 6.5m is distributed between collapsed and washed away.

Wooden buildings shown in **Figure 6.7** (c) and other lightweight constructions building shown in **Figure 6.7** (d) are expressing almost similar damage distributions. For both cases, inundation depth less than 1.5m causes low, slightly, moderate (observed only for others) damages. Wooden and other fragile building material for inundation depth range of 1.5-4.0m are mostly collapsed and the inundation depth of 4.0m is the threshold for washed away buildings.

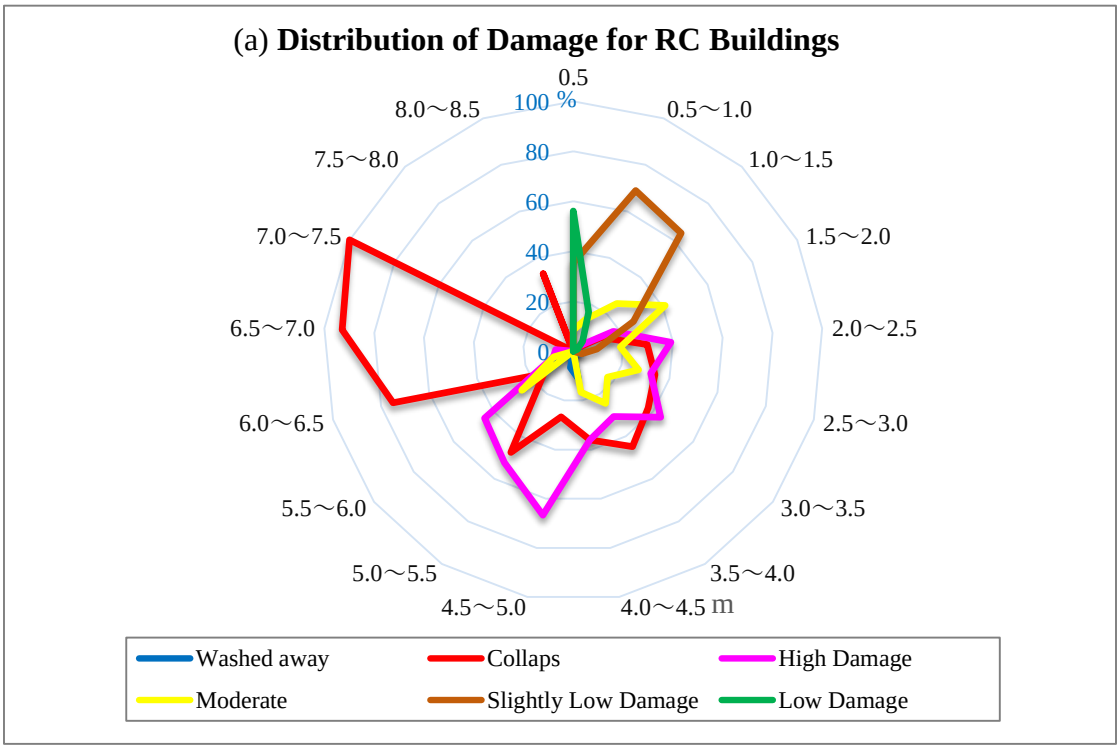

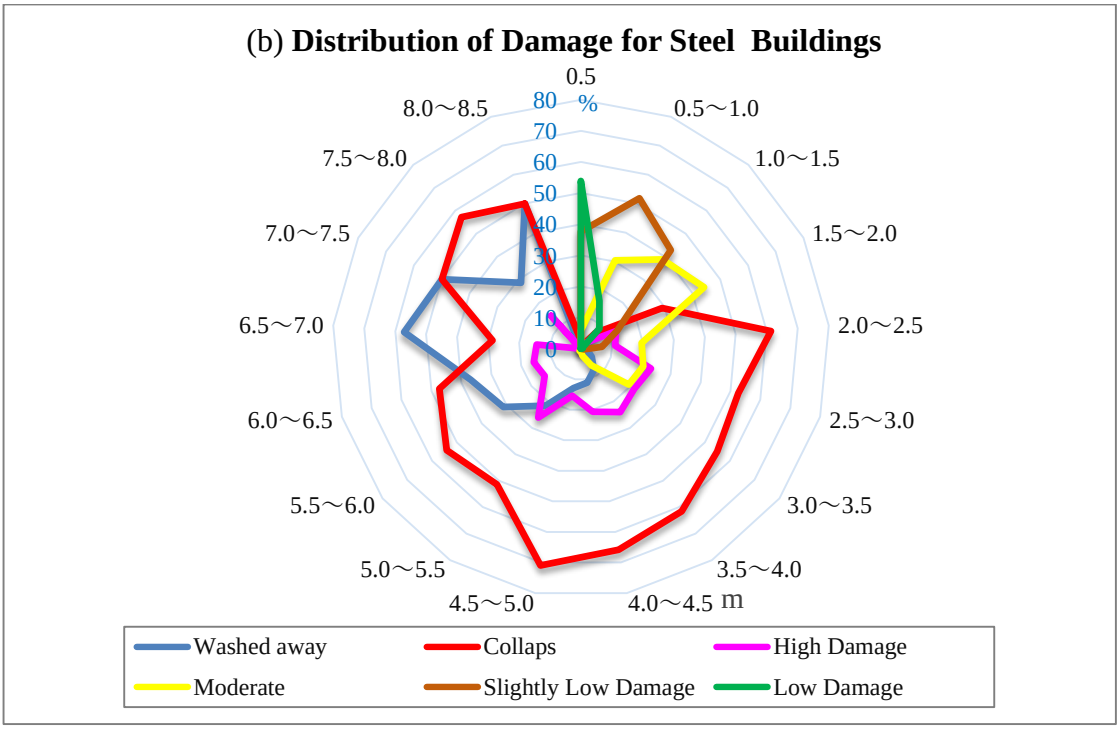
(b) Distribution of Damage for Steel Buildings
0.5
0.5～1.0
1.0～1.5
1.5～2.0
2.0～2.5
2.5～3.0
3.0～3.5
3.5～4.0
4.0～4.5
4.5～5.0
5.0～5.5
5.5～6.0
6.0～6.5
6.5～7.0
7.0～7.5
7.5～8.0
8.0～8.5
80
70
60
50
40
30
20
10
0
%
m
Washed away
Collaps
High Damage
Moderate
Slightly Low Damage
Low Damage

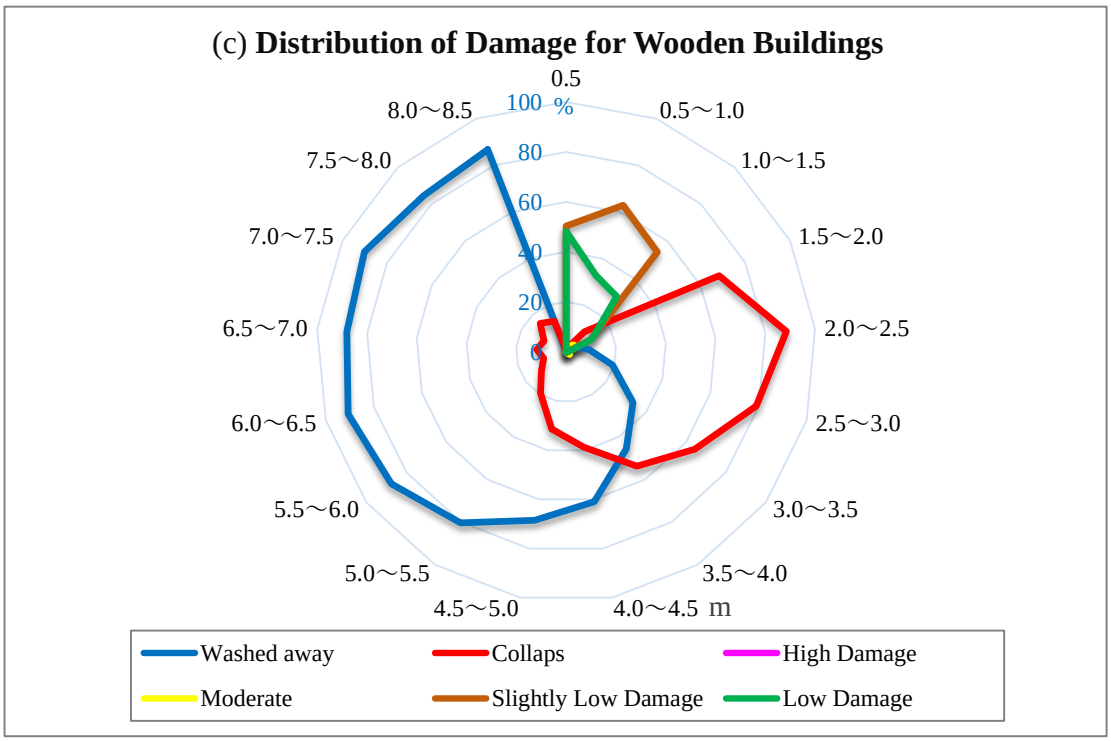
(c) Distribution of Damage for Wooden Buildings
0.5
0.5～1.0
1.0～1.5
1.5～2.0
2.0～2.5
2.5～3.0
3.0～3.5
3.5～4.0
4.0～4.5
4.5～5.0
5.0～5.5
5.5～6.0
6.0～6.5
6.5～7.0
7.0～7.5
7.5～8.0
8.0～8.5
100
80
60
40
20
0
%
m
Washed away
Collaps
High Damage
Moderate
Slightly Low Damage
Low Damage

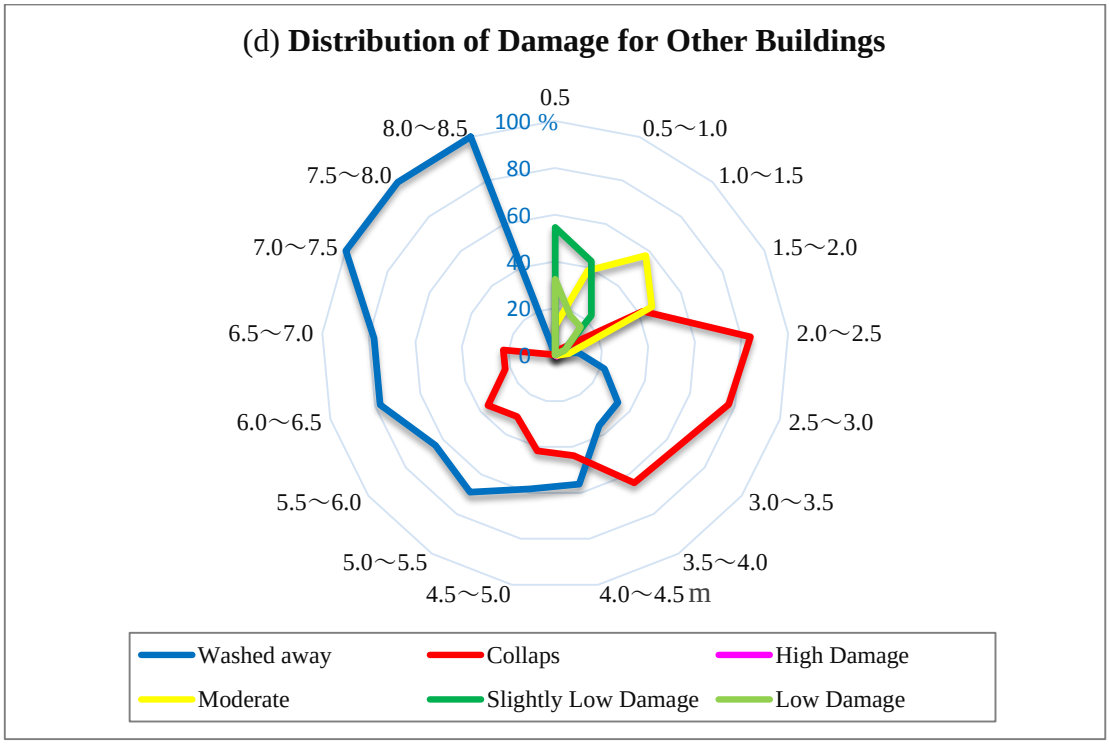


**Figure 6.7** Comparison of tsunami damage for different building material in Ishinomaki city separated for building material as a) RC, b) Steel, c) Wood and d) Others.

With considering inundation depth, the same data used in **Figure 6.7** are classified according to the levels of damage to better illustration of each construction materials distribution in amount of the damage in each level. The results are shown in **Figure 6.8**These classifications are also valuable because the comparison between different materials becomes possible. For instance by looking at **Figure 6.8** (a), the washed away inundation depth threshold is 3.0m for wooden and other fragile building material and for steel building over 4.0m while RC buildings are rarely influenced. It is also comprehended that for the washed away damage level, and for inundation threshold of 4.0m over half of the wooden or other weak buildings are washed away with similar graphical presentation. Also the collapse figure shown in **Figure 6.8** (b) Suggests the threshold of 1.5m to see this phenomena regardless of building material. It can be observed that wooden and other materials buildings start to collapse in much less inundation depth compared to RC buildings. According to **Figure 6.8** (c), only RC and steel are exposed to high damage. According to **Figure 6.8** (d), moderate damage for all building material are distributed for inundation depth range of 1.0-2.0m. Slightly low damage buildings are observed for mostly inundation depth range of 0.5-1.0m for all building material as shown graphically in **Figure**

**6.8** (e). And finally, buildings with lower damage level are accumulated in inundation depth less than 0.5m shown graphically in **Figure 6.8** (f).

(a) **Distribution of Damage for Washed away Buildings**

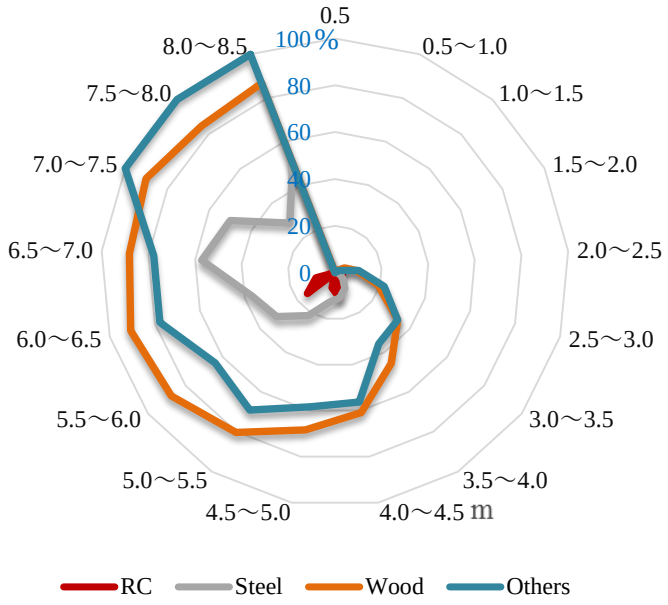


(b) **Distribution of Damage for Collaps Buildings**

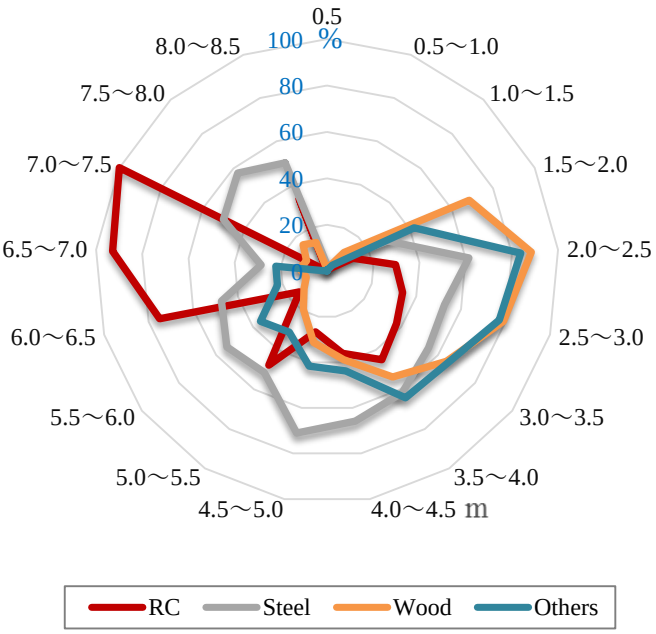

(c) **Distribution of Buildings for High Damage Classification**

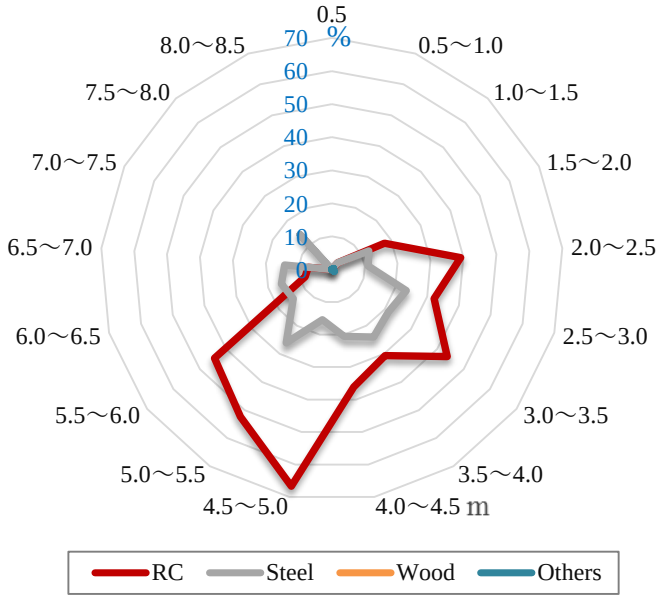


(d) **Distribution of Buildings for Moderate Damage Classification**

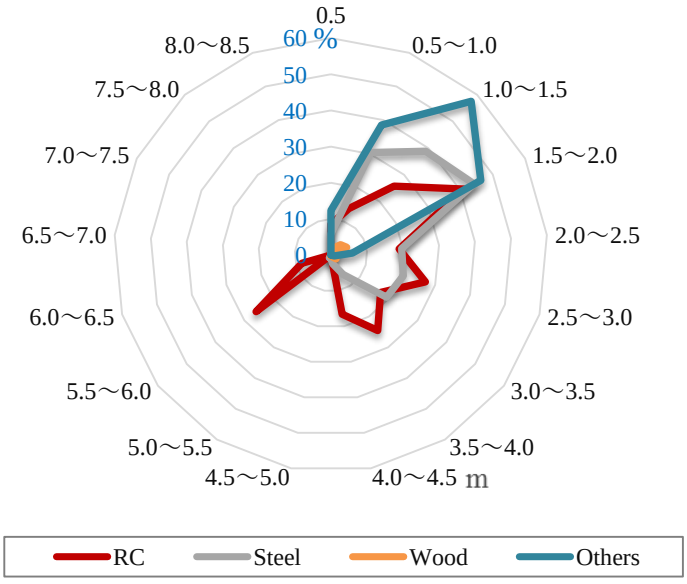

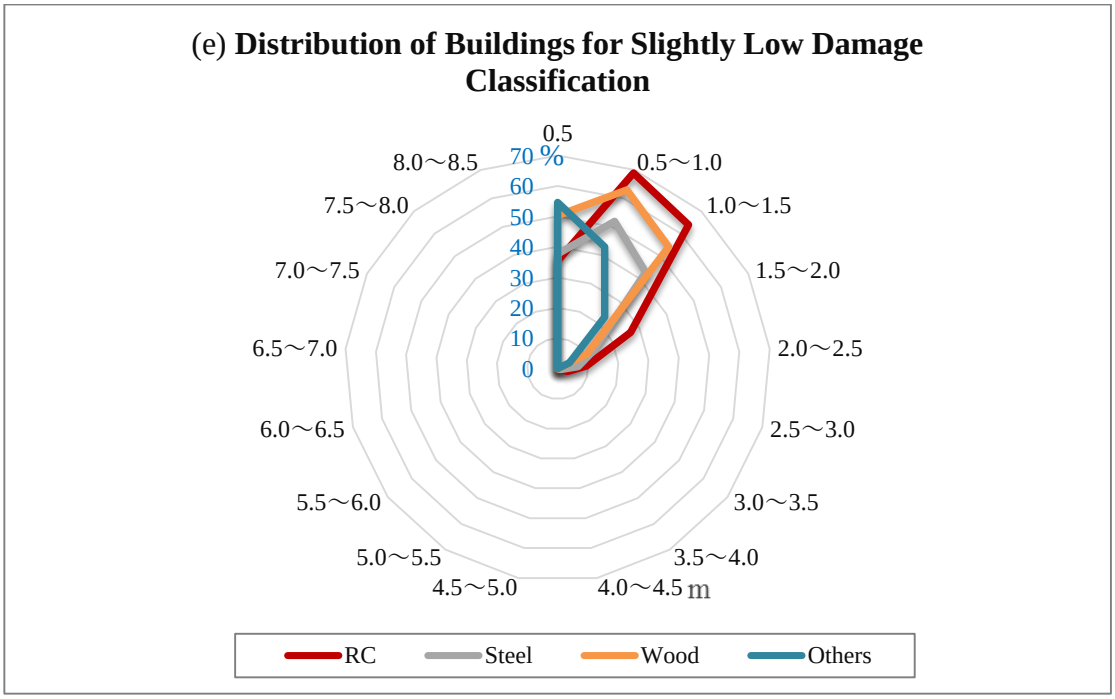


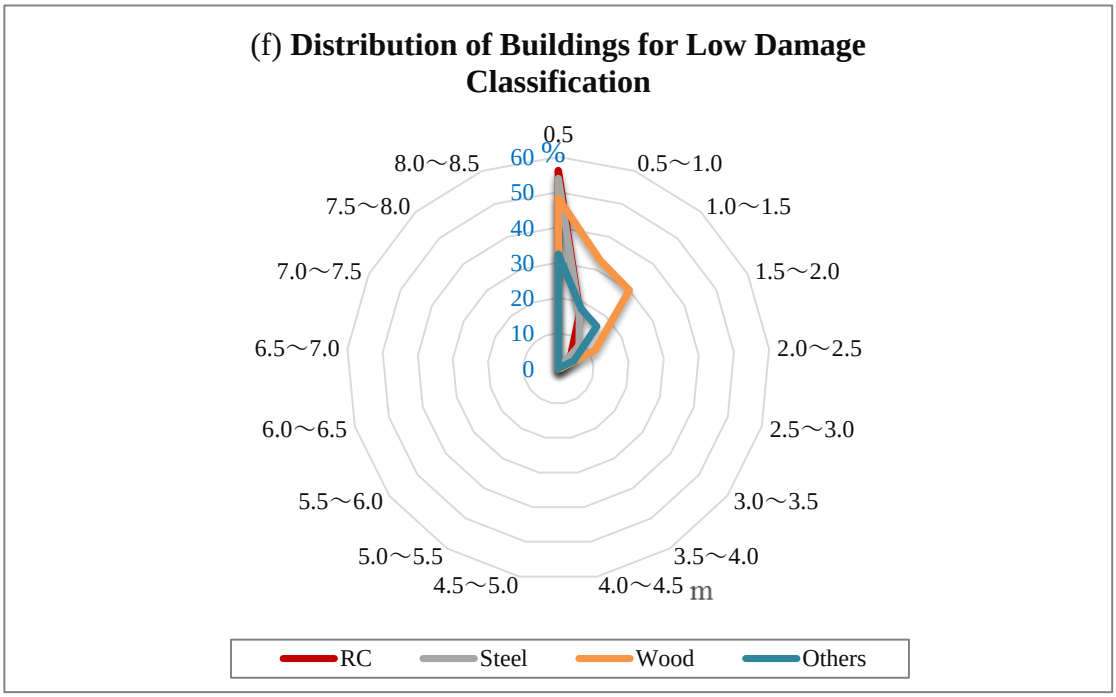


**Figure 6.8** Comparison of tsunami damage for different building material in Ishinomaki plain coast separated for six different damage levels. a) Washed away, b) Collapsed, c) High damage, d) Moderate damage, e) Slightly low damage f) low damage.

As it is mentioned earlier, the number of stories also plays an important role in the extent of damage where the statistics for the plain coast are classified and showed in the **Table 6.5** and **Figure 6.9** indicating that the buildings with multiple stories were less vulnerable to damage.

**Table 6.5** Distribution of the number of buildings based on the damage classification and the number of stories in Ishinomaki plain coast area.

| Classification | Number of Stories | | | | | | | | | |
|---|---|---|---|---|---|---|---|---|---|---|
| | 2 | 3 | 4 | 5 | 6 | 7 | 8 | 9 | 11 | 14 |
| Washed away | 3,357 | | | | | | | | | |
| High Damage | 915 | 3 | | | | | 1 | | | |
| Moderate Damage | 276 | 2 | 5 | | 1 | | | | | |
| Low Damage | 456 | 5 | 1 | | | | | | | |
| No Damage | 27,862 | 379 | 152 | 32 | 12 | 6 | 4 | 2 | 1 | 1 |
| Total | 32,866 | 389 | 158 | 32 | 13 | | 5 | 2 | 1 | 1 |

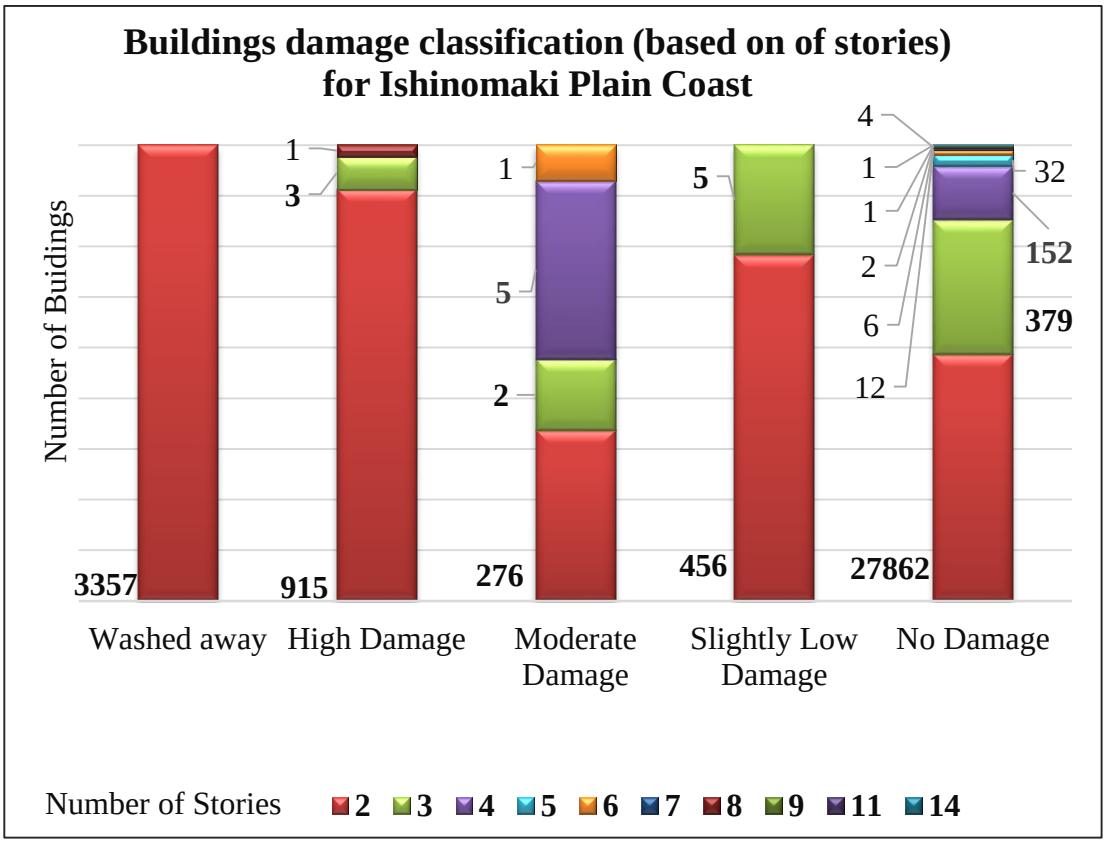


**Figure 6.9** Building damage classification based on the number of stories in Ishinomaki plain coast area.

## *6.4 Tsunami damage map*

**Figure 6.10** shows the tsunami damage area map in the Ishinomaki area as output of this calculation. We estimated the statistics of the tsunami damage map based on the damage classification of five factors used in this study is shown in **Table 6.6** while the damage

index of 125,548.39 grid cells are ranged between 1 to 5, with a standard deviation of 0.645. The GIS produced tsunami damage map is shown in **Figure 6.11** which is in good agreement (94.98%) with the historical data recorded by "GSI" and "2011 Earthquake Tsunami Joint Survey Group"

**Table 6.6** Tsunami damage classification based on the inundated area.

| Damage index | Damage Area Classification | | | |
|---|---|---|---|---|
| | Damage Classification | Damage Value in Tsunami Damage Map | Area ($km^2$) | Area (%) |
| 1 | Low | 1.30 - 1.59 | 2.65 | 18.69 |
| 2 | Slightly low | 1.59 - 1.87 | 3.22 | 22.77 |
| 3 | Medium | 1.87 - 2.34 | 3.02 | 21.35 |
| 4 | Slightly high | 2.34 - 2.97 | 3.07 | 21.71 |
| 5 | High | 2.97 - 4.32 | 2.19 | 15.48 |

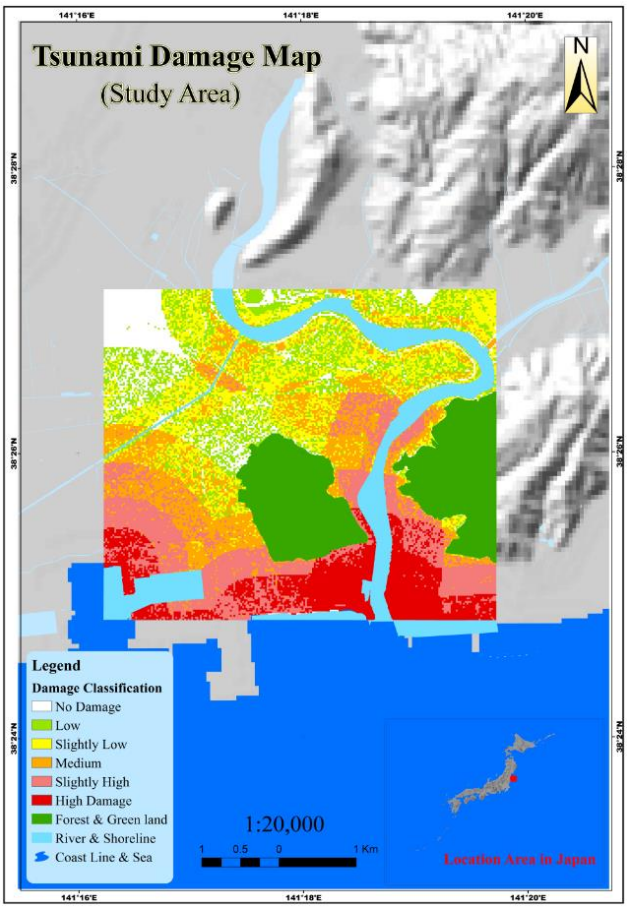


**Figure 6.10** Tsunami damage map of study area in Ishinomaki city.

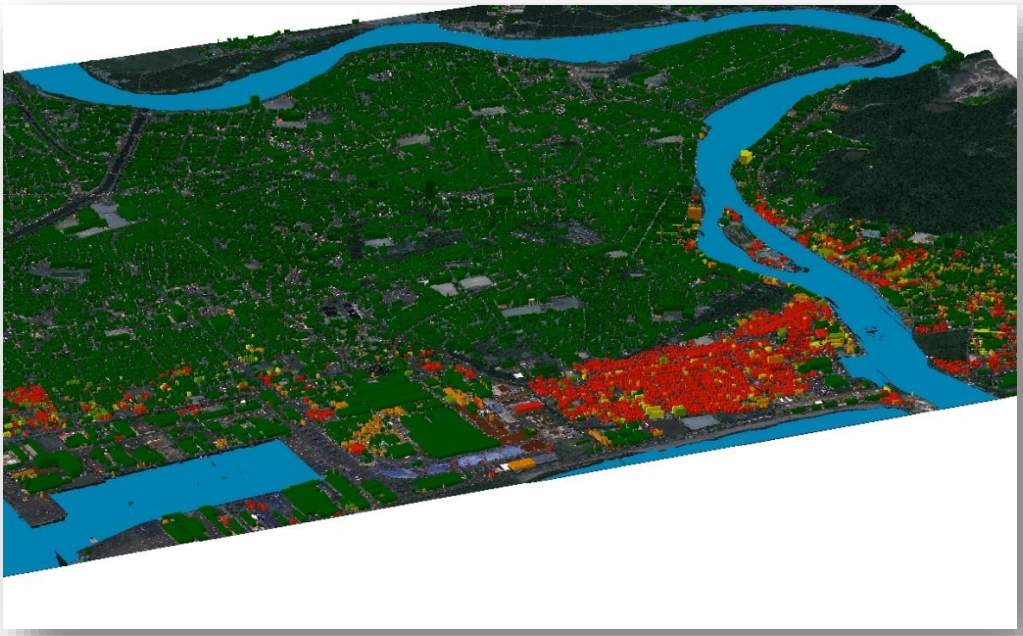

**Figure 6.11** Tsunami 3D-damage map of study area in Ishinomaki city.

Based on the result of our study, which is shown in **Figure 6.12** the inundation damage area was 14.16km$^2$, while GSI reported that the inundation damage area in Ishinomaki in the 2011 Japan tsunami was 13.45km$^2$.

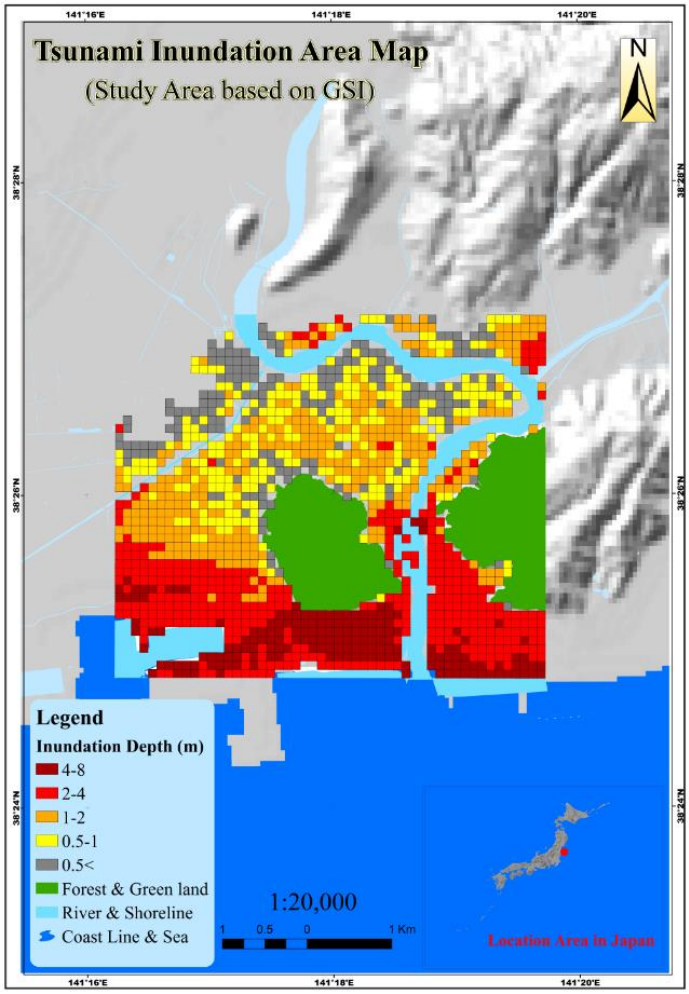


**Figure 6. 12** Tsunami inundation map in Ishinomaki- plain coast (Published by GSI).

## *6.5 Summary*

Building damage data of Ishinomaki city, with special attention to the plain coast affected area, were classified and analyzed using data surveyed by the MLIT for more than 52,000 structures. The classification includes information on six levels of damage, four types of building materials and damage percentage due to tsunami inundation for each building material which are necessary information for an effective hazard mitigation.

The main findings of this study and their applicability are summarized as below:

• The MLIT survey data of Ishinomaki city and its plain coast were classified to obtain key material factors controlling the amount of damage. RC, steel, wooden and other building materials were compared in different inundation depth. The results show a better resistant performance of RC and steel buildings over wood or other buildings.

• For each damage level class different inundation depth threshold were founded. For different materials, the damage levels distribution under the same inundation depth was found and compared between different materials.
• For each material, the damage behavior of the buildings due to the inundation depth were graphically illustrated that will be a great conclusion to assess the damages due to inundation depth.
• It is also found that coastal topography can have a significant influence on building damage. By means of GIS tool the inundation depth can be estimated and by means of presented data in construction material section, one can assess the amount of damage for a given area map.

These are important considerations in designing a tsunami evacuation building, material and location, and assessing the damages for other cities in danger of future tsunami attach.

In other words, the damage is not only controlled by the tsunami height which is dependent highly to coastal topography, but also highly dependent on the building materials.

By using multiple geospatial variables of topographic elevation, relation to tsunami direction, coastal proximity, and coastal shape incorporated by the AHP, an appropriate pair-wise comparison of AHP are proposed to construct a weighting scheme for the geospatial variables and assessing tsunami vulnerability. However, the damage is not only controlled by the tsunami height which is dependent highly to coastal topography, but also highly dependent on the building materials. By knowing the fragility of different building material for each inundation depth, as shown in this study, one can assess with a good precision the amount of damage. We propose using the illustrated figures of damage for different building materials due to different inundation depths together with GIS results as a powerful approach to assess the damages on buildings for an area attacked by tsunami storms. This approach can be employed to evaluate the assessment of the vulnerable areas that could be affected by tsunami hazard in future natural disasters.

# Chapter 7

## Disaster Management and Mitigation Strategy

In this chapter, the aim of disaster management and mitigation is to reduce the consequences of an event. These consequences include saving of lives and capitals. The prerequisite for this purpose is to know how will be the extent of the damages and how much is the quantities to enable us for an appropriate preparedness program. The more exact the data of the vulnerabilities, the more effective the management of its effects. Previous chapters presented an integrated approach for vulnerability assessment using the most effective and fast method combining the advantages of remote sensing and GIS systems. This chapter introduce the frame work of disaster mitigation and management and shows how we can utilize the previous outputs from vulnerability assessment process for better disaster management in tsunami events.

### *7.1 Important elements in comprehensive disaster management*

Topics concerning overall disaster prevention measures for metropolitan areas have been organized and categorized here. In order to establish a framework for future disaster management, the following five critical elements must be considered

#### *7.1. 1 Natural and social phenomena*

We cannot simply categorize disasters as natural phenomena. An earthquake and its tsunami with the greatest magnitude cannot be classified as a disaster if there is nothing in its proximity to sustain damage. On the other hand, a tsunami that is small, but causes substantial impacts to population and the built environment is however, disaster management has focused on damage caused by tsunami largely from the perspective of natural science. That is, disasters have been assessed on the basis of human casualties

and physical damage to structural systems. **Figure 7.1** shows integrated research fields for disaster mitigation and emergency response.

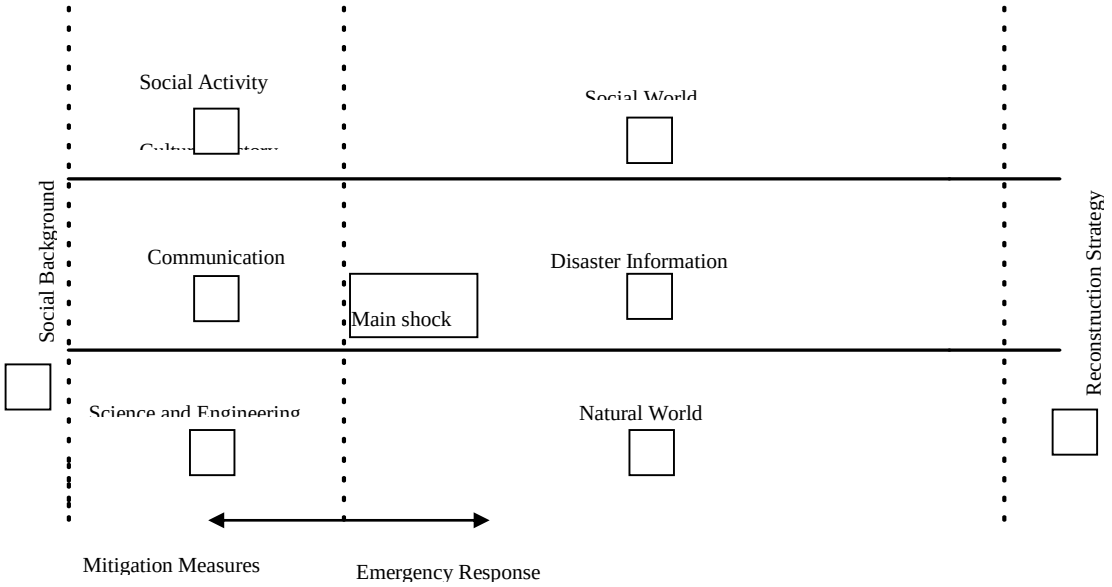


**Figure 7.1** Integrated research fields for disaster mitigation

### *7.1.2 Pre-disaster mitigation and post-disaster management measures*

There are two facts to disaster-management measures: pre-disaster damage mitigation and post-disaster management. The tsunami dramatically revealed the inadequacies of Japan's disaster mitigation measures. Concurrently, post-disaster management systems employed for the minimization of earthquake and tsunami damage and the prevention of secondary hazards were found to be insufficient as well. With these facts in mind, an appropriate balance is needed in effective pre- and post-disaster management procedures.

### *7.1.3 Information management*

Two types of phenomena exist in disaster management that are physical and social, which affect each of the two facets of disaster, being pre- and post-disaster. The correlation of these attributes contributes to chain reaction damage over time, and disasters evolve both rapidly and extensively. In order to meet the demands of evolving circumstances, an overall grasp of the situation is required and an information management system capable of deciphering the correlation of each of the disaster's attributes needed.

### *7.1.4 Disaster Management Philosophy*

As the basis of disaster management measures, a consensus must be reached as to what should be protected in society, who will do the protecting, how the protecting will be done and how much protection will be extended. The disaster prevention measures may be achieved based upon the self-awareness of each and every citizen regarding this matter. How safety and assurance are conceived is of fundamental importance. This is, in effect, the philosophy of disaster management.

### *7.1.5 Disaster and social management*

The development of a comprehensive approach to disaster management cannot be achieved if disaster management measures are devised in isolation of the many problems to which society is subjected. In this regard disaster management becomes an indispensable function within an ideal society.

## *7.2 Issues Requiring Future Disaster Mitigation Strategy*

Following in **Table 7.1** shows 18 issues are to be discussed as topics for disaster mitigation.

**Table 7.1** Discussion topics for disaster mitigation

| | |
|---|---|
| 1. Crisis Management | 10. Disaster Information |
| 2. Psychology of Disaster victims | 11. Traffic Functions |
| 3. Victims － Search and Rescue | 12. Maritime Functions |
| 4. Victims － Emergency Shelters | 13. Lifelines |
| 5. Volunteers | 14. Damage to Structures |
| 6. Disaster Prevention Plans － Legal Aspects | 15. Landslide Damage |
| 7. Disaster Prevention Plans － Planning Aspects | 16. Foundation Damage |
| 8. Disaster Prevention Plans － Economic Aspects | 17. Earthquake Motion |
| 9. Disposal of Debris | 18. Active Faults, Tectonics, Changes in marine phenomena |

In the past, investigations of earthquake disasters in metropolitan areas were performed first with the understanding of the natural phenomenon and then in terms of the development into a disaster that caused a chain reaction of damage. In contrast to this simple cause-and-effect approach, our working groups were instructed to begin their investigations with the social impact of the quake. In this fashion, the components required in constructing a framework for the comprehensive study of disaster management were formed.

## *7.3 Utilizing the vulnerability results from integrated remote sensing and GIS for disaster management*

### *7.3.1 General Framework*

Disaster management planning is structured around the disaster management cycle model. **Figure 7.2** shows the disaster management cycle which consists of four stages reduction, readiness, response and recovery. Remotely sensed data can provide a valuable source of information at each of these stages, helping to understand spatial phenomena, and providing scientists and authorities with objective data sources for decision making. The challenge with disaster management is that the inherent unpredictability and range of hazards does not allow for a single all-encompassing solution to be developed and explored.

Remote sensing can be used to assist risk reduction initiatives through identification of hazard zones associated with flood plains, coastal inundation and erosion, and active faults. It can also be used to verify hazard models by measuring the location and magnitude of actual events. Imagery is widely used by meteorologists for providing weather forecasting and warnings of potentially severe weather events, providing the public and emergency responders with information that can assist decision making around short term readiness. These images are commonly presented in print, television and on the internet, and they are well accepted by viewers around the world.


**Figure 7.2** The disaster management cycle

### *7.3.2 Utilization Steps and Objectives*

Mitigation of natural disasters can be successful only when detailed knowledge is obtained about the expected frequency, character, and magnitude of hazardous events in an area. Many types of information that are needed in natural disaster management have an important spatial component. Spatial data are data with a geographic component, such as maps, aerial photography, satellite imagery, GPS data, rainfall data, borehole data etc. Many of these data will have a different projection and co-ordinate system, and need to be brought to a common map-basis, in order to superimpose them. We now have access to information gathering and organizing technologies like remote sensing and geographic information systems (GIS), which have proven their usefulness in disaster management.

First of all, remote sensing and GIS provides a data base from which the evidence left behind by disasters that have occurred before can be interpreted, and combined with other information to arrive at hazard maps, indicating which areas are potentially dangerous. The zonation of hazard must be the basis for any disaster management project and should supply planners and decision-makers with adequate and understandable information. Remote sensing data, such as satellite images and aerial photos allow us to map the variabilities of terrain properties, such as vegetation, water, and geology, both in space and time. Satellite images give a synoptic overview and provide very useful

environmental information, for a wide range of scales, from entire continents to details of a few meters.

Secondly, many types of disasters, such as floods, drought, cyclones, volcanic eruptions, etc. will have certain precursors. The satellites can detect the early stages of these events as anomalies in a time series. Images are available at regular short time intervals, and can be used for the prediction of both rapid and slow disasters.

Then, when a disaster occurs, the speed of information collection from air and space borne platforms and the possibility of information dissemination with a matching swiftness make it possible to monitor the occurrence of the disaster. Many disasters may affect large areas and no other tool than remote sensing would provide a matching spatial coverage. Remote sensing also allows monitoring the event during the time of occurrence while the forces are in full swing. The position of satellites makes it ideal for us to think of, plan for and operationally monitor the event. GIS is used as a tool for the planning of evacuation routes, for the design of centers for emergency operations, and for integration of satellite data with other relevant data in the design of disaster warning systems.

In the disaster relief phase, GIS is extremely useful in combination with Global Positioning Systems (GPS) in search and rescue operations in areas that have been devastated and where it is difficult to orientate. The impact and departure of the disaster event leaves behind an area of immense devastation. Remote sensing can assist in damage assessment and aftermath monitoring, providing a quantitative base for relief operations.

In the disaster rehabilitation phase, GIS is used to organize the damage information and the post -disaster census information, and in the evaluation of sites for reconstruction. Remote sensing is used to map the new situation and update the databases used for the reconstruction of an area, and can help to prevent such a disaster that occurs again.

In order to utilize the previous study for disaster management the following objectives are considered:

- Evaluate the spatial data requirements in disaster risk management
- Use GIS and RS as a tools for hazard, vulnerability and risk (HVR) assessment
- Use risk information in planning disaster reduction intervention through spatial multi-criteria analysis
- Utilize existing sources of past disaster information and elements at risk data

- Assess spatial data availability and understand the importance of Spatial Data Infrastructure (SDI), for data sharing by organizations involved in disaster risk management
- Apply GIS and RS for designing implementations of large scale early warning systems
- Use participatory GIS (PGIS) at community level
- Application of remote sensing data and image processing techniques to monitor hazardous events and assess damage
- Damage assessments in order to generate information for recovery planning
- Evaluate Spatial Data Infrastructure (SDI), for data sharing by organizations involved in disaster risk management
- Design and implement their own GIS projects that integrate remote sensing data, GPS-based field information, and HVR models and analysis in a proper geospatial and cartographic framework

The key elements to facilitate the usefulness of remote sensing data in support of the disaster management community are being able to provide the appropriate information in a spectrally, temporally, and spatially relevant context. Additionally, one must be aware of the information requirements of that disaster management community, and tailor the remote sensing information to meet those needs. That can only come through close collaborations between the disaster management community and the remote sensing / geospatial community.

### *7.3.3 Implementation*

The volume of data needed for disaster management, particularly in the context of integrated development planning, clearly is too much to be handled by manual methods in a timely and effective way. For example, the post disaster damage reports on buildings in an earthquake or tsunami stricken city, may be thousands. Each one will need to be evaluated separately in order to decide if the building has suffered irreparable damage or not. After that all reports should be combined to derive at a reconstruction zoning within a relatively small period of time [140]-[142].

The data required for disaster management is coming from different scientific disciplines, and should be integrated. Data integration is one of the strongest points of GIS. In general the following types of data are required:

• Data on the disastrous phenomena (e.g. landslides, floods, earthquakes), their location, frequency, magnitude etc.

• Data on the environment in which the disastrous events might take place: topography, geology, geomorphology, soils, hydrology, land use, vegetation etc.

• Data on the elements that might be destroyed if the event takes place: infrastructure, settlements, population, socioeconomic data etc.

• Data on the emergency relief resources, such as hospitals, fire brigades, police stations, warehouses etc.

The amount and type of data that has to be stored in a GIS for disaster management depends very much on the level of application or the scale of the management project. Natural hazards information should be included routinely in development planning and investment project preparation. Development and investment projects should include a cost/benefit analysis of investing in hazard mitigation measures, and weigh them against the losses that are likely to occur if these measures are not taken. Although the selection of the scale of analysis is usually determined by the intended application of the mapping results, the choice of an analysis technique remains open. This choice depends on the type of problem, the availability of data, the availability of financial resources, the time available for the investigation, as well as the professional experience of the experts involved in the survey.

Based on the analyses in the previous chapters we have shown the data required to be used for disaster management. In order to estimate the fatalities and injuries and thus the help and rescue works to be done we need to match the population map and vulnerability map. **Figure 7.3** shows the population map of the region under study.

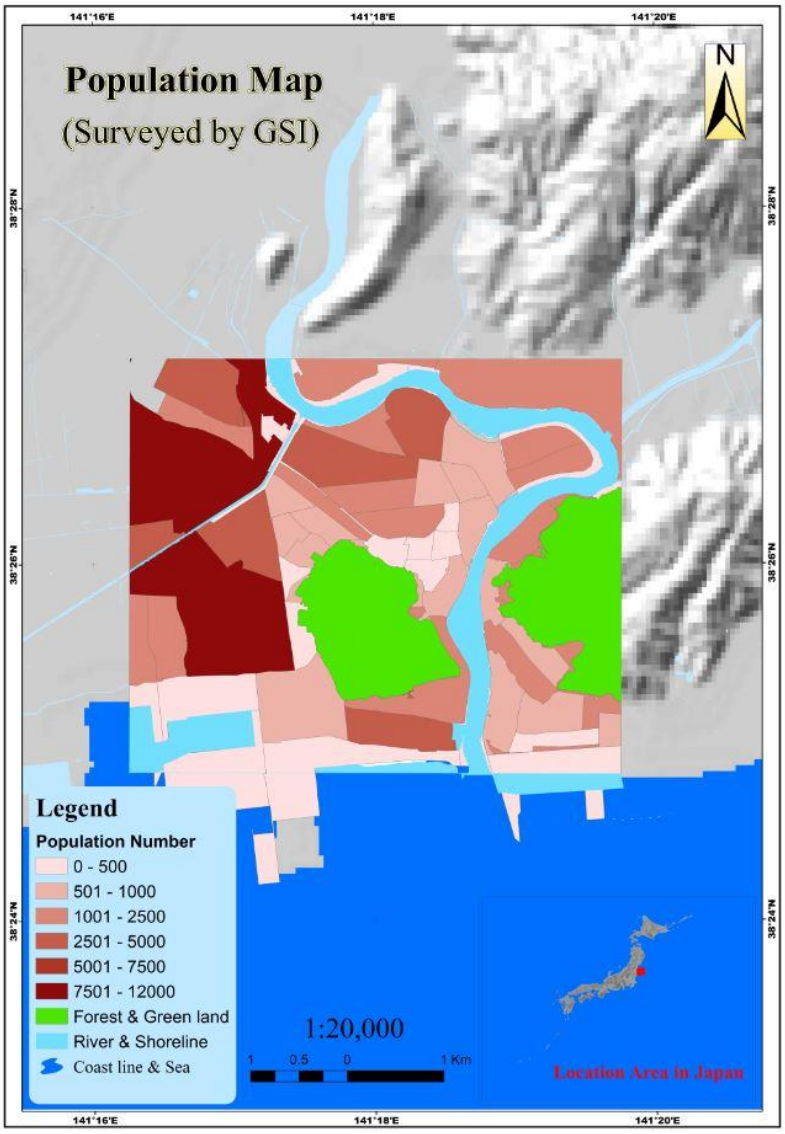


**Figure 7.3** The population map of the region under study

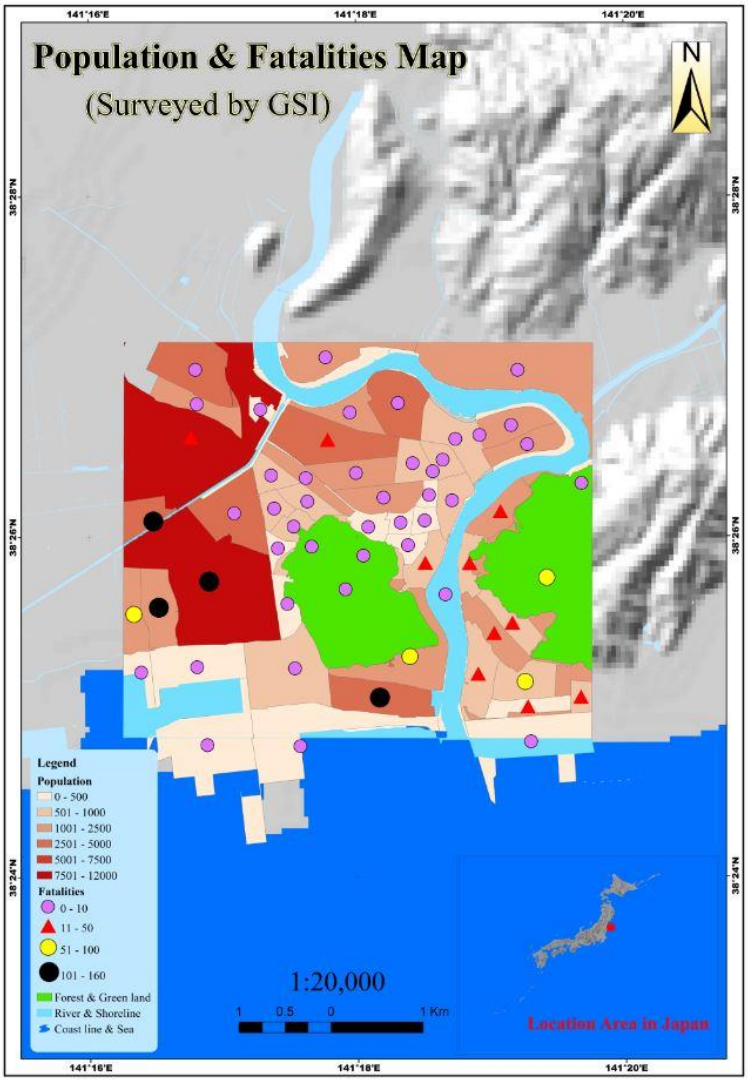


**Figure 7.4** The distribution of the number fatalities based on damage map

Thus at the first step the following priorities might be considered:

- Distribution of fatalities to arrange for rescue operations
- Distribution of emergency building such as hospital for mitigation of the rescue process
- Distribution of capitals and important facilities and lifeline sources to help for decision making for restoration process

**Figure 7.4** shows the map for the number of fatalities in the region. Such a map help to concentrate the rescue operation and find the zones for implementation of that. **Figure 7.5** shows the distribution of the hospitals and those located in damaged areas and also those can be used for rescue and mitigation process.

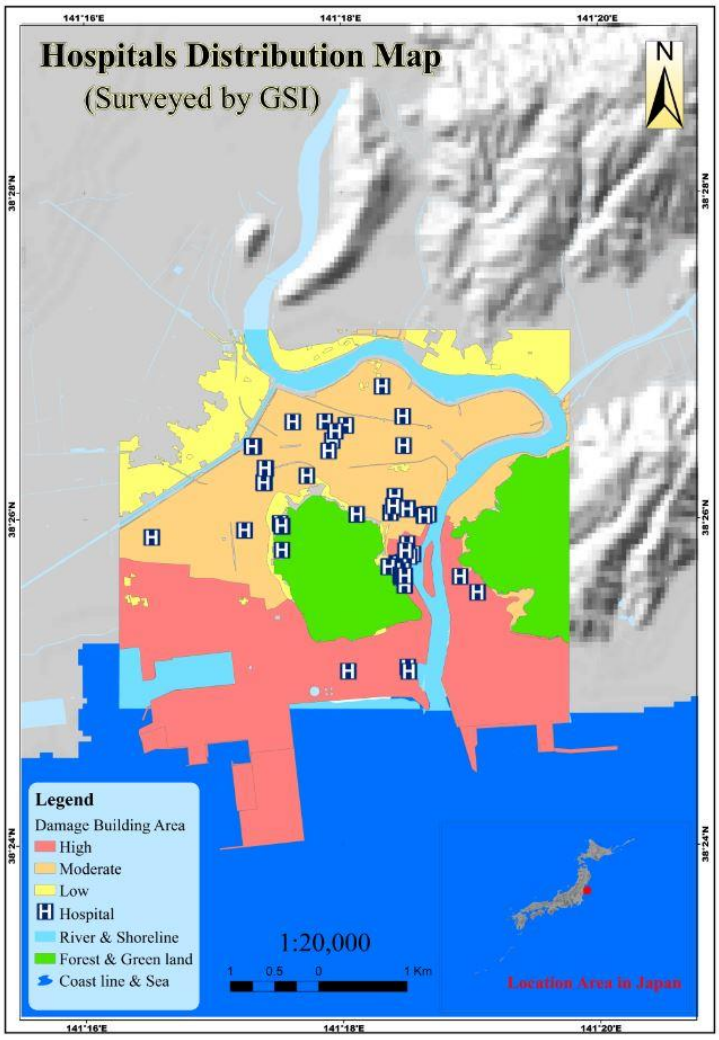


**Figure 7.5** The distribution of the hospitals as one of the emergency covering items

One of the other items which is important to know is the concentration points of population. This will held the disaster manager to know where he should send the most rescue team. The distribution of the training centers to estimate the concentration of the rescue operation are shown in **Figure 7.6** **Figure 7.7** shows the maps of distribution of important facilities which are necessary to be used for restoration operation. The existence and service ability of these facilities play an important role in the disaster management. **Figure 7.8** presents the location of capitals or the distribution of industrial facilities which are to be saved or also be used as a next step after rescue operation and emergency process.

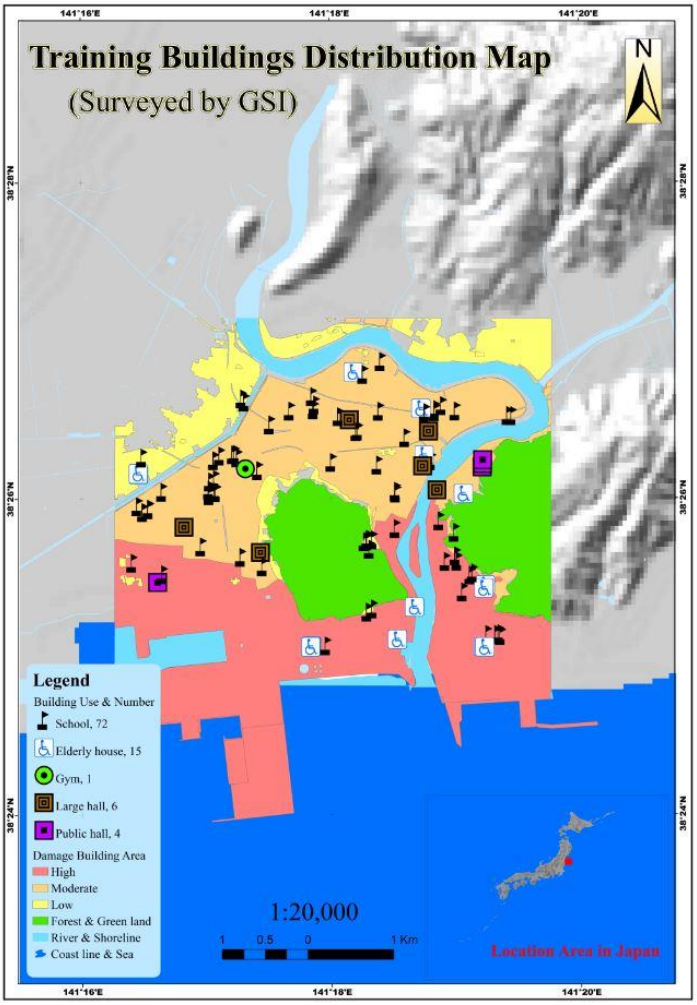


**Figure 7.6** The distribution of the training centers to estimate the concentration of the rescue operation

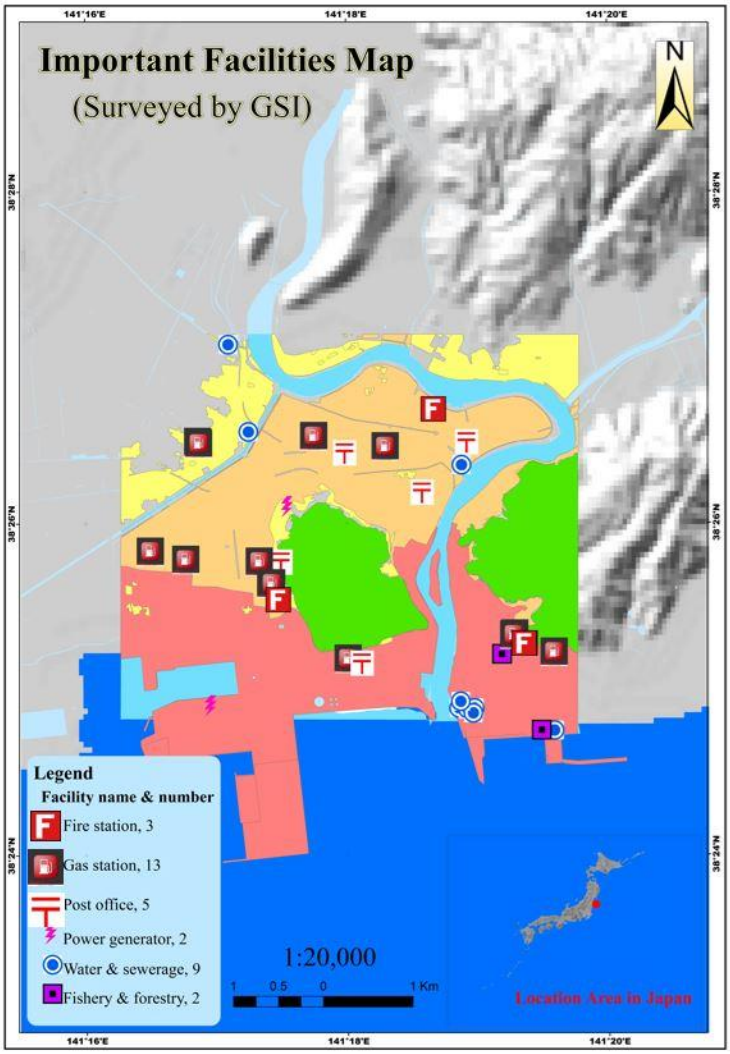


**Figure 7.7** The map of distribution of important facilities for restoration operation

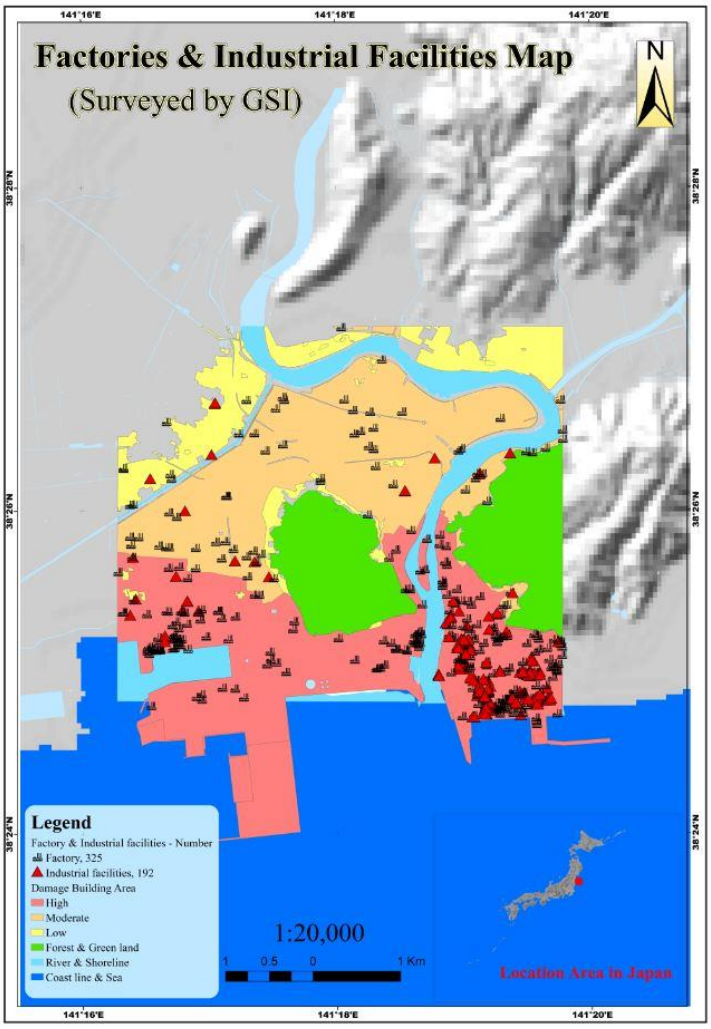


**Figure 7.8** The distribution of industrial buildings and areas for management of capital saving process

Based on the above analyses experts are provided with the data required to be used for disaster management. In order to estimate the fatalities and injuries and thus the help and rescue works to be done, the population map and vulnerability map and other auxiliary maps are given above. These maps are also necessary during critical time and recovery and reconstruction phases.

# Chapter 8

## Conclusion

In this research, we proposed the combined analysis of digital elevation data, very high resolution satellite images, tsunami historical data, together with an Analytical Hierarchy Process (AHP) method with proper factors and suitable scores to produce the vulnerability and damage maps. It is a first attempt for assessing tsunami vulnerability by using the factors of shoreline distance, river distance, elevation, vegetation, and slope through applying the AHP method combined with raster overlay tools through GIS processing in Ishinomaki area. The AHP has been extensively applied to decision-making problems, and extensive research has been carried out to apply AHP to risk assessment. For spatial multi-criteria analysis by means of GIS, the input data as a set of maps and attribute tables that include the spatial information of the study area, are grouped, standardized and weighted. The output is one or more composite index maps, which indicates the realization of the vulnerable hazardous areas.

It has been shown that remote sensing can be capable to achieve information about the input factors for tsunami vulnerability mapping and impact assessment. In the study area, several indicators of vulnerability can be achieved using a very high resolution satellite. It is very useful to derive data about the DEM in high spatial resolution so the output of the research will have more accuracy.

It is shown that a suitable set of factors, including elevation, slope, coastal proximity, hydrological feature, vegetation, and land use can be used to obtain an appropriate output, which is close enough to the actual event such as tsunami vulnerability, tsunami disaster management, and tsunami impact assessment. Using very high resolution satellite images and GIS approach, recovery and reconstruction progress can be monitored and studied in future works.

In another main study, building damage data of Ishinomaki city, with special attention to the plain coast affected area, are classified and analyzed using data surveyed by the Ministry of Land, Infrastructure and Transportation of Japan (MLIT) for more than

52,000 structures. The classification includes information on six levels of damage, four types of building materials and damages due to tsunami inundation for each building material which are necessary information for an effective hazard mitigation. Notably, damage levels percentage distribution of different building materials are plotted for different inundation depth ranges in several sets of figures. This graphical illustration not only shows a better resistant performance of reinforced concrete and steel buildings over wood or other buildings for all inundation depth ranges, but also can explain clearly the inundation-induced damage behavior for each building material as well as the threshold depth for each damage level.

Moreover, this research contains an analysis of building damage characteristics due to the topographical factors. Surveyed data provided by Geospatial information authority of Japan (GSI) that classifies the Ishinomaki plain coast area into three classes are compared with the building damage map produced using analytical hierarchy process (AHP) methodology in ArcGIS 10.2 environment. The influence of key geographical features on tsunami-induced building damage, notably Kitakami river and water canals flooding, is taken into account with respect to the weighting of factors. A good agreement produced building damage map with surveyed GSI data shows the power of GIS tool based on the AHP approach for tsunami damage assessment.

The disaster management and mitigation scopes and frame work was described in this study. The aim was to reduce the consequences of tsunami event which include saving of lives and capitals. As prerequisite for this purpose the extent of the damages was obtained from vulnerability studies. Then the quantities to enable us for an appropriate preparedness program can be estimated based on the frame work presented. The more exact the data of the vulnerabilities, the more effective the management of its effects. It was shown that which data from vulnerability analysis can more help to disaster management and how we can extract these data for quantifying the needs for disaster management and also planning and preparedness issues. It was quantitatively shown that the more exact the data of the vulnerabilities, the more effective the management of its effects. It was also shown that considering the priorities such as distribution of fatalities to arrange for rescue operations, distribution of emergency building such as hospital for mitigation of the rescue process and distribution of capitals and important facilities and lifeline sources to help for decision making for restoration process a very effective and

robust disaster management plan can be developed and this is dedicated to the quickly available outputs from integrated condition assessment using GIS and remote sensing.

This study proposes an effective approach to assess the vulnerability of an area to tsunamis and a good method to analyze the building damage data based on surveyed databases. Results are practical for researchers in the field of disaster management to create the tsunami vulnerability and building damage maps.

# Reference


[1] F. Imamura, “Hyogo Framework for Action 2005-2015: Building the Resilience of Nations and Communities to Disasters”, Focusing on 2011 Great East Japan Earthquake, Tohoku University, Japan, 2014.

[2] F. Ranghieri and M. Ishiwatari, “Learning from Megadisasters-Lessons from the Great East Japan Earthquake”, 2014.

[3] National Geophysical Data Center/World Data Service (NGDC/WDS), 2014.

[4] REPORT OF THE INTERGOVERNMENTAL OCEANOGRAPHIC COMMISSION ON ITS ACTIVITIES (2014-2015), 38th Session, Paris, 2015

[5] Http://pubs.usgs.gov/circ/c1187/ (Tsunami generation).

[6] http://www.tsunami-alarm-system.com/en/phenomenon-tsunami/phenomenon-tsunami-occurrences.html

[7] Tsunami Terminology, http://nthmp-history.pmel.noaa.gov/terms.html

[8] Intergovernmental Oceanographic Commission, Tsunami Glossary, UNESCO, 2008.

[9] Yeh, H., and Stein, R., “Seismic Risk Mitigation Leadership Forum”, San Francisco, 5/2-3. Oregon State University and USGS, 2011.

[10] http://www.jma.go.jp/jma/en/2011_Earthquake/2011_Earthquake.html

[11] http://www.mapsofworld.com/thematic-maps/earthquake/japan.html

[12] CASCADIA, “News & information from the Oregon Department of Geology and Mineral Industries”, WINTER 2012.

[13] National Police Agency of Japan, 2011. Damage situation and police countermeasures associated with 2011 Tohoku district - off the Pacific Ocean earthquake, Accessed July 5, 2011 from http://www.npa.go.jp/archive/keibi/biki/index_e.htm

[14] http:// www.coastal.jp/ttjt/index.php?plugin=ref&page=FrontPage&src=survey.jpg

[15] http://earthquake.usgs.gov/earthquakes/shakemap

[16] http://quake.abag.ca.gov/shaking/mmi/

[17] osdma.org, Understanding Tsunami

[18] Pelling, M., "The vulnerability of Cities: Natural Disasters and Social Resilience", Earthscan Publication, London, 2003.

[19] Bollin, C., Cardenas, C., Hahn, H., and Vasta, K., S., Disaster Risk Management by Communities and Local Governments, Inter-American Development Bank, Washinton, DC, 2003.

http://www.iadb.org/sds/doc/GTZ%2DStudyFinal.pdf.

[20] Karen E., Joyce, Kim C., Wright, Sergey V., Samsonov and Vincent G., "Remote Sensing and The Disaster Management Cycle, Advances in Geoscience and Remote Sensing", Gary Jedlovec (Ed.), ISBN:978-953-307-005-6, 2009.

[21] Yamazaki, F., Kouchi, K. and Matsuoka, M., "Tsunami damage detection using moderate-resolutuion satellite imagery", Proceeding of the 8th U.S. National Conference on Earthquake Engineering, California, US, 2006.

[22] Yamazaki, F., and Matsuoka, M., "Remote sensing technology in post-disaster damage assessment, Journal of Earthquakes and Tsunamis, World Scientific Publishing Company, vol. 1, no.3, pp. 193-210, 2007.

[23] Carver, S., J., "Integrating multi-criteria evaluation with geographical information systems", International Journal of Geographical Information Systems, Vol. 5 No. 3, pp. 321-339. http://dx.doi.org/10.1080/02693799108927858, 1991.

[24] Jankowski, P., "Integrating geographic information systems and multiple criteria decision making methods", International Journal of Geographic Information System, Vol. 9 No. 3, pp. 251-273. http://dx.doi.org/10.1080/02693799508902036, 1995.

[25] Eckert, S., Jelinek, R., Zeug, G. and Krausmann, E., "Remote sensing-based assessment of tsunami vulnerability and risk in Alexandria", Egypt, Applied Geography, Vol. 32 No. 2, pp. 714-723., 2012.

[26] Romer, H., Willroth, P., Kaiser, G., Vafeidis, A.T., Ludwig, R., Sterr, H. and Diez, J.R, "Potential of remote sensing techniques for tsunami hazard and vulnerability analysis - a case study from Phan-Nga province, Thailand", Natural Hazards and Earth System Sciences, Vol. 12 No. 6, pp. 2103-2126, 2 012.

[27] Mahendra, R. S., Mohanty, P. C., Bisoyi, H., Kumar, T. S. and Nayak, S., Assessment and management of coastal multi-hazard vulnerability along the Cuddalore Villupuram, east coast of India using geospatial techniques, Ocean & Coastal Management, Vol. 54 No. 4, pp. 302-311, http://dx.doi.org/10.1016/j.ocecoaman.2010.12.008, 2011.

[28] Strunz, G., Post, J., Zosseder, K., Wegscheider, S., Muck, M., Riedlinger, T., Mehl, H., Dech, S., Birkmann, J., Gebert, N., Harjono, H., Anwar, H. Z., Sumaryono, Khomarudin, R. M. and Muhari, A., "Tsunami risk assessment in Indonesia, Natural Hazards and Earth System Science", Vol. 11, pp. 67-82. http://dx.doi.org/10.5194/nhess-11-67-2011, 2011.

[29] Sinaga, T. P., Adhi, N., Yang-Won Lee, and Yongcheol, S., "GIS mapping of tsunami vulnerability: case study of the Jembrana Regency in Bali, Indonesia", KSCE Journal of Civil Engineering, Vol. 15 No. 3, pp. 537-543.http://dx.doi.org/10.1007/s12205-011-0741-8, 2011.

[30] Hsien, L., C., and Sheng, C., H., "The use of spatial analysis techniques in mapping potential natural hazard areas: a case study of Taiwan, Procedia Environmental Sciences", Vo. 10, Part B, pp. 1092-1097, 2011.

[31] Gokon, H., and Koshimura, S., "Mapping of building damage of the 2011 Tohoku earthquake tsunami in Miyagi Prefecture", Coastal Engineering Journal, World Scientific Publishing Company and Japan Society of Civil Engineers, Vol. 54 No. 1, pp. 12, 2012.

[32] Mori, N. and Takahashi, T., Nationwide Field Survey of the 2011 Off the Pacific Coast of Tohoku Earthquake Tsunami, The 2011 Tohoku Earthquake Tsunami Joint Survey Group, Journal of Japan Society of Civil Engineers, Series B, Vol. 67, No.1 pp.63-66, 2011.

[33] Dall'Osso, F., Bovio, L., Cavalletti, A., Immordino, F., Gonella, M., and Gabbianelli, G., "A novel approach (the CRATER method) for assessing tsunami vulnerability at the regional scale using ASTER imagery", Italian Journal of Remote Sensing, vol. 42, no. 2, pp. 55-74., 2010.

[34] Papathoma, M., Dominey-Howes, D., Zong, Y. and Smith, D., Assessing tsunami vulnerability, an example from Herakleio, Crete, Nat. Hazards Earth Syst. Sci., Vol. 3, pp. 377 389, http://dx.doi.org/10.5194/nhess-3-377-2003, 2003.

[35] Papathoma, M., and Dominey-Howes, D., "Tsunami vulnerability assessment and its implications for coastal hazard analysis and disaster management planning, Gulf of Corinth, Greece", *Natural Hazards and Earth System Sciences,* Vol. 3 No. 6, pp. 733-747, http://dx.doi.org/10.5194/nhess-3-733-2003, 2003.

[36] Dall'Osso, F., Gonella, M., Gabbianelli, G., Withycombe, G., and Dominey-Howes, D., "A revised (PTVA) model for assessing the vulnerability of buildings to tsunami damage", Nat. Hazards Earth Syst. Sci., vol. 9, pp. 1557 1565, doi: 10.5194/nhess-9-1557-2009, 2009.

[37] Blaikie, P., "At risk: natural hazards, people's vulnerability and disasters", London etc., Routledge, 1994.

[38] Turner, B. L., and Kasperson, R. E., "A framework for vulnerability analysis in sustainability science", Proceedings of The National Academy of Sciences of The USA, 100(14): 8074-8079, 2003.

[39] UN – ISDR, "Living with Risk", UN, http://www.unisdr.org/eng/about_isdr/bd-lwr-2004-eng.htm, 2004.

[40] Birkmann, J., "Danger need not spell disaster-But how vulnerable are we?", Research Brief of the United Nations University, No. 1, 2005.

[41] http://www.proventionconsortium.org/

[42] United Nations Disaster Relief Organization (UNDRO), Mitigating Natural Disasters: Phenomena, Effects and Options: A Manual for Policy makers and Planners, New York: United Nations, 1991.

[43] Villagrán de Leon, J. C., Vulnerability a Conceptual and Methodological Review, 2006.

[44] UN – ISDR, "Living with Risk, UN", http://www.unisdr.org/eng/about_isdr/bd-lwr-2004-eng.htm, (2004).

[45] UNU-EHS. UNU. No 4/2006.

[46] Bogardi, J., and Birkmann, J., "Vulnerability Assessment: the first step towards sustainable risk reduction". Disasters and Society - From hazard assessment to risk reduction. D. Malzahn and T. Plapp. Berlin, Logos Verlag: 75-82, 2004.

[47] Cardona, O., D., "Environmental Management and Disaster Prevention: Two Related topics: A Holistic Risk Assessment and management Approach", in: J.Ingleton, ed., Natural Disaster Management, London: Tudor Rose, 1999.

[48] Saaty, T., L., "The Analytic Hieharchy Process, Planning, Priority Setting, Resource Allocatio", McGraw-Hill, New York, 1980.

[49] T. L. Saaty and L. G. Vargas, "Decision Making with the Analytic Network Process", University of Pittsburgh, USA, 2001.

[50] Proctor, W., "Towards sustainable forest management-an application of multi-criteria analysis to Australian forest policy", In: Third International Conference of the European Society for Ecological Economics, May 3-6, Vienna, Austria, 2000.

[51] T. L. Saaty, "A Scaling Method for Priorities in Hierarchical Structures", Journal of Mathematical Psycology, Vol. 15, pp. 234-281, 1977.

[52] Rao, M., Sastry, S., V., C., Yadar, P., D., Kharod, K., Pathan, S., K., Dhinwa, P.,S., Majumdar, K.,L., Sampat Kumar, D., Patkar, V., N., and Phatak, V., K., "A Weight Index Model for Urban Suitability Assessment a GSI Approach", Bombay Metropolitan Regional Developtment Authority, Bombai, India. 1991.

[53] Westen and Kingma,, "*Elements at risk.* In: Multi-hazard Risk Assessment", United Nations University, ITC School on Disaster Geoinformation, pp. 1-43, 2009.

[54] Abella, E., A., C., "Multi-scale Landslide Risk Assessment in Cuba", ITC the Netherlands, 2008.

[55] Thirumalaivasan D., Karmegam, M., and Venugopal, K., "AHP-DRASTIC: software for specific aquifer vulnerability assessment using DRASTIC model and GIS", Environmental Modelling & Software, pp. 645 656, 2003.

[56] Belward, A.S., Stibig, H.J., Eva, H., Rembold, F., Bucha, T., Hartley, A., Beuchle, R., Khudhairy, D., Michielon, M., and Mollicone, D., "Mapping Severe Damage to Land Cover Following the Indian Ocean Tsunami using Moderate Spatial Resolution Satellite Imagery", International Journal of Remote Sensing, 28 (13), pp. 2977- 2994, 2004.

[57] McAdoo, B., G., Richardson, N., and Borrero, J., "Inundation Distances and Run-up Measurements from ASTER, QuickBird and SRTM Data", Aceh Coast, Indonesia. International Journal of Remote Sensing, 28 (13-14), pp. 2961-2975, 2007.

[58] Iverson, L., R., and Prasad, A., M., "Using Landscape Analysis to Assess and Model Tsunami Damage in Aceh Province, Sumatra" Landsc. Ecol., 22, pp. 323-331, 2007.

[59] Chatenoux B., and Peduzzi P., "Impacts from the 2004 Indian Ocean Tsunami: Analysing the Potential Protecting Role of Environmental Features", Natural Hazards, 40, pp. 289 304, 2007.

[60] Suppasri, A., Koshimura, S., Matsuoka, M., Gokon, H., and Kamthonkiat, D., "Application of Remote Sensing for Tsunami Disaster", Remote Sensing of Planet Earth, Dr Yann Chemin (Ed.), ISBN: 978-953-307-919-6, InTech, Available from: http://www.intechopen.com/books/remotesensing-of-planet-earth/application-of-remote-sensing-for-tsunami-disaster, 2012.

[61] http://eoimages.gsfc.nasa.gov/images/imagerecords/49000/49648/sendai_ast_20110 73_lrg.jpg.

[62] http://www.geoimage.com.au/media/satellite_pdfs/GeoEye_FactSheet_comb.pdf

[63] http://www.landinfo.com/geo.htm

[64] http://www.geoimage.com.au/media/satellite_pdfs/GeoEye_FactSheet_comb.pdf

[65] https://directory.eoportal.org/web/eoportal/satellite-missions/g/geoeye-1

[66] http://fgd.gsi.go.jp/download/GsiDLSelFileServlet.

[67] Worboys., "GIS: A Computer Science Perspective", London, Bristol, ISBN 3540603921, pp. 413-430, 1995.

[68] Abdul-Rahman and Pilouk., "Spatial Data Modelling for 3D GIS:]", Springer, 2007.

[69] Smith, M., Goodchild, M. F. and Longley, P. A., "Geospatial Analysis; a Comprehensive Guide to Principle", Techniques and Software Tools, Matador, Leicester, UK, 2007.

[70] Saaty, T., L., and Vargas, L. G., "Prediction, Projection, and Forecasting: Application of The Analytic Hierarchy Process in Economics", Finance, Politics, Games, and Sports, Kluwer Academic Publishers, Boston, 1991.

[71] Saaty, T., L., "Decision Making for Leaders; The Analytical Hierarchy Process for Decisions in a Complex World", RWS Publication, Pittsburgh, 1982.

[72] N. E. Podger, W. B. Colwell and M. H. Taylor., "GeoEye-1 Radiance at Aperture and Planetary Reflectance, 2011.

[73] Z. Jiang, A.R. Huete, J. Chen, Y. Chen, J. Li, G. Yan and X. Zhang., "Analysis of NDVI and scaled difference vegetation index retrievals of vegetation fraction", Remote Sensing of Environment 101, pp. 366‑378, 2006.

[74] P.M. MATHER and M. KOCH, "Computer Processing of Remotely-Sensed Images: An Introduction", 4th Edition, ISBN: 978-0-470-74239-6, 2010.

[75] Exelis Visual Information Solutions, Inc. All Rights Reserved, 2013.

[76] Abu Bakar Sambah, Tsunami Vulnerability Assessment Using Integrative Remote Sensing and GIS Approaches, Yamaguchi University, 2014.

[77] Hideomi Gokon and Shunichi Koshimura, Disaster Control Research Center, Graduate School of Engineering, Tohoku University., "MAPPING OF BUILDING DAMAGE OF THE 2011 TOHOKU EARTHQUAKE TSUNAMI IN MIYAGI PREFECTURE", 24 March 2012.

[78] Tadashi Ishii, "Medical response to the Great East Japan Earthquake in Ishinomaki City", 2011.

[79] Okayama. T., "Disaster Debris Management in Miyagi Prefecture and Ishinomaki City Following the 2011 East Japan Earthquake", ARB Symposium, Hokkaido University, Japan, 1-8, 2013.

[80] Google map, 2015

[81] Gao. Y, Mas. J.F., "A COMPARISON OF THE PERFORMANCE OF PIXEL-BASED AND OBJECT-BASED CLASSIFICATIONS OVER IMAGES WITH VARIOUS SPATIAL RESOLUTIONS," On Line Journal of Earth Sciences 2, 27-35, 2008.

[82] Aplin. P, Smith. G.M., "ADVANCES IN OBJECT-BASED IMAGE CLASSIFICATION," 725-728, 2008.

[83] Angelos Tzotsos., "A SUPPORT VECTOR MACHINE APPROACH FOR OBJECT BASED IMAGE ANALYSIS", 2006.

[84] Dang Huu Nghi, Luong Chi Mai., "An object oriented classification techniques for high resolution satellite imagery", 1-6, 2008.

[85] Bokhary, Marwa A. M., "Comparison between Pixel Based Classification and Object Base Feature Extraction Approaches for a Very High Resolution Remote Sensed Image", 2008.

[86] EXELIS, Feature Extraction with Example-Based Classification Tutorial, ENVI Tutorial, 2012.

[87] Katharina Tschanen., "Evaluation of Adaptive Image Characteristics for Image Classification", 2012.

[88] R. Duda, P. Hart, and D. Stork, Pattern Classification, John-Wiley., "Support Vector Machines (SVM)", 2001.

[89] Yutaka Sasaki., "The truth of the F-measure", School of Computer Science, University of Manchester, 2007.

[90] http://www.pasco.co.jp/eng/products/geoeye-1, 14 September 2014.

[91] Tabarroni. A., "Remote Sensing and Image Interpretation Change Detection Analysis: Case Study of Borgo Panigale and Reno Districts", Master II Livello in Sistemi Informativi Geografici, 27-35, 2010.

[92] Department of Regional Development and Environment Executive Secretariat for Economic and Social Affairs Organization of American States. "Primer on Natural Hazard Management in Integrated Regional Development Planning", Washington, D.C, 1991.

[93] Roxana L. Ciurean , Dagmar Schröter and Thomas Glade., "Conceptual Frameworks of Vulnerability Assessments for Natural Disasters Reduction", INTECH Published, pp. 1-32, 2013.

[94] Omar-Dario Cardona, Maarten K. van Aalst., "Determinants of Risk: Exposure and Vulnerability", Cambridge University Press, Cambridge, UK, and New York, NY, USA, pp. 65-108, 2012.

[95] Masashi Matsuoka, and Fumio Yamazaki., "Use of Satellite SAR Intensity Imagery for Detecting Building Areas Damaged Due to Earthquakes", Earthquake Spectra, Volume 20, No. 3, pp. 975–994, 2004.

[96] FEMA, Applications of GIS for Emergency Management, Lesson 1: Introduction and Course Overview, IS-922, available at https://emilms.fema.gov/is922/GISsummary.htm. Accessed on 16 August 2015.

[97] STEPHEN J. CARVER., "Integrating multi-criteria evaluation with geographical information systems", GEOGRAPHICAL INFORMATION systems, 1991, VOL. 5, No.3, 321-339, University of Newcastle upon Tyne, U.K, 2007.

[98] Soheil Boroushaki and Jacek Malczewski., "Participatory GIS: A Web-based Collaborative GIS and Multicriteria Decision Analysis", URISA Journal, Vol. 22, No. 1, pp. 23-32, 2010.

[99] Jacek Malczewski., "GIS-based land-use suitability analysis: a critical overview", Department of Geography, University of Western Ontario, London, Ont., Canada, pp. 3-65, 2004.

[100] Tariful Islam and Sugianto Saman., "Spatial information-based approach for integrated coastal resource management in Asian tsunami-affected countries", FAO Regional office Asia and Pacific, The Regional Workshop on Information Management and Coordination Mechanisms of Tsunami Emergency and Rehabilitation Operations in Agriculture, Fisheries and Forestry, pp. 287-311, 2006.

[101] James C. Ascough, Harriet D. Rector, Dana L. Hoag, Gregory S. McMaster, Bruce C. Vandenberg, Marv in J. Shaffer, Mark A. Weltz, and Lajpat R. Ahjua., "Multicriteria Spatial Decision Support Systems: Overview, Applications, and Future Research Directions", pp. 175-180, 2002.

[102] Uwe Deichmann, Daniele Ehrlich, Christopher Small, Gunter Zeug., "Using high resolution satellite data for the identification of urban natural disaster risk", European Union and World Bank, 2011.

[103] Abu Bakar Sambah, Fusanori Miura., "Remote Sensing, GIS, and AHP for Assessing Physical Vulnerability to Tsunami Hazard", World Academy of Science, Engineering and Technology International Journal of Environmental, Ecological, Geological and Mining Engineering, Vol. 7, No. 10, 2013.

[104] Fakultät für Geowissenschaften., "ASSESSING BUILDING VULNERABILITY TO TSUNAMI HAZARD USING INTEGRATIVE REMOTE SENSING AND GIS APPROACHES", Dissertation Thesis , 2010.

[105] William Cadell., "Report on the generation and analysis of DEMs for spatial modeling", pp. 11-15, 2002.

[106] Robert C. Weih, Jr. and Tabitha L.Mattson., "Modeling Slope in a Geographic Information System", Journal of the Arkansas Academy of Science, Vol. 58, pp. 100-108, 2004.

[107] Hitoshi Tanaka, Kosuke Kayane, Mohammad Bagus Adityawan, and Mohammad Farid., "THE EFFECT OF BED SLOPE TO THE TSUNAMI INTRUSION INTO RIVERS", Coastal Dynamics, pp. 1601-1610, 2013.

[108] Harry Yeh, Elena Tolkova, David Jay, Stefan Talke, and Hermann Fritz., "Tsunami Hydrodynamics in the Columbia River", Journal of Disaster ResearchVol.7, No.5 , 2012.

[109] Mohammad Bagus ADITYAWAN, Min ROH, Hitoshi TANAKA, and Mohammad FARID., "The Effect of River Mouth Morphological Features on Tsunami Intrusion", pp. 75-83, 2012.

[110] FUKUI, Tsuneaki., "Considering the Extent of Damage in Ishinomaki from a Civil Engineering Perspective", Disaster, Infrastructure and Society: Learning from the 2011 Earthquake in Japan No.2, pp. 14-21, http://hdl.handle.net/10086/23128, 2012.

[111] Jonathan E. Campbell, Michael Shin., "Geographic Information System Basics" (v. 1.0), Chapter 6, pp. 133-163, 2012.

[112] Suraj Kumar Singh, Vikas Chandel, Himanshu Kumar and Hemant Gupta., "RS & GIS BASED URBAN LAND USE CHANGE AND SITE SUITABILITY ANALYSIS FOR FUTURE URBAN EXPANSION OF PARWANOO PLANNING AREA, SOLAN, HIMACHAL PRADESH (INDIA)", International Journal of Development Research Vol. 4, Issue. 8, pp. 1491-1503, 2014.

[113] Thomas L. Saaty., "Decision making with the analytic hierarchy process", Int. J. Services Sciences, Vol. 1, No. 1, 2008.

[114] Thomas L. Saaty., "A Scaling Method for Priorities in Hierarchical Structures", JOURNAL OF MATHEMATICAL PSYCHOLOGY, Vol. 15, pp. 234-281, 1977.

[115] Kardi Teknomo., "ANALYTIC HIERARCHY PROCESS (AHP)", 2006.

[116] Thomas L. Saaty., "Decision Aiding Decision-making with the AHP: Why is the principal eigenvector necessary", European Journal of Operational Research 145 85–91, 2003.

[117] Proceedings of the 6th European Conference on Management Leadership and Governance, Poland, 2010.

[118] R. V. Rao., "Decision Making in the Manufacturing Environment Using Graph Theory and Fuzzy Multiple Attribute Decision Making Methods, Chapter 2 Improved Multiple Attribute Decision Making Methods", http://www.springer.com/978-1-4471-4374-1, 2013.

[119] Geospatial Authority of Japan (GSI), Map of inundation area due to the 2011 Great East Japan Earthquake, Map number 12 available at http://www.gsi.go.jp/common/000059847.pdf, Accessed on 2 November 2015.

[120] Samo Drobne and Anka Lisec., "Multi-attribute Decision Analysis in GIS: Weighted Linear Combination and Ordered Weighted Averaging", pp. 459–474, 2009.

[121] N. Chandrasekar, J. L. Immanuel, J. D.Sahayam, M. Rajamanickam, S.Saravanan., "Appraisal of tsunami inundation and run-up along the coast of Kanyakumari District, India – GIS analysis", OCEANOLOGIA, 49 (3), pp. 397–412, 2007.

[122] E. A. Gencer, The Interplay Between Urban Development,Vulnerability, and Risk Management, Mediterranean Studies 7, Chapter 2, "Natural Disasters, Urban Vulnerability,and Risk Management: A Theoretical Overview", 2013.

[123] M. Papathoma-Köhle, T. Ulbrich, M. Keiler, L. Pedoth, R. Totschnig, Th. Glade, S. Schneiderbauer, U. Eidswig, Vulnerability to Heat Waves, Floods, and Landslides in Mountainous Terrain: Test Cases in South Tyrol, Assessment of Vulnerability to Natural Hazards A European Perspective, Elsevier publications, pp.179-201, 2014.

[124] National Police Agency (2011) Damage condition of the 2011 earthquake off the Pacific coast of Tohoku http://www.npa.go.jp/archive/keibi/biki/higaijokyo.pdf. Accessed 20 July 2012.

[125] Gokon H, Koshimura S, Matsuoka M, Namegaya Y (2011) Developing tsunami fragility curves due to the 2009 tsunami disaster in American Samoa. In: Proceedings of coastal engineering conference, Japan. Society of Civil Engineers, Morioka, 9–11 November 2011.

[126] Ruangrassamee A, Yanagisawa H, Foytong P, Lukkunaprasit P, Koshimura S, Imamura F Investigation of Tsunami-induced damage and fragility of buildings in Thailand after the December 2004 Indian Ocean Tsunami. Earthquake Spectra 22:377–401, 2006.

[127] Arikawa T Structural behavior under impulsive tsunami loading. J Disaster Res 4(6):377–381, 2009.

[128] Dominey-Howes D, Papathoma M Validating the ‘‘Papathoma Tsunami Vulnerability Assessment Model’’ (PTVAM) using field data from the 2004 Indian Ocean tsunami. Nat Hazards 40(1):113–136, 2007.

[129] Matsutomi H, Harada K Tsunami–trace distribution around building and its practical use. In: Proceedings of the 3rd international tsunami field symposium, Sendai, Japan, 10–11 April 2010, session 3–2, 2010.

[130] Matsutomi H, Shuto N Tsunami inundation depth, current velocity and damage to houses. In:Proceedings of coastal engineering conference, Japan Society of Civil Engineers, 41, 246–250, 1994.

[131] Suppasri A, Koshimura S, Imai K, Mas E, Gokon H, Muhari A, Imamura F Field survey and damage characteristic of the 2011 Tohoku tsunami in Miyagi prefecture. Coast Eng J 54:1250005, 2012a.

[132] Suppasri A, Koshimura S, Matsuoka M, Gokon H, Kamthonkiat D Remote sensing of planet earth: application of remote sensing for tsunami disaster, InTech, ISBN 979-953-307-541-8, 2012b.

[133] Suppasri A, Mas E, Koshimura S, Imai K, Harada K, Imamura F Developing tsunami fragility curves from the surveyed data of the 2011 Great East Japan tsunami in Sendai and Ishinomaki Plains Coast Eng J 54:1250008, 2012c.

[134] Suppasri A, Imai K, Imamura F, Koshimura S Comparison of casualty and building damage between Sanrikuria coast and Sendai plain coast based on the 2011 Great East Japan tsunami. In: Proceedings of international sessions in coastal engineering, JSCE, ed., vol 3, 2012d.

[135] Porter K, Kennedy R, Bachman R Creating fragility functions for performance-based earthquake engineering. Earthquake Spectra 23(2):471–489, 2007.

[136] Reese S, Cousins WJ, Power WL, Palmer NG, Tejakusuma IG, Nugrahadi S Tsunami vulnerability of buildings and people in South Java – field observations after the July 2006 Java tsunami. Nat Hazards Earth Syst Sci 7:573–589, 2007.

[137] A. Suppasri, E. Mas, I. Charvet, R. Gunasekera, , K. Imai, Y. Fukutani, Y. Abe, and F. Imamura., 'Building damage characteristics based on surveyed data and fragility curves of the2011 Great East Japan tsunami', Natural Hazards, 66(2), pp. 319–341, 2013.

[138] Tanimoto, K.: On the Hydraulic Aspects of Tsunami Breakwaters in Japan, Proc. of the International Tsunami Symposium by IUGG Tsunami Commission, pp. 423-435, 1983.

[139] http://www.reidsteel.com/information/tsunamiresistant_building.html

[140] Cees VAN WESTEN, "REMOTE SENSING FOR NATURAL DISASTER MANAGEMENT", International Archives of Photogrammetry and Remote Sensing, Vol. XXXIII, Part B7. Amsterdam, 2000.

[141] Karen E. Joyce, Kim C. Wright, Sergey V. Samsonov and Vincent G. Amborsia, "Remote sensing and the disaster management cycle", www.intechopen.com, 2009.

[142] Nirupama, Slobodan P. Simonovic, "ROLL OF REMOTE SENSING IN DISASTER MANAGEMENT", ICLR Research, Paper Series – No. 21, 2002.

# Publication List

## Journal Articles

[1] Mohammad Reza Poursaber and Yasuo Ariki: "Estimation of Tsunami Hazard Vulnerability Factors by Integrating Remote Sensing, GIS and AHP based Assessment", OALIB Journal, January 2016.

[2] Mohammad Reza Poursaber and Yasuo Ariki: Integrated GIS, Remote Sensing and Survey Data for Damage Assessment of Buildings in Tsunami Event, Journal of Geographic Information System, March 2016.

## International Conferences

[1] Mohammad Reza Poursaber, Yasuo Ariki, and Mohammad Safi: "Selection of appropriate interpretation techniques of satellite images for natural disaster management", SPIE Remote Sensing - International Conference, United Kingdom- Edinburgh- Sep. 2012.

[2] Mohammad Reza Poursaber, Yasuo Ariki, Nemat Hassani and Mohammad Safi: "Variability of Change Detection Results for 2011 Tohoku, Japan Earthquake Using Very High-Resolution Satellite Images", SPIE Asia Pacific Remote Sensing (International Conference) China- Beijing, Oct. 2014.

[3] Mohammad Reza Poursaber, Yasuo Ariki, and Mohammad Safi: "Prioritization criteria of objective index for disaster management by satellite image processing", SPIE Remote Sensing (International Conference), Netherlands- Amsterdam- Sept. 2014.

## University Published Papers

[1] Mohammad Reza Poursaber, Yasuo Ariki and Mohammad Safi: "Research study on appropriate interpretation techniques of satellite images for natural disaster management", RCUSS- Kobe University- 2012.

[2] Mohammad Reza Poursaber, Yasuo Ariki and Mohammad Safi: "Updating satellite image processing results based on mapping during disaster management", RCUSS-Kobe University- 2013.

[3] Mohammad Reza Poursaber, Yasuo Ariki and Mohammad Safi: "Comparative study of pixel and object based classification of GeoEYE-1 imagery for natural disaster management; case study on Ishinomaki city under tsunami 2011", RCUSS- Kobe University- 2014.